MReadings: MR in RT

7th Edition 2021

siemens-healthineers.com/magnetom-world-rt

Not for distribution in the US

SIEMENS
Healthineers

The entire editorial staff at Medical University of Vienna and at Siemens Healthineers extends their appreciation to all the radiation oncologists, radiologists, technologists, physicists, experts, and scholars who donate their time and energy – without payment – in order to share their expertise with the readers of MAGNETOM Flash and the MReadings.

We welcome your questions and comments about the editorial content of MAGNETOM Flash. Please contact us at
magnetomworld.team@siemens-healthineers.com

Manuscripts as well as suggestions, proposals and information are always welcome; they are carefully examined and submitted to the editorial board for attention. MAGNETOM Flash is not responsible for loss, damage, or any other injury to unsolicited manuscripts or other materials. We reserve the right to edit for clarity, accuracy, and space. Include your name, address, and phone number and send to the editors, address above.

MReadings: MR in RT is also available online:

www.siemens-healthineers.com/magnetom-world-rt

External laser bridge for MR treatment planning
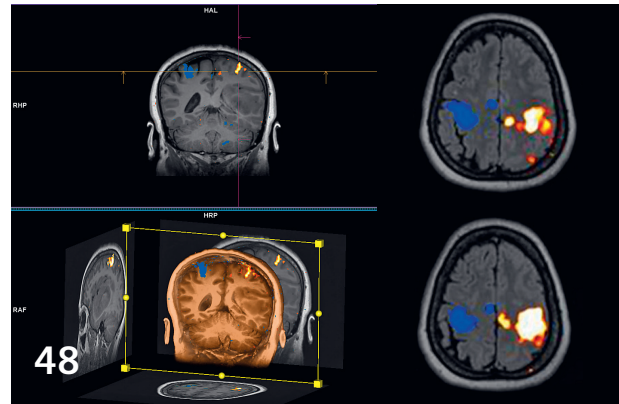
fMRI for Radiosurgery

Editorial Comment

Radiation Therapy

A History of Innovations

Meet Siemens Healthineers

*Cover image from JM Balter, et al.
Clinical Evaluation of a Receiver Coil
Custom Designed for MR Simulation
of Immobilized Patients*

Dr. Christian Kirisits, Associate Professor
Department of Radiation Oncology, Comprehensive Cancer Center, Medical University of Vienna, Austria

Christian Kirisits studied Technical Physics at the Vienna University of Technology in Austria and the first phase of Human Medicine at the University of Vienna. In 2000, he received a Doctor of Technical Science degree from the Vienna University of Technology. After completing an additional thesis ('Habilitation') while also working at the Medical University of Vienna, he was appointed to Associate Professor in 2005. His main fields of research are Medical Physics and Acoustics. Christian Kirisits is author or co-author of more than 150 peer-reviewed scientific articles in international journals and more than 10 book chapters. He has also made numerous contributions to conference proceedings, as a book editor and as a regular speaker at international and national conferences. He performed various functions in several professional and scientific societies and working groups, including chairman of the European Brachytherapy Committee, the GEC European Society for Radiotherapy & Oncology (ESTRO) Committee. He was a Coordinator of the Committee for the International Commission on Radiation Units and Measurements (ICRU) 89 report on Gynecological Brachytherapy and is currently one of the Coordinators of the International EMBRACE I and II clinical trials.

20 Years of MRI-guided Brachytherapy for Adaptive Radiation Oncology

Dear readers and colleagues,

This 7th edition of the *MReadings: MR in RT* contains a wide range of very interesting articles describing the integration of MRI into radiation oncology. Many of these individual experiences are similar to the long process of introducing MRI into brachytherapy. MRI-guided radiotherapy for external beam adaptive radiation oncology became an essential modality during recent years [1, 2]. Its use for brachytherapy already has a history that spans more than two decades. Initial experiences have been reported for several clinical disease sites, but clinical application in the treatment of gynecological and prostate cancer has been described by far the most [3]. For cervical cancer therapy, MRI-guided brachytherapy became state of the art in daily clinical routine. Back in 1992, Schoeppel et al. [4] described the use of "magnetic resonance imaging during intracavitary gynecologic brachytherapy" and showed the relation between the dose delivery device, the brachytherapy applicator, and the surrounding anatomy, especially the tumor. Mayr et al. identified in that early period the clear benefit of MRI in addition to clinical examination and with a clear advantage compared with CT-based tumor delineation [5].

MRI for brachytherapy is well established at the Department of Radiotherapy (now Radiation Oncology), Medical University of Vienna (known at that time as the University of Vienna) in Austria. There, a dedicated MR scanner for radiotherapy was installed as early as 1997

under Professor Richard Pötter. With the idea of using it together with the Division of Interventional Radiology, a low-field, open bore scanner was chosen (MAGNETOM Open Viva 0.2T, Siemens Healthcare, Erlangen, Germany). There was no specific support from the industry for its use in radiotherapy or brachytherapy. This created a substantial demand for research and development as well as quality assurance, especially taking into account image acquisition and distortion [6]. Essentially, it was possible to achieve high accuracy in the center of the field and in the pelvic area [7]. In brachytherapy, this region contains the delivery device, the applicator, and the clinical target volume. It was therefore possible to introduce MRI for cervical cancer brachytherapy clinically in 1999 [8]. Another advantage of MRI for brachytherapy application is the energy spectrum: The use of Iridium-192 instead of the higher energies used with Cobalt-60 or linear accelerators means that the energy spectrum and the predominant Compton effect allows dose planning based on water equivalent assumptions without clinically relevant uncertainties inside the pelvis [9].

Still, the misconception remains that brachytherapy treatment planning needs additional CT imaging to enable accurate dose calculations. Furthermore, there is a myth that only deformable image registration would allow the combination of external beam radiotherapy and brachytherapy for cervical cancer. However, the homogenous

external beam dose present at those volumes and organ parts that are of main interest for total dose constraints (external beam plus brachytherapy) allows a very good dose estimation without deformable image registration. There are even major limitations from the underlying target concepts so that it is questionable that such methods would result in a clinical benefit or improvement of the workflow [10].

The main issue in the initial phase of MRI integration in brachytherapy treatment planning was the lack of treatment planning software with the option to import sectional imaging from MRI. First, sectional images in general were not supported, later it was still difficult to import non-axial, oblique image orientations. The interim solutions for the first clinical applications were then based on the already state-of-the-art 3D reconstructions with orthogonal or semi-orthogonal radiographs (often called 2D planning, although the two radiographs allowed the reconstruction of the applicator and anatomical points in 3D). Applicators and some limited anatomical structures were digitized. These 3D datasets were used for dose calculation and could subsequently be registered to axial MR images for dose evaluation. The first rigid registration of radiographic approximation and MRI was established. The evaluation of isodose lines directly visualized on MRI slices was a major development and a particular advantage in daily clinical practice. Suddenly, the dose to individual parts of the tumor, the clinical target volume, and to organs and their substructures could be analyzed in detail. However, in first instance this did not result in reproducible plan evaluations and dose prescriptions at all. The first major step was the calculation of dose volume histograms for structures directly contoured on MR slices [11]. Although this was performed in daily clinical practice, the workflow itself became extremely time-consuming until the first planning systems to allow direct reconstruction of the brachytherapy source path and contouring in one MRI dataset, also consisting of several image orientations. This resulted in the first clinically applied MRI-only treatment plans in radiation oncology.

Image orientation was an essential topic, as the radiation oncologist performing the brachytherapy was used to an applicator's eye view – comparable to the beam's eye view in external beam. MRI with its possibility to orientate the slice orientation perpendicular to the tandem applicator located in the intrauterine channel was a major step toward the development of contouring guidelines with reduced inter- and intraobserver variations [12].

The clinical target definition and appropriate concepts for dose prescribing, recording, and reporting became essential when introducing MRI. The initial experience in Vienna demonstrates this process [13]. The clinical outcome in terms of local control improved substantially. Especially for larger tumors, the local control increased

from 64% in 1998–2000 to 82% in 2001–2003. And even more importantly, this increase in tumors larger > 5 cm was related to significant improvement in overall survival from 28% to 58%.

What were the main reasons for this success?

Target concept and dose metrics for prescribing and reporting

From my personal experience, the initial phase started with a major breakthrough: MR images at diagnosis with their soft-tissue contrast showing the gross tumor volume (GTV) with high signal intensity as well as the entire cervix, uterus, and, especially, potential infiltration into the parametrium were not new. A special learning phase included the understanding of MRI at the time of brachytherapy, in particular, the residual GTV and definition of gray zones, areas of tumor infiltration at diagnosis with a response to the external beam treatment usually performed prior to brachytherapy. But showing isodose lines in relation to these volumes of initial GTV, residual GTV, and a high-risk CTV (including gray zones) and analysis of dose volume histograms were the major step forward. However, without a clear target concept, inter- and intraobserver variations for the contours were huge and treatment plans were highly individual. Dose variations for target and organs at risk were substantial and lacked clear dose constraints.

These imaging and technological advances provided the initial impulse for groups like ICRU and GEC-ESTRO to found working groups. Richard Pötter from Vienna, together with Christine Haie-Meder, Villejuif, Paris, France, and Erik van Limbergen, Leuven, Belgium, representing different traditional treatment schools for cervix cancer radiotherapy succeeded in agreeing on a detailed target-concept and dose-reporting concept. From the beginning, these groups included medical physicists. Their concept was based on MRI with integration of the information from the clinical examination. It provided the basis for the internationally successful GEC-ESTRO recommendations I and II, two of the most cited articles in radiotherapy and oncology [14, 15]. The GEC-ESTRO recommendation III was dedicated to the principles and parameters of MR imaging within the framework of image-based adaptive cervix cancer brachytherapy [16] while part IV added the essential component of 3D registration [17]. All of these guidelines were finally extended to the international ICRU 89 report, supported by experts from Europe, North America, and Asia [18]. This comprehensive report allowed to define target volumes and organs at risk and provided a clear concept for prescribing, recording, and reporting dose. Definition of the initial GTV, residual GTV, as well as a risk-based clinical target volume concept using MRI are a key message in this report.

Optimizing dose delivery

The second major issue was dose delivery. The sudden clear picture of target volumes and organs at risk in relation to the dose distribution revealed major limitations of the application techniques that had been applied so far in daily clinical practice as "state of the art" based on standard point A dose prescription. Dose optimization by changing the dwell-time distribution could only partially compensate for the limited dose coverage. Especially large tumors and situations with unsuitable topography of target and organs at risk could not be sufficiently covered.

Optimized dose delivery became possible mainly by increasing the degrees of freedom with additional applicators placed inside the target volumes. Pioneering work has been done by developing compatible applicators and their visualization on MRI. This has been described first by using interstitial needles for the prostate especially, but also titanium needles [19, 20]. Especially the use of non-metallic tandem-rings and tandem-ovoid applicators in combination with these types of needles, visualized directly on MRI, allowed highly individualized dose distribution [21]. Dose could be increased to the clinical target volumes and gross tumor volume without increasing dose to surrounding organs. For asymmetric tumor topography, it allowed a higher conformality and often even a decrease in organ dose.

Adaptive workflow

Another major development was the adaptive workflow compared with image-guided external beam therapy. From the very beginning of fractionated high-dose-rate brachytherapy, a fully adaptive process was performed. MRI at the time of diagnosis and MRI at the time of brachytherapy (usually after a major amount of external beam dose delivery) allowed to study the pattern of response for the specific tumor situation. This allowed a detailed target definition based on GTV at diagnosis, the residual GTV, and the visible situation at the time of treatment.

Offline MRI is used by performing a pre-treatment MRI. This method allows to get the tumor situation at diagnosis and after external beam the radiochemotherapy response at a timepoint directly before brachytherapy. In such cases, the pre-treatment MRI is used to delineate the GTV and CTV on conventional CT plans.

However, online, MRI-guided interfraction adaptive RT became the real state of the art. In one sequence, it visualizes the GTV, CTV, organs at risk, the dose delivery device, and brachytherapy applicators with a high degree of accuracy. It would be comparable to an image visualizing the tumor, the organs, and the linear accelerator all at once. Only small uncertainties are introduced during the final dose delivery even hours after contouring and treatment planning. This was demonstrated in multiple studies, even resulting in a special issue of the Green Journal (multicenter analysis of uncertainties in [22]). These "intrafraction" variations are limited as demonstrated by repeated MRI scans after or directly before dose delivery for a second time.

Key to all the aforementioned developments was the highly interdisciplinary approach. All major guidelines and studies were generated through an intensive and balanced interaction between radiation oncologists and medical physicists as major contributors.

The integration of MRI into the brachytherapy planning process resulted in considerable improvements in treatment planning with an increase in target coverage and dose as well as a decrease in OAR doses. This was expected to translate into clear clinical benefits. This process could only become successful with clinical concepts including adaptive radiotherapy, adaptive in terms of adaptation of the target volume at the time of boost treatment (brachytherapy), adaptation of application technique, and optimized dose delivery.

And 20 years later? What is the status now? After several encouraging retrospective mono-institutional reports, it took a long time until a clear benefit of all these efforts could finally be demonstrated through a prospective clinical trial. The observational, multi-center EMBRACE I trial has provided comprehensive evidence that MRI works for radiotherapy (brachytherapy) of cervical cancer in clinical practice (1,416 patients from 24 centers from 2008–2015) and leads to excellent clinical results. The evidence relates to technology (MR imaging and the introduction of interstitial brachytherapy), dosimetric parameters (high target doses, also in advanced disease and limited OAR doses), as well as disease and morbidity outcomes. Local control was 92% at 5 years and was not significantly different between more limited and advanced local tumor stages (IB2-IVA). Overall survival at 5 years was outstanding at 74% [23].

MRI-based, image-guided, adaptive brachytherapy therefore represents a paradigm shift in the treatment of cervical cancer. It is currently leading to a change in clinical practice in Europe, North America, and in Asia. For any future developments, this MRI-based treatment approach should be used as the benchmark.

Christian Kirisits

References

1 Otazo R, Lambin P, Pignol JP, Ladd ME, Schlemmer HP, Baumann M, et al. MRI-guided Radiation Therapy: An Emerging Paradigm in Adaptive Radiation Oncology. Radiology. 2021;298(2):248-260.

2 Menard, C. van der Heide UA. Introduction: Magnetic resonance imaging comes of age in radiation oncology. Semin Radiat Oncol. 2014;24(3): 149-150.

3 Tanderup K, Viswanathan AN, Kirisits C, Frank SJ. Magnetic resonance image guided brachytherapy. Semin Radiat Oncol. 2014;24(3):181-91.

4 Schoeppel SL, Ellis JH, LaVigne ML, Schea RA, Roberts JA. Magnetic resonance imaging during intracavitary gynecologic brachytherapy. Int J Radiat Oncol Biol Phys. 1992;23(1):169-74.

5 Mayr NA, Tali ET, Yuh WT, Brown BP, Wen BC, Buller RE, et al. Cervical cancer: application of MR imaging in radiation therapy. Radiology. 1993;189(2):601-8.

6 Fransson A, Andreo P, Pötter R. Aspects of MR image distortions in radiotherapy treatment planning. Strahlenther Onkol. 2001;177(2):59-73.

7 Petersch B, Bogner J, Fransson A, Lorang T, Pötter R. Effects of geometric distortion in 0.2T MRI on radiotherapy treatment planning of prostate cancer. Radiother Oncol. 2004;71(1):55-64.

8 Wachter-Gerstner N, Wachter S, Reinstadler E, Fellner C, Knocke TH, Pötter R. The impact of sectional imaging on dose escalation in endocavitary HDR-brachytherapy of cervical cancer: results of a prospective comparative trial. Radiother Oncol. 2003;68(1):51-9.

9 Kirisits C, Rivard MJ, Baltas D, Ballester F, De Brabandere M, van der Laarse R, et al. Review of clinical brachytherapy uncertainties: analysis guidelines of GEC-ESTRO and the AAPM. Radiother Oncol. 2014;110(1):199-212.

10 Swamidas J, Kirisits C, De Brabandere M, Hellebust TP, Siebert FA, Tanderup K. Image registration, contour propagation and dose accumulation of external beam and brachytherapy in gynecological radiotherapy. Radiother Oncol. 2020;143:1-11.

11 Kirisits C, Pötter R, Lang S, Dimopoulos J, Wachter-Gerstner N, Georg D. Dose and volume parameters for MRI-based treatment planning in intracavitary brachytherapy for cervical cancer. Int J Radiat Oncol Biol Phys. 2005;62(3):901-11.

12 Petric P, Dimopoulos J, Kirisits C, Berger D, Hudej R, Pötter R. Inter- and intraobserver variation in HR-CTV contouring: Intercomparison of transverse and paratransverse image orientation in 3D-MRI assisted cervix cancer brachytherapy. Radiother Oncol. 2008;89(2):164-71.

13 Pötter R, Dimopoulos J, Georg P, Lang S, Waldhausl C, Wachter-Gerstner N, et al. Clinical impact of MRI assisted dose volume adaptation and dose escalation in brachytherapy of locally advanced cervix cancer. Radiother Oncol. 2007;83(2):148-55.

14 Haie-Meder C, Pötter R, Van Limbergen E, Briot E, De Brabandere M, Dimopoulos J, et al. Recommendations from Gynaecological (GYN) GEC-ESTRO Working Group (I): concepts and terms in 3D image based 3D treatment planning in cervix cancer brachytherapy with emphasis on MRI assessment of GTV and CTV. Radiother Oncol. 2005;74(3):235-45.

15 Pötter R, Haie-Meder C, Van Limbergen E, Barillot I, De Brabandere M, Dimopoulos J, et al. Recommendations from Gynaecological (GYN) GEC ESTRO Working Group (II): concepts and terms in 3D image-based treatment planning in cervix cancer brachytherapy: 3D dose volume parameters and aspects of 3D image-based anatomy, radiation physics, radiobiology. Radiother Oncol 2006;78(1):67-77.

16 Dimopoulos JC, Vos VD, Berger D, Petric P, Dumas I, Kirisits C, et al. Inter-observer comparison of target delineation for MRI-assisted cervical cancer brachytherapy: Application of the GYN GEC-ESTRO recommendations. Radiother Oncol. 2009;91(2):166-72.

17 Hellebust TP, Kirisits C, Berger D, Pérez-Calatayud J, De Brabandere M, De Leeuw A, et al. Recommendations from Gynaecological (GYN) GEC-ESTRO Working Group: considerations and pitfalls in commissioning and applicator reconstruction in 3D image-based treatment planning of cervix cancer brachytherapy. Radiother Oncol. 2010;96(2):153-60.

18 Prescribing, Recording, and Reporting Brachytherapy for Cancer of the Cervix. J ICRU. 2013;13(1-2):NP.

19 D'Amico AV, Cormack R, Tempany CM, Kumar S, Topulos G, Kooy HM, et al. Real-time magnetic resonance image-guided interstitial brachytherapy in the treatment of select patients with clinically localized prostate cancer. Int J Radiat Oncol Biol Phys. 1998;1;42(3):507-15.

20 Popowski Y, Hiltbrand E, Joliat D, Rouzaud M. Open magnetic resonance imaging using titanium-zirconium needles: improved accuracy for interstitial brachytherapy implants? Int J Radiat Oncol Biol Phys. 2000;47(3):759-65.

21 Kirisits C, Lang S, Dimopoulos J, Berger D, Georg D, Pötter R. The Vienna applicator for combined intracavitary and interstitial brachytherapy of cervical cancer: design, application, treatment planning, and dosimetric results. Int J Radiat Oncol Biol Phys. 2006;65(2):624-30.

22 Nesvacil N, Tanderup K, Hellebust TP, De Leeuw A, Lang S, Mohamed S, et al. A multicentre comparison of the dosimetric impact of inter- and intra-fractional anatomical variations in fractionated cervix cancer brachytherapy. Radiother Oncol. 2013;107(1):20-5.

23 Pötter R, Tanderup K, Schmid MP, Jürgenliemk-Schulz I, Haie-Meder C, Fokdal LU, et al. MRI-guided adaptive brachytherapy in locally advanced cervical cancer (EMBRACE-I): a multicentre prospective cohort study. Lancet Oncol. Accepted 2021.

MRI in Radiotherapy Planning: Our Experience so far

Rhydian Powell[1]; Bernadette McCafferty[1]; Lynn Doy[2]; Dr David Stewart[1]; Dr Darren Brady[1]; Dr Ciara Lyons[1]; Dr Ahmed Bedair[1]; Stephen Gilroy, M.Sc.[1]; Aisling Haughey, M.Sc.[1]; Elaine Reilly[1]; Andrew Reilly, Ph.D.[1]

[1]Department of Oncology, North West Cancer Centre, Altnagelvin Area Hospital, Londonderry, Northern Ireland
[2]Department of Radiology, Altnagelvin Area Hospital, Londonderry, Northern Ireland

Background

Advances in radiotherapy have made tumor definition increasingly important. There is extensive literature on the advantages of using magnetic resonance imaging (MRI) for tumor-volume and organ-at-risk delineation compared to computed tomography (CT) alone, with patients potentially receiving more accurate treatment at higher doses and with fewer side effects. Yet despite the many advantages, introducing MRI into the radiotherapy planning pathway is a challenge and far from standard practice in the UK and Ireland.

The Radiotherapy Department at the North West Cancer Centre in Altnagelvin, Northern Ireland, is a new facility equipped with state-of-the-art equipment capable of delivering some of the most technologically advanced radiotherapy treatment regimens currently in use anywhere in the world. However, although the treatment regimens can be delivered, accuracy and efficacy depend on precisely locating and defining the treatment-planning target volumes. Current treatment-planning technology dictates that CT imaging is the essential standard, as electron-density values derived from the scans are required for accurate dose calculation. However, CT imaging is not the modality of choice for visualizing soft tissue.

The advancement of treatment technologies has enabled more precise delivery of radiation to the target volume. This may permit reducing the volume of irradiated tissue but with these reduced volumes, the risk of a geographical miss increases and consequently there is a greater need for improved imaging for better visualization of tumour and organs at risk (OARs). With its superior
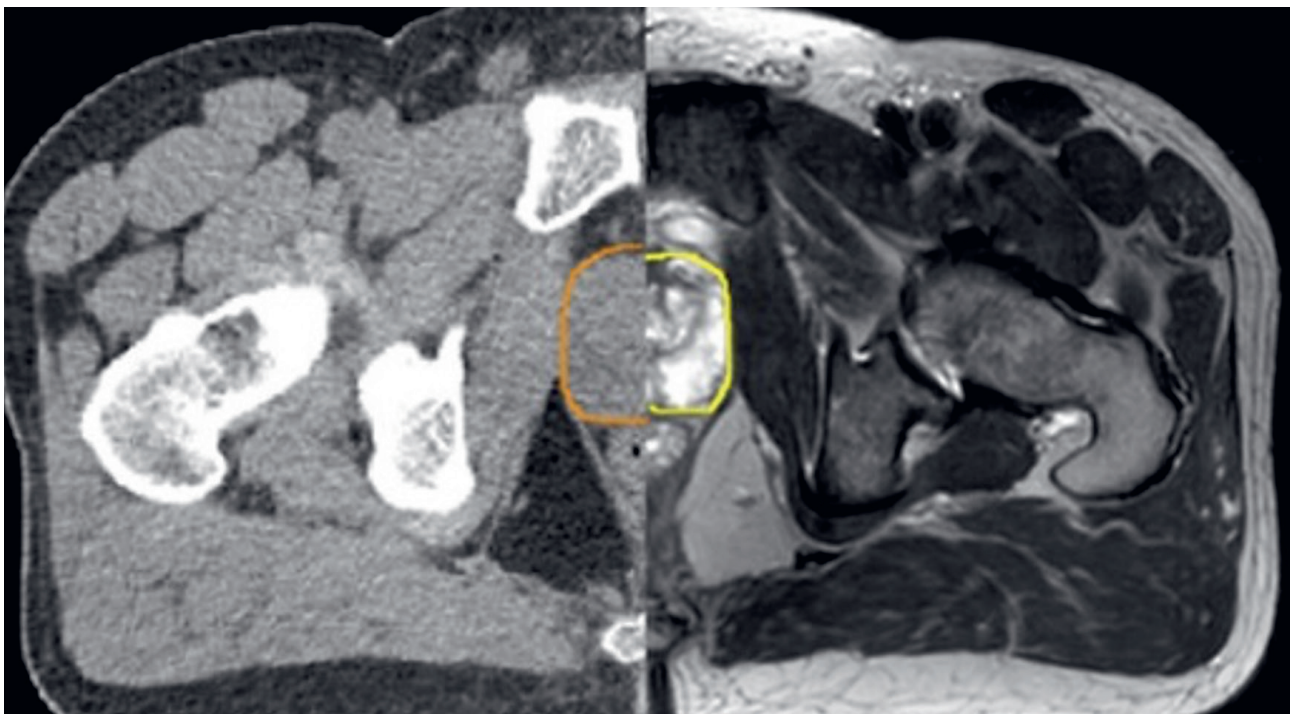
soft-tissue visualization capabilities (Fig. 1), wide range of image contrasts, and the availability of numerous functional imaging techniques, MRI has become a powerful tool for helping to accurately delineate treatment-planning target volumes.

MRI was introduced into the radiotherapy-planning pathway in September 2017. A multidisciplinary team of diagnostic and therapeutic radiographers, treatment planners, medical physicists, and clinicians was convened to establish this service, and close collaboration and cross-disciplinary training between all members of the team was vitally important for its successful implementation. Planning MRI was carried out in the days immediately following conventional CT simulation. All patients underwent identical preparation prior to both CT and MRI scans. They were immobilized in the treatment position using MR-compatible equipment. T2 SE axial and sagittal images were acquired (1.5T MAGNETOM Aera with software version *syngo* MR E11, Siemens Healthcare, Erlangen, Germany), imported into the Eclipse planning system (V15.5, Varian Medical Systems Inc., Palo Alto, CA, USA), and registered to the planning CT for volume delineation.

The service was initially offered to all patients for radical radiotherapy to the prostate at the North West Cancer Centre. The service was expanded in August 2018 to include patients for radical radiotherapy to the head and neck. As of December 2020, over 667 patients have been successfully scanned. Treatment review has shown that these patients have tolerated their radiotherapy well, with minimum side effects.

In this article, we describe some of our experience so far, and highlight the benefits of introducing MRI into the radiotherapy-planning pathway.

Treatment planning

To understand the benefits of introducing MRI into the radiotherapy-planning pathway, it is useful to understand the principles of target-volume delineation. In essence, we deliver a treatment to a volume much larger than the visible tumor itself. This is to account for multiple uncertainties and to avoid missing the tumor during daily radiotherapy treatments.

The geometric concepts of gross tumor volume (GTV), clinical target volume (CTV), and planning target volume (PTV) form the basis of modern radiotherapy planning.

The GTV refers to the position and extent of the gross tumor, i.e., what can be seen, palpated, or imaged.

The CTV contains the GTV, plus a margin for subclinical disease spread that cannot be fully visualized. The CTV is important because it must be adequately treated to achieve cure.
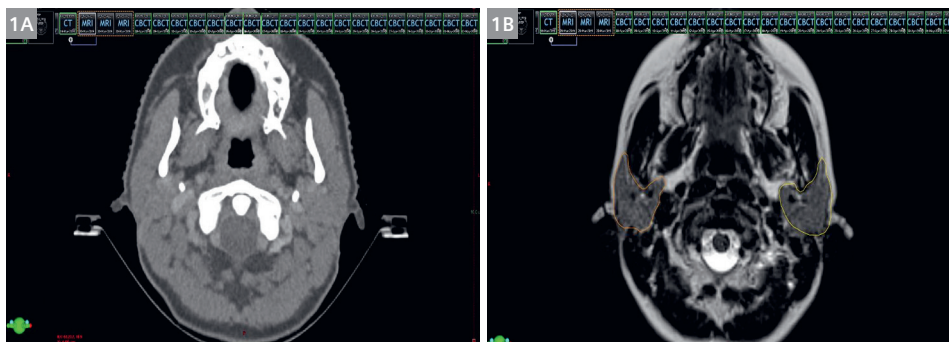
1 Superior soft-tissue contrast seen on MRI (1B) compared to CT scan (1A).
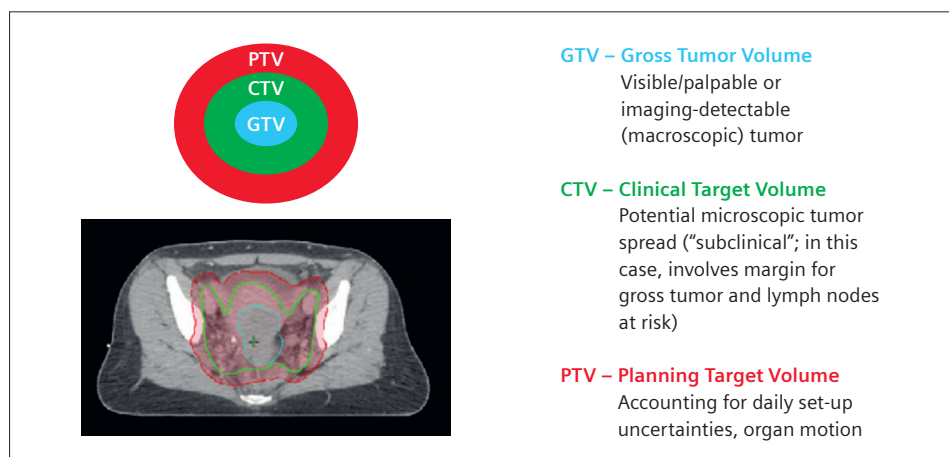
2 Radiotherapy target volumes.

GTV – Gross Tumor Volume
Visible/palpable or imaging-detectable (macroscopic) tumor

CTV – Clinical Target Volume
Potential microscopic tumor spread ("subclinical"; in this case, involves margin for gross tumor and lymph nodes at risk)

PTV – Planning Target Volume
Accounting for daily set-up uncertainties, organ motion

The PTV allows for uncertainties in planning or treatment delivery. It is a geometric concept designed to ensure that the radiotherapy dose is actually delivered to the CTV.

Radiotherapy planning must always consider critical normal tissue structures, known as organs at risk (OARs). An example of an OAR is the spinal cord, where damage to a small amount of normal tissue would be potentially life-threatening or life-changing.

Accurate delineation of these volumes using CT alone can be problematic. Determining tissue interfaces when delineating OARs such as the penile bulb and genitourinary (GU) diaphragm can be difficult using CT alone (Fig. 3), and the inferior image contrast often means that the same volume can be defined very differently by different users (Fig. 4). This has been shown to often lead to the GTV being defined larger than the true volume. Our experience is that prostate volumes defined using MRI fusion can be up to 30% smaller than those defined using CT alone, which in turn can affect the degree of genitourinary and gastrointestinal toxicity.

For head and neck cancers, precise delineation of intracranial OARs is crucial for accurate dose calculation, as radiotherapy can lead to visual or auditory deficits along with hormonal impairment or neurocognitive changes. Using CT imaging alone means that important normal structures are not always easily discernible. One area in which we have found MRI very useful is when delineating the optic chiasm (Fig. 5). The optic chiasm has a lower radiation tolerance than the surrounding cranial nerves, and over-irradiation of this structure can result in radiation-induced optic neuropathy. MRI has given our clinicians increased confidence in the accuracy of their delineation of this structure and other OARs within this region.
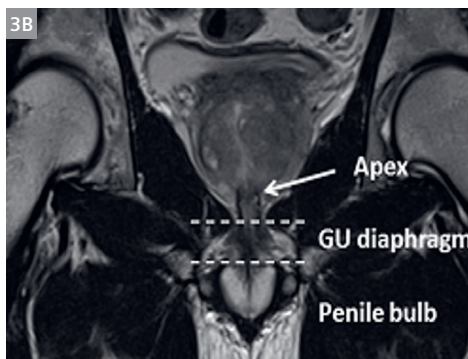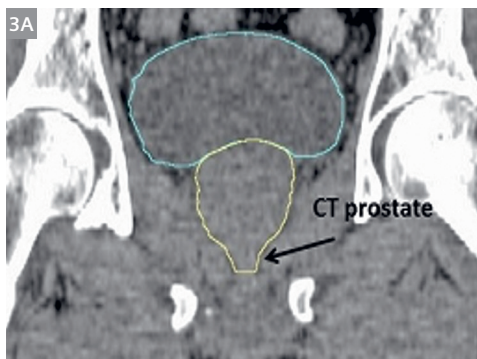
3 CT **(3A)** vs. MRI **(3B)** when delineating the penile bulb and GU diaphragm.
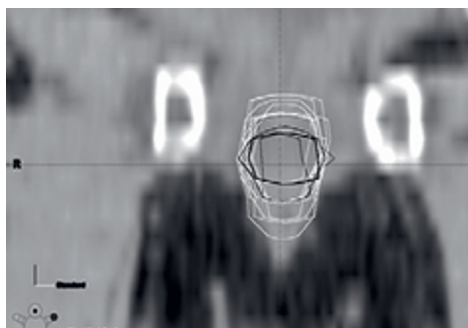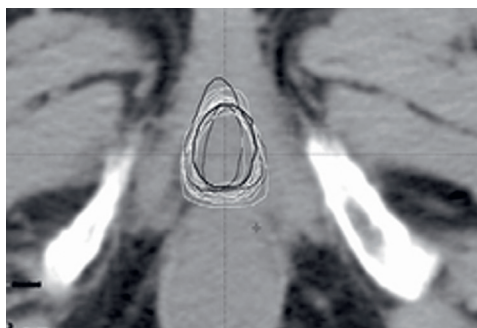
4 Inter User Variability. Images showing variability between users when defining planning volumes with CT alone.
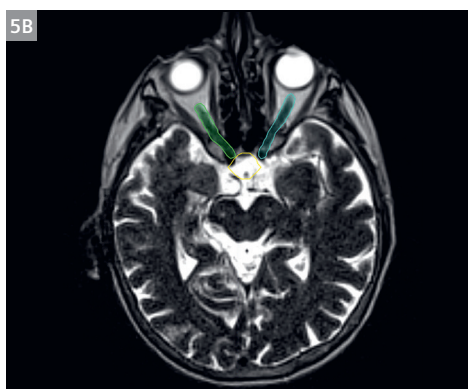
5 Optic nerves (blue and green) and optic chiasm (yellow) on CT **(5A)** and MRI **(5B)**. *Reproduced with permission from [1].*

MRI allows us to acquire our planning images in multiple planes. Sagittal and coronal images are particularly useful when defining the superior and inferior extent of the GTV, and although CT allows us to retrospectively reconstruct sagittal and coronal images, they are of inferior quality when compared to MRI, as you can see from the sample images below (Fig. 6).

Another area in which MRI has proven very useful is when planning patients with prostheses[1]. Metal artifacts can often obscure the region of interest on a CT planning scan, even after the use of iterative metal artifact reduction (iMAR) algorithms (Fig. 7).

MRI sees the prostheses as a void, but importantly it allows us to visualize all the central structures clearly. Co-registering the MRI image against the planning CT image enables clinicians to accurately determine the volume of all relevant structures with increased confidence.

Pre-treatment imaging

It is important that both, the CT and MRI planning images are acquired in the same reproducible position to minimize any problems with image registration and geometric distortion.

Our 1.5T MAGNETOM Aera scanner was purchased primarily for diagnostics. However, its wide (70 cm) short bore, large field of view (FOV), and uniformity in the static magnetic field (B_0) for minimizing geometric distortion allow us to accommodate the auxiliary RT positioning equipment and adapted MR coil positioning required to reproduce almost any radiotherapy treatment position – including arms above head within the bore – and achieve excellent image quality.

As MRI radiotherapy planning is becoming more common, the main manufacturers of MRI and radiotherapy equipment have responded to the demands of radiotherapy users and now provide auxiliary, MR-conditional equipment to enable most examinations to take place in the treatment position. A flat table top is required if we are to reproduce the CTSim positioning. We use an MRI-conditional, indexed flat table top that allows us to place all our immobilization devices in exactly the same position as for the CT scanner, which helps ensure accurate image registration (Figs. 8, 9).

The inclusion of RT-specific immobilization equipment – such as knee and ankle immobilization, indexing bars, wing boards, thermoplastic masks, and vacuum bags – is also necessary if we wish to exactly

---

[1]The MRI restrictions (if any) of the metal implant must be considered prior to patient undergoing MRI exam. MR imaging of patients with metallic implants brings specific risks. However, certain implants are approved by the governing regulatory bodies to be MR conditionally safe. For such implants, the previously mentioned warning may not be applicable. Please contact the implant manufacturer for the specific conditional information. The conditions for MR safety are the responsibility of the implant manufacturer, not of Siemens Healthineers.
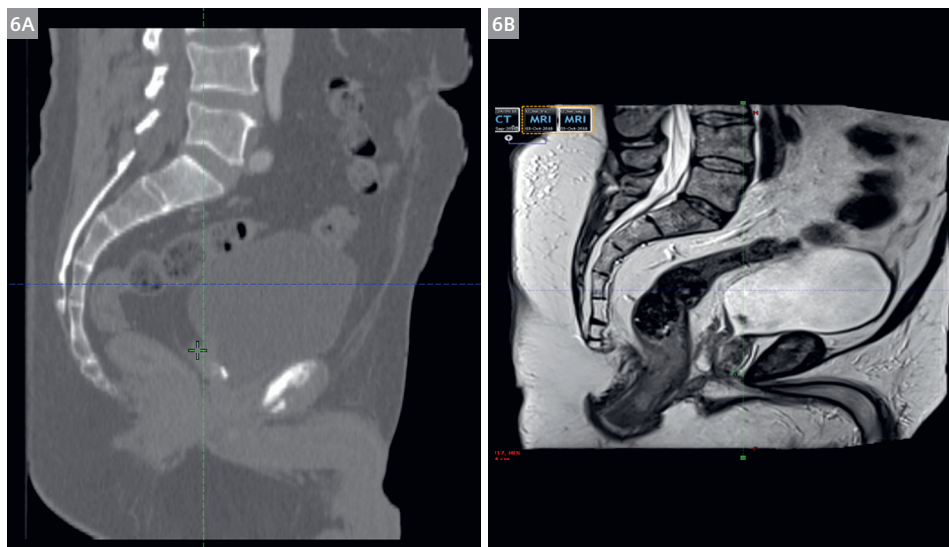
6 Sagittal MPR from CT **(6A)** compared with sagittal MRI **(6B)**.
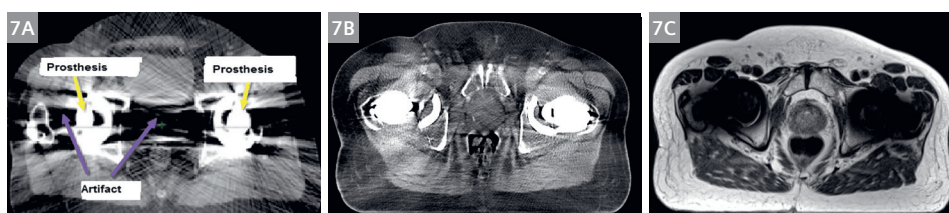
7 Hip prostheses on CT, pre- **(7A)** and post- **(7B)** iMAR, and on MRI[1] **(7C)**.

replicate the patient's treatment position. It is imperative that MR-conditional RT equipment is sourced and appropriately labelled before use. Scanning patients in the radiotherapy treatment position and the need for larger FOV coverage often mean that diagnostic coils cannot be used, as they are not designed to fit around RT positioning aids. Flexible surface coils in combination with coil bridges have to be used instead. Coil bridges prevent the surface coil from touching and distorting the patient's skin surface,

and adjusting the bridge height ensures coil proximity to the patient.

Radiotherapy treatment positions are reproduced by using tattoos on the patient's skin and a laser positioning system. Standard positioning lasers on the MRI scanner are primarily used to center the patient to the magnet isocenter for optimal imaging, but they are not suitable for RT purposes. An RT-specific laser system (Fig. 10) is required to help align the patient according to their treatment tattoos when positioning for MRI scans.

8 An example of a prostate set-up for MR treatment planning, showing immobilization, coil supports, and coil positioning.
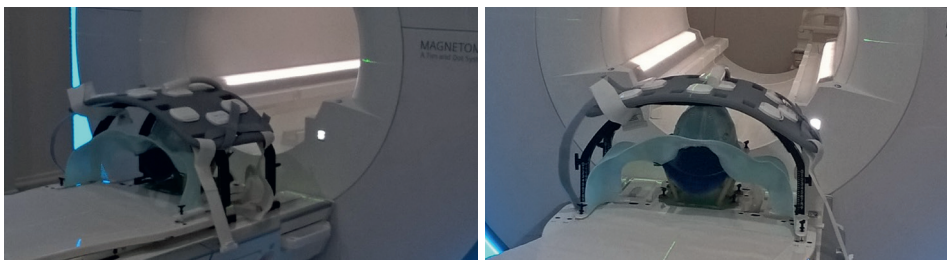
9 An example of a head-and-neck set-up for MR treatment planning, showing immobilization, coil supports, and coil positioning.

10 External laser bridge for MR treatment planning.

The RT laser is used to set-up the patient, whereas the MRI bore lasers are used to define the isocenter of the imaging volume. This ensures that the same position is replicated in both CT and MRI, aids in the image fusion of the two scans, and is supported by the addition of an RT Dot Engine software package.

Sequence requirements

Imaging requirements for therapy planning are different to those for diagnostic imaging, with the emphasis being placed on reducing geometric distortion as much as possible. Geometric inaccuracies caused by different patient positioning and the magnetic-field distortions inherent to MR images can significantly affect treatment doses to the patient as a result of inaccurate volume delineation if not minimized or corrected for. We can mitigate some of the factors that cause geometric distortions by, for example, ensuring the MRI scan is undertaken in the radiotherapy treatment position. However, other things need to be considered, too, such as choice of sequences and coil arrangements to maintain the balance between accuracy, patient comfort, and image quality.

Staffing and training

Integrating MRI planning into the pathway is very much a multi-disciplinary team effort, and the contribution from our medical physicists, dosimetrists, and clinicians has been invaluable.

Traditionally, the role of diagnostic radiographers has been limited to a diagnostic setting, where they are responsible for optimizing imaging for diagnosis. In contrast, the role of therapeutic radiographers is in the planning and treatment of patients once a diagnosis has been made. These roles would rarely ever overlap, but we have drawn many parallels between implementing MRI and when we first started using CT in radiotherapy.

The first lesson we learned was to make friends with the MRI radiographers, as they were the people we interacted with the most and the people who could answer our questions (of which there were many!).

Successful integration requires radiographers to have a better understanding of both the RT and diagnostic work processes. Diagnostic MR radiographers have had to adapt to using different coil positioning and imaging techniques. In the future, therefore, we would like the diagnostic team to rotate into CT simulation so that they can gain an understanding of basic and advanced treatment set-ups to ensure these can be accurately replicated in the MRI scanner. The radiographers should also receive training in CT-MR image registration and volume delineation so that they can appreciate how the MR images are utilized, allowing for greater optimization of imaging parameters to better suit the requirements for radiotherapy treatment planning.

As a therapy team, we are currently responsible for patient preparation and positioning, but we do not currently acquire the MR planning images. We have undergone some local training to gain a better understanding of the basics of MRI and MR safety. However, to develop our role further, we are looking to complete more comprehensive training organized by academic institutions or vendors after the pandemic, followed by in-house competency training that will allow us to perform the planning scans under the supervision of the lead MR radiographer.

Patients scanned as of December 2020

By the beginning of December 2020, we had successfully scanned 667 patients in the CT/MRI fusion-planning pathway. Of these, 512 were prostate cancer patients, 145 were head and neck cancer patients, and 10 were rectal cancer patients who were scanned as part of a local study.
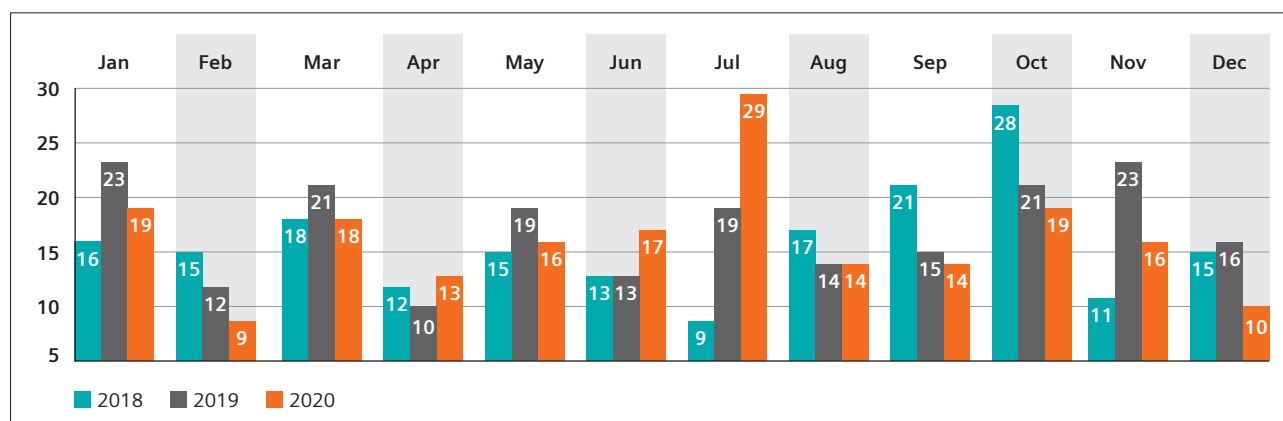
11 Patients scanned as of December 2020.

Treatment and post-treatment toxicity scoring is carried out routinely for all patients as part of their on-treatment review and post-treatment follow-up. A recent sample of 30 prostate patients showed that just under 80% reported toxicities graded 0 on the NCI CTC toxicity scoring scale (version 2.0, with RTOG), and less than 1% reported toxicities graded 3.

Conclusion

The use of MRI for radiotherapy planning is part of our evolving image-guided radiotherapy strategy, and local studies are planned to assess its impact so far with a view to reducing planning margins and associated toxicities in the near future. In the long term, clinicians have expressed an interest in functional imaging for tumor boosts, and for using MRI to plan stereotactic ablative radiotherapy (SABR) and adaptive treatments.

This truly collaborative service has had a positive impact on our staff and patients, examples of which include
- cross-disciplinary training resulting in upskilling, enhanced skills and knowledge, and evolving roles for staff;
- the introduction of new technologies into routine clinical practice, offering our patients access to the most up-to-date, effective treatments;
- improved inter-professional communication, facilitating better working relationships and environments, which impacts directly on patient care and experience.

The close collaboration between all members of the multi-disciplinary team with their differing skill sets has helped overcome a number of challenges and has provided a gateway for improved clinical outcomes and further research.

References

1 Dubec M, Speight R. The role of MRI in radiotherapy. RAD Magazine 2020;46(543):15–16.
2 Brouwer C, Steenbakkers R, Bourhis J, Budach W, Grau C, Gregoire V, et al. CT-based delineation of organs at risk in the head and neck region: DAHANCA, EORTC, GORTEC, HKNPCSG, NCIC CTG, NCRI, NRG Oncology and TROG consensus guidelines. Radiother Oncol. 2015;117(1):83–90.
3 Chandarana H, Wang H, Tijssen RHN, Das IJ. Emerging role of MRI in radiation therapy. J Magn Reson Imaging. 2018;48(6):1468–1478.
4 Rai R, Kumar S, Batumalai V, Elwadia D, Ohanessian L, Juresic E, et al. The integration of MRI in radiation therapy: collaboration of radiographers and radiation therapists. J Med Radiat Sci. 2017;64(1):61–68.
5 Schmidt MA, Payne GS. Radiotherapy planning using MRI. Phys Med Biol. 2015;60(22): R323–61.
6 Hu Q, Yu VY, Yang Y, O'Connell DP, Woods KE, Cao M. Practical Safety Considerations for Integration of Magnetic Resonance Imaging in Radiation Therapy. Pract Radiat Oncol. 2020;10(6):443–453.

Contact

Rhydian Powell
Department of Oncology
North West Cancer Centre
Altnagelvin Area Hospital
Londonderry, BT47 6SB
Northern Ireland
Rhydian.Powell@Westerntrust.HSCNI.net

Optimization of Pre-biopsy bp-MRI of the Prostate

Lynn Doy[1]; Niall MacKenzie[1]; Salman A. Siddiqui[1]; Gautham Mukerjhee[2]; Rebecca Sands[1]

[1]Department of Radiology, North West Cancer Centre, Altnagelvin Area Hospital, Londonderry, Northern Ireland
[2]Department of Radiotherapy Physics, North West Cancer Centre, Altnagelvin Area Hospital, Londonderry,
 Northern Ireland

Interprofessional teamwork and collaboration between diagnostic and therapeutic radiographers in the evolution of an MR radiotherapy-planning (MR RTP) service was pivotal to the success of this study, and to the eventual implementation of our current standard prostate-imaging protocol.

Key points

- Escalating demands in the early diagnosis and management of prostate cancer is placing considerable pressure on MRI departments across the UK.
- Adopting a combined approach to image optimization and investing in both technical and patient-related aspects to reduce artifacts can improve image quality and reduce scan times.
- Learning experiences in the development of an MR RTP service led to research to ascertain whether adminstration of a micro-enema before prostate imaging could influence image interpretation in diagnostics.
- Micro-enema administration demonstrates a significant benefit to image quality in bp-MRI of the prostate and should be considered as an integral part of the imaging procedure.

Introduction

Prostate cancer is now the most common malignancy in men and the second leading cause of cancer in the UK [1]. The clinical behavior of prostate cancers can range from low-grade cancers that do not progress to lethal disease, to invasive tumors that rapidly progress and become metastatic [2]. With the incidence of prostate cancer expected to double by 2030 [3], early diagnosis of clinically significant disease, performed at reasonable cost and in achievable time frames, is of increasing importance.

The publication of the Prostate Imaging Reporting and Data System (PI-RADS) in 2012 [4] brought together the importance of standardizing optimal sequences, now widely known as multi-parametric MRI (mp-MRI), with structured reporting systems to aid interpretation and diagnostic evaluation of the prostate. The publication of PI-RADS v2 in 2015 [5] aimed to further standardize image acquisition and interpretation in mp-MRI, providing guidance on technical optimization, detailing the minimal acceptable sequences and parameters in image acquisition, with the current emphasis on the more widely available sequences. Accurate interpretation and staging of disease with mp-MRI is now considered to play an additional key role in identifying prognostic factors, such as extracapsular extension, seminal vesicle extension, and lymphovascular invasion. These significant image findings indicate a higher risk of recurrence [2], aiding in risk

stratification of cases and defining optimal treatment pathways for the large cohort of diagnosed patients.

Pre-biopsy mp-MRI now plays a central role in the management pathway of prostate cancer in the UK, being performed on up to 75% of men with a clinical suspicion of prostate cancer [6], so it is essential that diagnostic mp-MRI of the highest quality is increasingly accessible.

PI-RADS v2 does acknowledge that there are many challenges in achieving standardization of image acquisition. Equipment availability and capability, patient factors, and radiology interpretation all differ across imaging sites. To achieve excellence in clinical performance, diagnostic processes need to be robust, encompassing high-quality imaging by radiographers and accurate image interpretation by radiologists working together with urologists in multidisciplinary teams.

Zonal anatomy and key sequences

At least 75% of all prostate cancers occur in the peripheral zone (PZ), but when differentiating benign and malignant disease, and determining prognostic factors, special attention should also be given to the transitional zone (TZ), prostate capsule, seminal vesicles, neurovascular bundles, and rectoprostatic angles to identify any extracapsular extension [7]. Zonal anatomy of the prostate gland and MRI appearances of extracapsular structures are shown in Figures 1 and 2, respectively.

Sequence choice in prostate MRI is widely debated, but T2-weighted (T2W) high-resolution imaging is considered to be the preferable sequence for local staging and identification of cancers in the TZ, as it also identifies the presence of extracapsular extension and seminal vesicle involvement [7]. Diffusion-weighted imaging (DWI) provides functional information based on the tissue cellularity, measuring the movement of water molecules within tissue. DWI is considered to be the best-performing sequence for detection of cancers in the PZ, with a restricted water diffusion playing a key role in defining
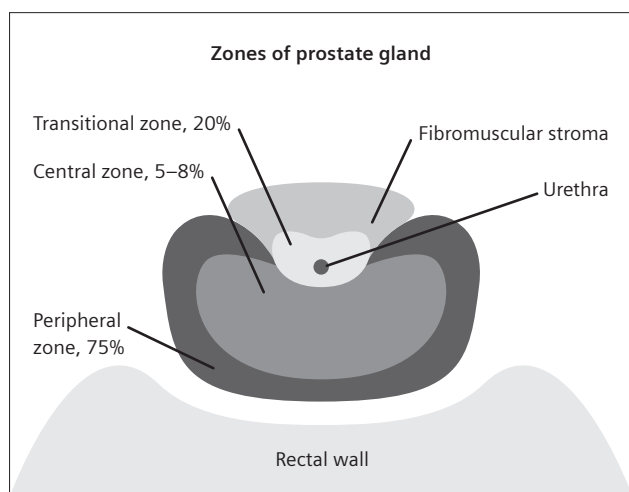
1 Anatomy of the zones of the prostate gland: schematic diagram in transverse plane with rectal wall at posterior aspect.
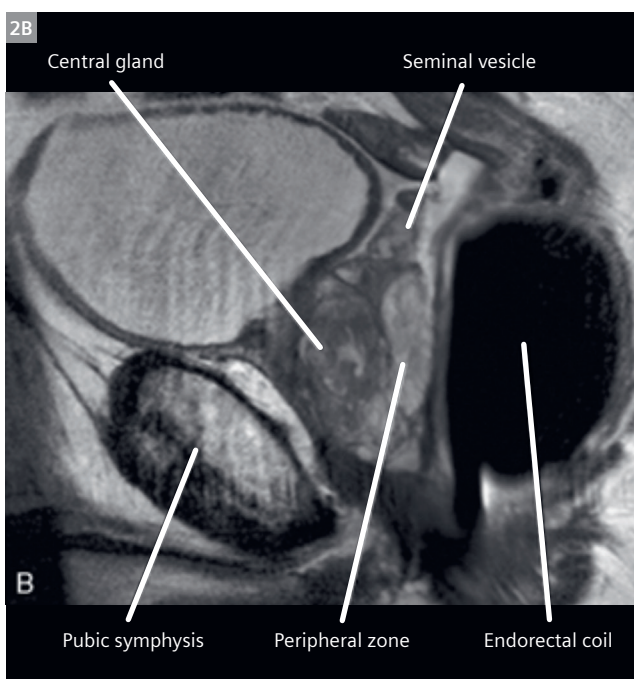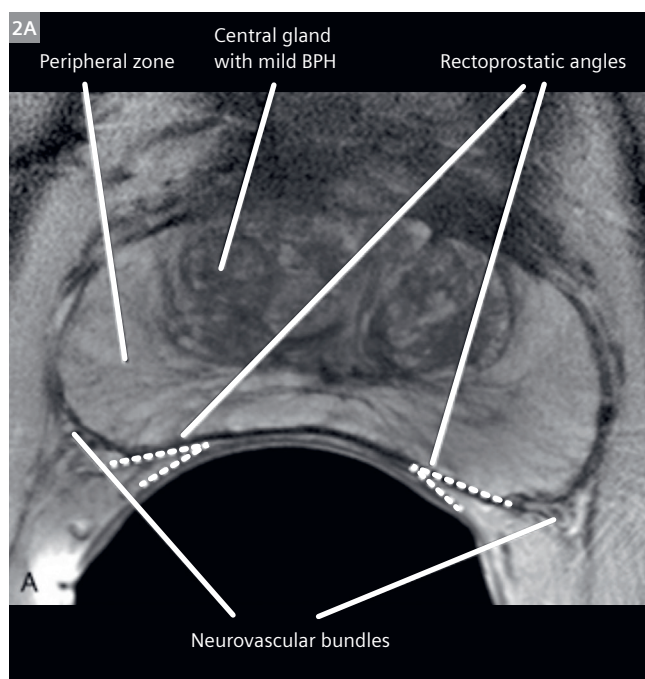
2 MR images of extracapsular structures: **(2A)** sagittal T2W and **(2B)** axial T2W showing anatomical landmarks.
Reproduced with permission from https://radiologykey.com/male-reproductive-system-2.

high-grade cancers [7]. PI-RADS v2.1, which was published in 2019 [8], now places most emphasis on DWI for PZ lesions and on T2W for TZ lesions; additional sequences like dynamic contrast-enhanced (DCE) are considered to play a limited role in lesion characterization, and MR spectroscopy is considered to be impractical for widespread use. As such, the term bi-parametric MRI (bp-MRI) is rapidly gaining favor, and although effectively reducing overall examination time, achieving a fully optimized examination becomes even more important to the overall clinical outcome.

Combined approach to optimization

As MR radiographers working as an integral part of a multi-disciplinary approach to cancer services, we must ensure that image quality is of the highest standard we can achieve, whilst also managing increasing clinical demand, often with limited scanner capability or resources. We have an array of tools at our disposal to optimize image quality. Primarily we consider image optimization to be technical in its approach, aiming to utilize a vast choice of sequences and imaging parameters to achieve artifact-free, high SNR and high-resolution images in reasonable scan times to provide good clinical outcomes, but this can be very dependent on the capability of the equipment available.

However, an important, yet often forgotten factor in overall image optimization can be the patient themselves. In prostate imaging, patient-related factors can be anything from gross patient movement or bowel peristalsis, to air and feces within the rectum. By addressing patient-related issues that may affect overall image quality due to artifacts or distortion, we can directly improve outcomes for our patients. The rest of this article will look at using a combined approach to image optimization.

Technical optimization of sequences

In focusing our efforts on bp-MRI only, it is imperative that the key sequences are fully optimized. The MAGNETOM Aera 1.5T system can easily achieve PI-RADS v2-compliant sequences in terms of SNR and resolution, but some specific sequence and parameter options are worth further consideration to ensure consistency across a wide range of patients.

All T2W and DWI sequences utilize GRAPPA to reduce scan times with relatively little compromise in SNR.

Where administration of an antispasmodic is contraindicated and the risk of motion artifacts from bowel movement is increased, T2W sequences are simply acquired with a lower resolution for speed, and interpolation is chosen to increase the apparent resolution. This has proved to be a robust alternative to BLADE, with radiology being more confident when tissue contrast is consistent with our standard protocol.

In DWI, distortion from metallic implants[1] may prove problematic. EPI sequences are usually preferred as they are more readily available and have the advantage of a higher SNR than some alternatives. However, in patients where distortion from metallic implants – e.g., total hip replacement (THR) – cannot be avoided, options like RESOLVE DWI may be preferred to take advantage of the superior distortion reduction and hopefully provide some correlation with the image appearances of T2W lesions.

Choice of b-value in DWI is widely debated, with longer b-values ≥ 1400 s/mm^2 being considered optimal in prostate imaging. Some systems will have the option to calculate or extrapolate higher b-value images from multiple acquired data sets with lower b-values and higher SNR. However, Grant et al. [9] conclude that the image quality of calculated high b-value DWI relative to corresponding acquired DWI decreases with an increase in b-value, and the radiology preference in our department is to invest in acquiring data with a b-value of 1400 s/mm^2.

Reduction of patient-related artifacts

Bowel peristalsis: The use of anti-peristaltic drugs to reduce artifacts from bowel movement in the pelvis and abdomen does have implications for the overall service: There are additional costs to consider, additional time is required for cannulation, and medical support is often needed for administration and prescription. However, Slough et al. [10] conclude that the IV administration of hyoscine butylbromide (HBB) immediately prior to MRI significantly improves the image quality of T2W images, a key sequence in mp-MRI. They advocate its use in routine patient preparation prior to prostate MRI, with the acquisition of T2W sequences during a short window of effectiveness, usually approximately 20 minutes.

Rectal distention: There is wide acceptance in diagnostic MRI that an air-filled rectum can lead to considerable geometric distortion on DWI at air-tissue interfaces. Recent publications [11, 12] discuss the negative impact that rectal distention and loading can have on the quality of both T2W and DW images. Caglic et al. [12] propose the use of bowel preparation prior to prostate mp-MRI to optimize image quality. However, they also note that PI-RADS v2 highlights a lack of evidence to specifically inform on patient preparation prior to mp-MRI.

---

[1]The MRI restrictions (if any) of the metal implant must be considered prior to patient undergoing MRI exam. MR imaging of patients with metallic implants brings specific risks. However, certain implants are approved by the governing regulatory bodies to be MR conditionally safe. For such implants, the previously mentioned warning may not be applicable. Please contact the implant manufacturer for the specific conditional information. The conditions for MR safety are the responsibility of the implant manufacturer, not of Siemens Healthineers.

3 Comparison of rectal distension in diagnostic MRI (3A) and RTP MRI (3B): **(3A)** sagittal T2W diagnostic image with rectal distension; **(3B)** sagittal T2W RTP image with no rectal distension.

Research study: Optimization of bp-MRI of the prostate using a self-administered enema

Background

During our collaborative MR radiotherapy-planning (RTP) sessions, a significant reduction in air-filled rectal distension was observed in sagittal RTP images (see Fig. 3). This led to local discussions about the standard procedure for the imaging and treatment of all prostate patients undergoing radiotherapy at NWCC. Minimal bowel preparation in the form of a self-administered micro-enema is used just prior to all RT imaging and treatment to evacuate the rectum prior to all scans. This facilitates accuracy in gross-tumor-volume (GTV) contouring for RT treatment planning, and during all subsequent treatments to ensure reproducibility of the anatomical position of the prostate gland and promote positional accuracy of the treatment beam. RT experiences, including evidence in the literature [13], have proven this to be a cost-effective and minimally invasive patient procedure that is easily tolerated by patients. MR radiographers were keen to explore any potential benefit to diagnostic MRI protocols, and a local study was set up.

Aims and objectives

The aim of this research was to ascertain whether using a micro-enema before prostate imaging influences image interpretation. The main objectives were to collect data on prostate image interpretation with and without use of a micro-enema, to compare data, and to reach a conclusion on the efficacy of micro-enema use with respect to image quality in bp-MRI for pre-biopsy imaging.

Methodology

Thirty consecutive pre-biopsy referrals for prostate MRI were asked to attend their MRI appointment 45 minutes early to self-administer a micro-enema approximately 30 minutes prior to MRI scanning. Thirty consecutive patients scanned prior to the trial period, without preparation, acted as the control. To ensure comparable findings, exclusion criteria were applied to both groups and included patients with THR in situ and patients who presented with any contraindications to IV antispasmodic drugs. A standard NWCC high-resolution, PI-RADS v2-compliant protocol was carried out on all patients. Two consultant radiologists experienced in reporting prostate bp-MRI individually scored all images according to the criteria shown in Table 1. Cases were randomized on reporting workstations, with both radiologists blinded to use of micro-enema and their colleague's scoring.

Results

- Scores for rectal distension are highly correlated between the two radiologists for prepared and unprepared patients ($r = 0.82$ and $r = 0.86$, respectively). This indicates improved visibility of the prostate bed when a micro-enema is administered compared to unprepared patients ($p = 0.16$ and $p = 0.04$).
- Scores for distortion on DWI demonstrated moderately correlated scores ($r = 0.76$ and $r = 0.67$), with statistically high significance for prepared patients compared to unprepared patients ($p = 0.0$ and $p = 0.28$).

Rectal distention on Sag T2		Distortion on DWI + ADC		Confidence in lesion conspicuity	
Clear	0	None	0	Poor	0
Minimal	1	Minimal	1	Fair	1
Partial	2	Moderate	2	Good	2
Fully	3	Severe	3	Excellent	3

Table 1: Radiological scoring criteria
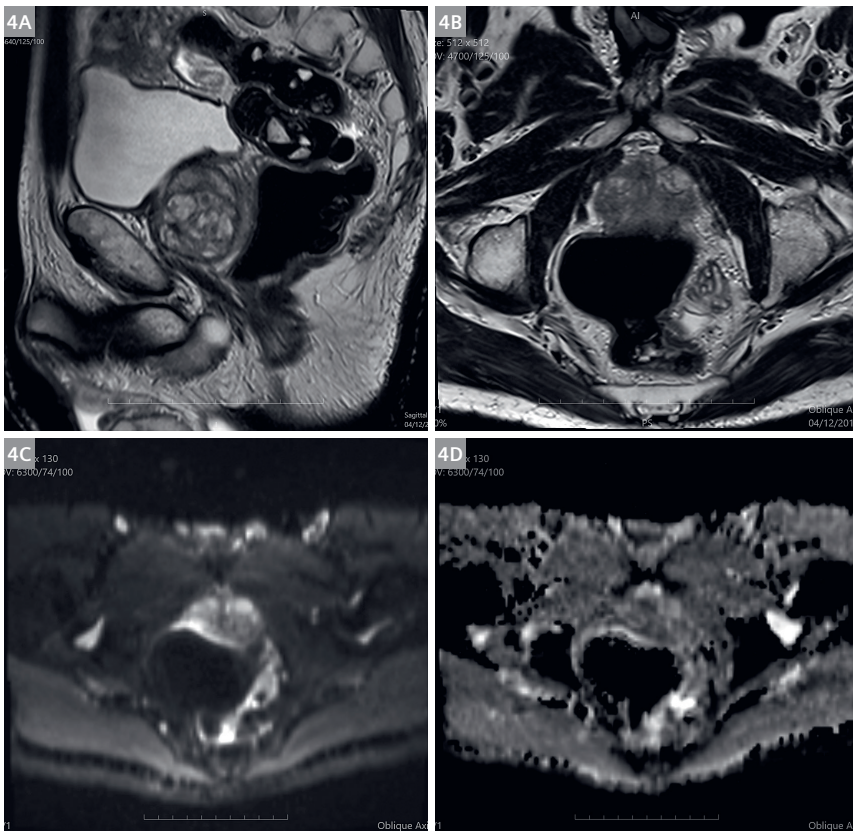
4 Sample images from control group (no bowel preparation):
(4A) Sag T2w TSE; **(4B)** Tra T2w TSE;
(4C) Tra DWI b-value = 800 s/mm^2;
(4D) ADC map.
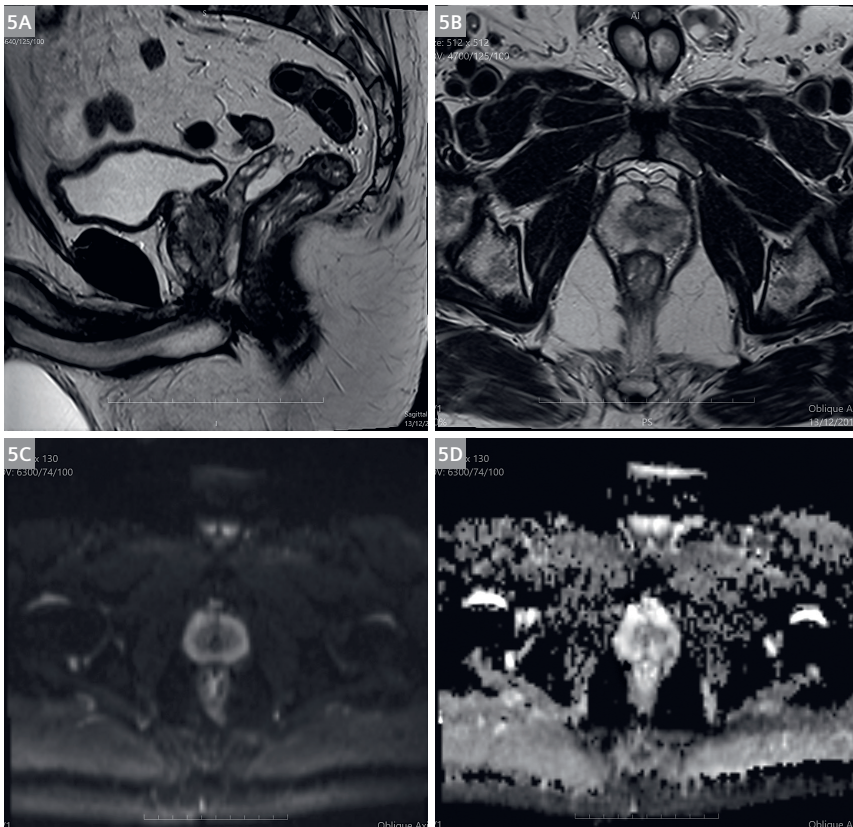
5 Sample images from study group (bowel preparation administered):
(5A) Sag T2w TSE; **(5B)** Tra T2w TSE;
(5C) Tra DWI b-value = 1400 s/mm^2;
(5D) ADC map.

- Scores for distortion on apparent diffusion coefficient (ADC) maps also demonstrated agreement on moderately correlated scores (r = 0.54 and r = 0.59), and also high significance (p = 0.0), which proves that visibility for identifying distortion is better in the case of prepared patients.
- There is a high correlation in lesion visibility on DWI (r = 0.50) and an overall improvement in confidence (p = 0.36) for prepared patients.
- Radiologist 2 has a higher variance in scoring than Radiologist 1, irrespective of whether patients were prepared or not. However, variance in scoring is reduced in prepared patients, which indicates a higher level of confidence in lesion visibility among the radiologists (see Fig. 6).

Conclusion

Micro-enema administration demonstrates a significant benefit to image quality in bp-MRI of the prostate and should be considered as an integral part of the imaging procedure.

Study outcomes

Improvements in image quality and the clinical effectiveness of the radiological report, for both clinically significant and insignificant disease, were demonstrated in prepared patients. This led to a change in standard practice for bp-MRI prostate imaging at NWCC. Improved radiological confidence has reduced the imaging protocol, with the emphasis now on fully optimized bp-MRI rather than mp-MRI, leading to shorter scan times for patients and the potential for increased patient capacity. Improved confidence in the radiology findings at multidisciplinary meetings (MDMs) is proving especially beneficial for patients with insignificant or benign disease confirmed on MRI, and the potential to ensure progression to targeted biopsy is limited to equivocal cases only, e.g., PI-RADS 3. This places fewer clinical demands on the urology service overall. Utilizing a low cost, established technique that is easily tolerated by patients and involves minimal operational issues for staff has greatly improved the quality of our prostate imaging service.

6A

Variance – prepared patients

6B

Variance – unprepared patients

■ Radiologist 2   ■ Radiologist 1
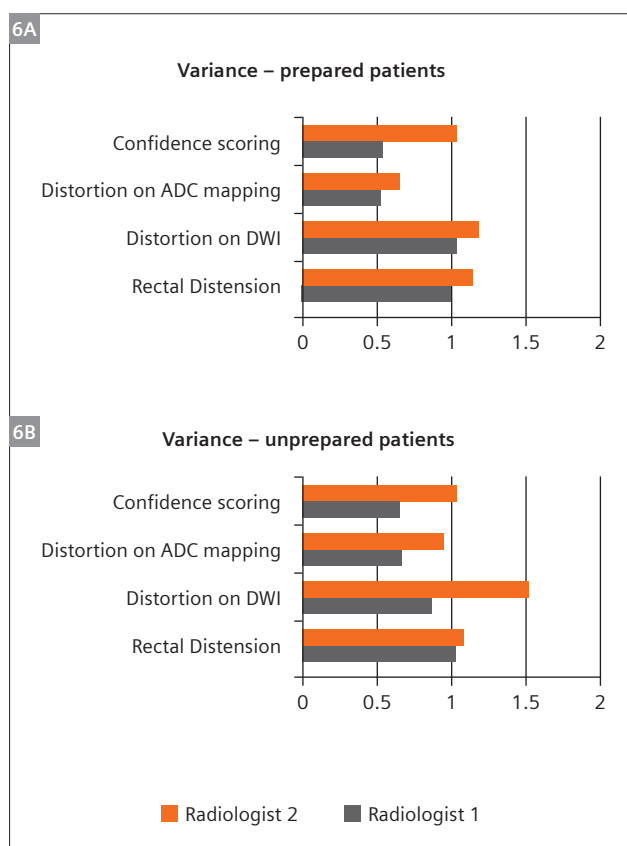
6 Comparison of variance in radiologist scoring in prepared (micro-enema) and unprepared patients.

Patient Information on Use of Micro-enema prior to MRI

You will be asked to use a form of bowel preparation called a micro-enema on arrival for your MRI. It falls within a group of medicines called laxatives, and is administered as a single dose to patients as a self-administered enema.

It is being used before your MRI scan to empty your rectum of stools and air to get better images of the prostate gland, and help the doctors plan any treatment you may need more carefully.

It may not be advisable to use if you suffer from any inflammatory bowel conditions, such as Crohn's disease, IBS, or colitis, so please make the staff aware of this.

A micro-enema allows the insertion of a liquid into your back passage to help your lower bowel empty. Instructions will be given to you by the MRI staff on arrival, and it is usually effective within 15 mins. Toilets are nearby for use.

How to Use a Micro-enema

- Sit on the toilet
- Pull or twist the cap off the plastic tube
- Squeeze a drop of the liquid onto the nozzle to help lubricate it.
- Put the full length of the nozzle into your back passage, and gently squeeze the tube until it is empty.
- Wait for 15 mins for the laxative to work.

As it's a single dose, there is no risk of using too much and there should be no risk of prolonged diarrhoea. Staff will be happy to answer any questions you may have.

Table 2: Patient information on use of micro-enema prior to MRI.

How we do it:
NWCC's current standard procedure and MR imaging protocol

Referral
Patients are all pre-biopsy urology referrals based on raised prostate-specific antigen levels (PSA) > 5.

Patient preparation
Patients are asked to arrive 45 minutes before their appointment time, so the only scheduling complication is around the first slot of the day. Information leaflets are sent out with appointment letters to advise patients of the need for bowel preparation on arrival (see Table 2). On patient arrival, MR radiographers go through the patient safety checklist to ensure there are no contraindications to MRI scanning that may negate the need for the enema. A drug checklist is also completed to ensure there are no inflammatory bowel conditions that could be aggravated by the enema, and no contraindications to the antispasmodic drug HBB 20 mg/mL (Buscopan), which is administered intravenously by radiographers guided by a local patient group directive (PGD). Radiologists are asked to prescribe the enema and, if PGD conditions are not met, the intravenous Buscopan.

An explanation of the procedure and its benefits for the imaging is provided to the patient in a private subwait area. If verbal consent is given, the patient is asked to proceed. Toilets are adjacent. A subsequent patient feedback audit demonstrated that most patients were well informed and tolerated the procedure well (see Fig. 7).

After 15–30 minutes, patients are brought in to have their IV cannulation for the Buscopan, which is administered once the patient is positioned on the scanner, due to its short-lived effect of only 15–20 minutes.

Additional patient preparation could be perceived as preventing radiographers from performing actual MR scans. However, as the bowel preparation is explained along with our MRI safety checklisting on arrival, and as radiographers insert all our cannulas anyway, it is seen as an integral part of the overall patient preparation procedure.

Equipment
Images were performed on a 24-channel 1.5T MAGNETOM Aera using an 18-channel Body Coil.

Patient positioning
Patients are always positioned supine, preferably head first unless claustrophobic, to ensure that whole-body SAR deposition is more accurately calculated.

The 18-channel Body Coil is positioned longitudinally on the patient's abdomen. This is acceptable as most of the anatomy to be imaged is midline, and it allows additional upper abdominal coverage for para-aortic nodes whilst providing improved patient comfort. Two transversely positioned body array coils would take longer to position, add extra weight on the patient's abdomen, and restrict the space available for their arms within the bore. Additional straps and coil size would also restrict access to the IV cannula for administration of Buscopan immediately prior to isocenter positioning.

Acquisition
The Dot Cockpit is fundamental to conducting these examinations efficiently and with an easily reproducible protocol of sequences that achieve consistency when multiple operators rotate through the department. Decision strategies built into the workflow are utilized to allow radiographers to adapt the protocol to patient-related scanning needs – e.g., when antispasmodic drug administration is contraindicated, or choosing the RESOLVE DWI option when THR is in situ. Orthogonal slice orientations are preferred by radiology, as they are easily reproduced to ensure consistency in imaging and to enable optimal calculation of gland volume. Imaging parameters are detailed in Table 3, and examples of images are shown in Figure 8.

How satisfied were you with the following?

	Not applicable	No	Yes
Aftercare information	1	0	19
Was it effective	1	6	13
Toilet proximity	0	0	20
Radiographer explanation	0	0	20
Prepared for scan	2	0	18
More/less information	2	17	1
Easy to understand	2	0	18
Information leaflet in the post	0	2	18
Ever used a Micralax enema before	0	19	1
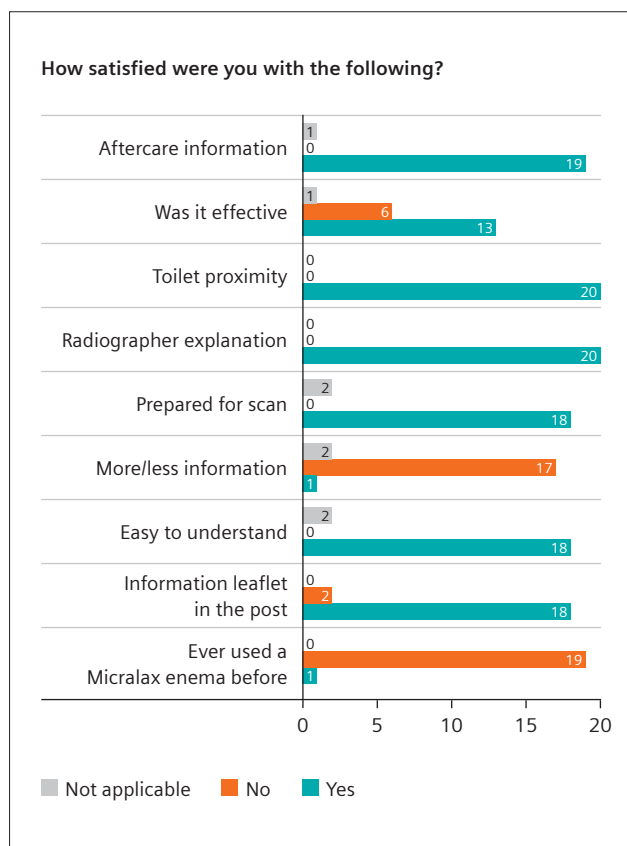
7 Outcomes of patient feedback audit.

Sequence	TR	TE	FOV	Slices			Matrix	Voxel size	iPAT	b-values s/mm^2	Averages	Scan time min.sec
				Number	mm	Gap						
Sag T2W TSE	5200	122	200 x 100	30	3	0	320 x 80%	0.6 x 0.6 x 3.0	2		3	4.48
Cor T2W TSE	5200	122	200 x 100	30	3	0	320 x 80%	0.6 x 0.6 x 3.0	2		3	4.48
Tra T2W TSE	5200	122	200 x 100	34	3	0	320 x 80%	0.6 x 0.6 x 3.0	2		3	4.48
TRA DWI (1) + ADC	5800	66	300 x 100	34	3	0	120 x 80%	2.5 x 2.5 x 3.0	2	50 400 800	1 4 6	4.46
TRA DWI (2)	7100	72	300 x 100	34	3	0	120 x 80%	2.5 x 2.5 x 3.0	2	1400	12	6.18

Table 3: Standard bp-MRI sequences and parameters; total acquisition time < 30 minutes.
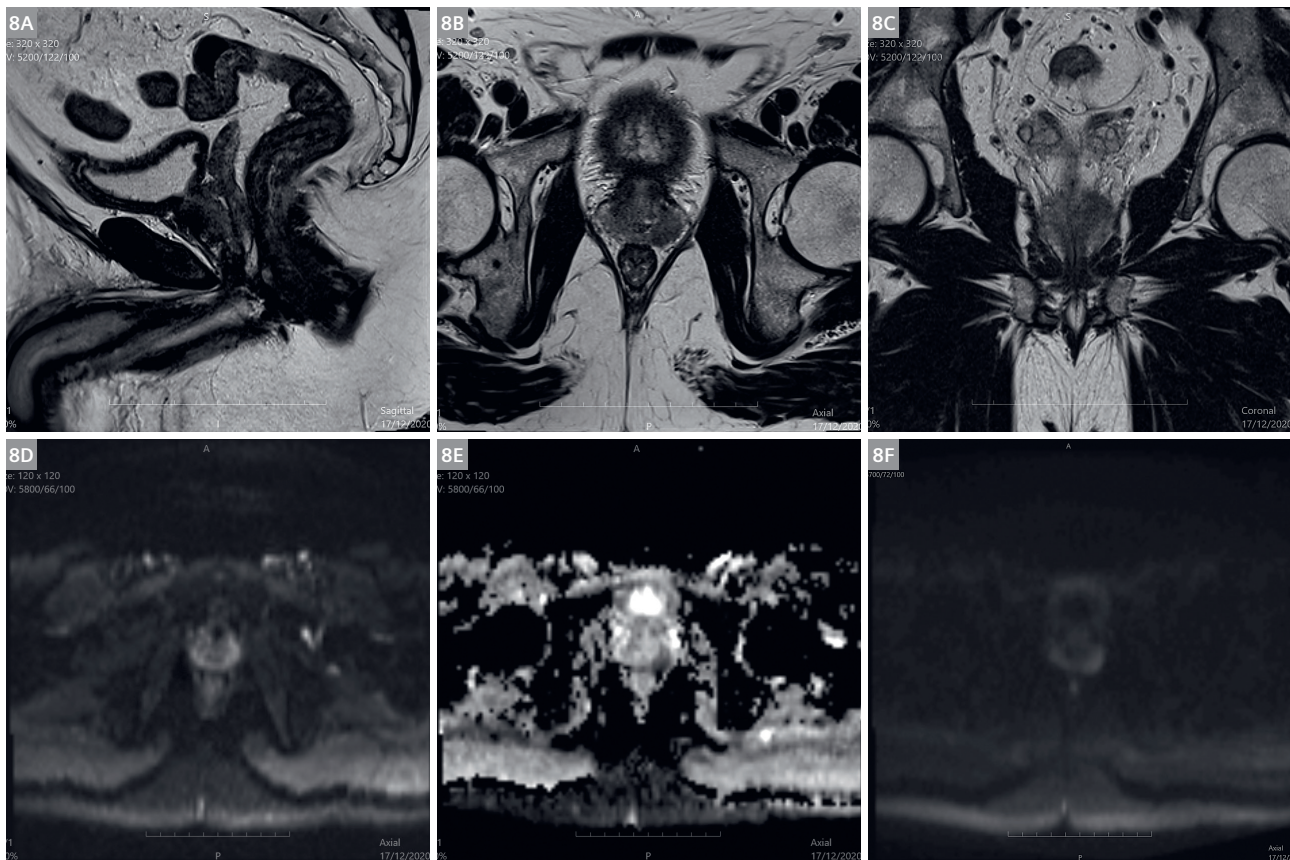
8   Examples of standard optimized protocol: **(8A)** Sag T2W, no rectal distension; **(8B)** Tra T2W; **(8C)** Cor T2W; **(8D)** Tra DWI b-value = 800 s/mm^2; **(8E)** Tra DWI ADC map; **(8F)** Tra DWI b-value = 1400 s/mm^2.

Conclusion

Fully optimizing bp-MRI in the assessment of prostate cancer using a combined technical and patient-focused approach has greatly increased our performance in several ways:

- A low-cost operational change with minimal impact on staff and patients has delivered a significant improvement in image quality, with reduced scan times.
- Dot delivers an efficient workflow to ensure a robust, easily reproduced protocol, which is acquired within 30 minutes and maximizes capacity.
- It has optimized patient flows within the department, minimizing the time patients spend on the scanner.
- Increased time spent with clinical staff prior to MRI has boosted patient confidence in the overall process and experience, and although no evidence is currently available, we do have a very low rate of claustrophobia and anxiety-related refusals.
- Much-improved and consistent image quality with minimal artifacts has increased confidence in diagnostic accuracy for radiologists, and in the decision strategies adopted for patient management at urology MDMs.

Acknowledgments

References

1 Prostate cancer: Diagnosis and Management, NICE guideline 131 [document on the Internet]. The National Institute for Health and Care Excellence; 2019 [cited October 21 2020]. Available from: https://www.nice.org.uk/guidance/ng131

2 Kizilay F, Çelik S, Sözen S, Özveren B, Eskiçorapçı S, Özgen M, et al. Correlation of Prostate-Imaging Reporting and Data Scoring System scoring on multiparametric prostate magnetic resonance imaging with histopathological factors in radical prostatectomy material in Turkish prostate cancer patients: a multicenter study of the Urooncology Association. Prostate Int. 2020;8(1):10–15.

3 Maddams J, Utley M, Møller H. Projections of cancer prevalence in the United Kingdom 2010–2040. Br J Cancer. 2012;107(7):1195–202.

4 Barentsz JO, Richenberg J, Clements R, Choyke P, Verma S, Villeirs G, et al. ESUR prostate MR guidelines 2012. Eur Radiol. 2012;22(4):746–57.

5 PI-RADS Prostate Imaging – Reporting and Data System: 2015 Version 2. [document on the Internet]. Reston, VA: American College of Radiology. 2015 [cited October 21 2020]. Available from: https://www.acr.org/-/media/ACR/Files/RADS/Pi-RADS/PIRADS-V2.pdf

6 Caglic I, Barrett T. Optimising prostate mpMRI: prepare for success. Clin Radiol. 2019;74(11):831–840.

7 Purysko AS, Rosenkrantz AB. Technique of Multiparametric MR Imaging of the Prostate. Radiol Clin North Am. 2018;56(2):211–222.

8 PI-RADS Prostate Imaging – Reporting and Data System: 2019 Version 2.1. [document on the Internet]. Reston, VA: American College of Radiology. 2019 [cited October 21 2020]. Available from: https://www.acr.org/-/media/ACR/Files/RADS/Pi-RADS/PIRADS-V2-1.pdf

9 Grant KB, Harsh KA, Shih JH, Bernardo M, Pang Y, Daar D, et al Comparison of calculated and acquired high b value diffusion-weighted imaging in prostate cancer. Abdom Imaging. 2015;40(3):578–586.

10 Slough RA, Caglic I, Hansen NL, Hansen NL, Barrett T. Effect of hyoscine butylbromide on prostate multiparametric MRI anatomical and functional image quality. Clin Radiol. 2018;73(2):216e9-216e14.

11 van Griethuysen JJM, Bus EM, Hauptmann M, Lahaye MJ, Maas M, Ter Beek LC, et al. Gas-induced susceptibility artifacts on diffusion-weighted MRI of the rectum at 1.5 T – Effect of applying a micro-enema to improve image quality. Eur J Radiol. 2018;99:131–137.

12 Caglic I, Hansen NL, Slough RA, Patterson AJ, Barrett T. Evaluating the effect of rectal distension on prostate multiparametric MRI Image quality. Eur J Radiol. 2017;90:174–180.

13 Padhani AR, Khoo VS, Suckling J, Husband JE, Leach MO, Dearnaley DP. Evaluating the effect of rectal distension and rectal movement on prostate gland position using cine MRI. Int J Radiat Oncol Biol Phys. 1999;44(3):525–33.

Contact

Lynn Doy, DCR(R) MSc
Department of Radiology
North West Cancer Centre
Altnagelvin Area Hospital
Glenshane Road, Londonderry, BT46 6SB
Northern Ireland
Lynn.Doy@westerntrust.hscni.net

MRI-only Based External Beam Radiation Therapy of Prostate Cancer: Early Evaluation of Workflow and Clinical Impact

Jean-François Cabana, M.Sc.[1]; Dany Thériault, Ph.D.[1,2,3]

[1]Centre régional intégré de cancérologie de Chaudière-Appalaches (CRIC), Lévis, QC, Canada
[2]Centre de recherche du CISSS de Chaudière-Appalaches, Lévis, QC, Canada
[3]Département de physique, de génie physique et d'optique, Université Laval, Québec, QC, Canada

Introduction

Treatment planning in external beam radiation therapy (EBRT) traditionally requires computed tomography (CT) images, with or without additional magnetic resonance (MR) images. These complementary imaging modalities both have properties that are useful or necessary for EBRT treatment planning.

On the one hand, CT provides excellent contrast for bone structures, but soft tissue contrast is limited. Furthermore, it is a requirement of treatment planning systems (TPS) to have a CT for accurate dose calculation. Modern TPS use a curve mapping CT number (or Hounsfield Unit (HU)-to-electron or mass density conversion), which is applied to patient CT data to allow for accurate calculation of energy transport and deposition in this heterogeneous environment. Moreover, a CT reference is also required for image guided radiation therapy (IGRT), either to generate digitally reconstructed radiographs (DRR) for kV imaging or as a direct reference for cone beam CT (CBCT) imaging.
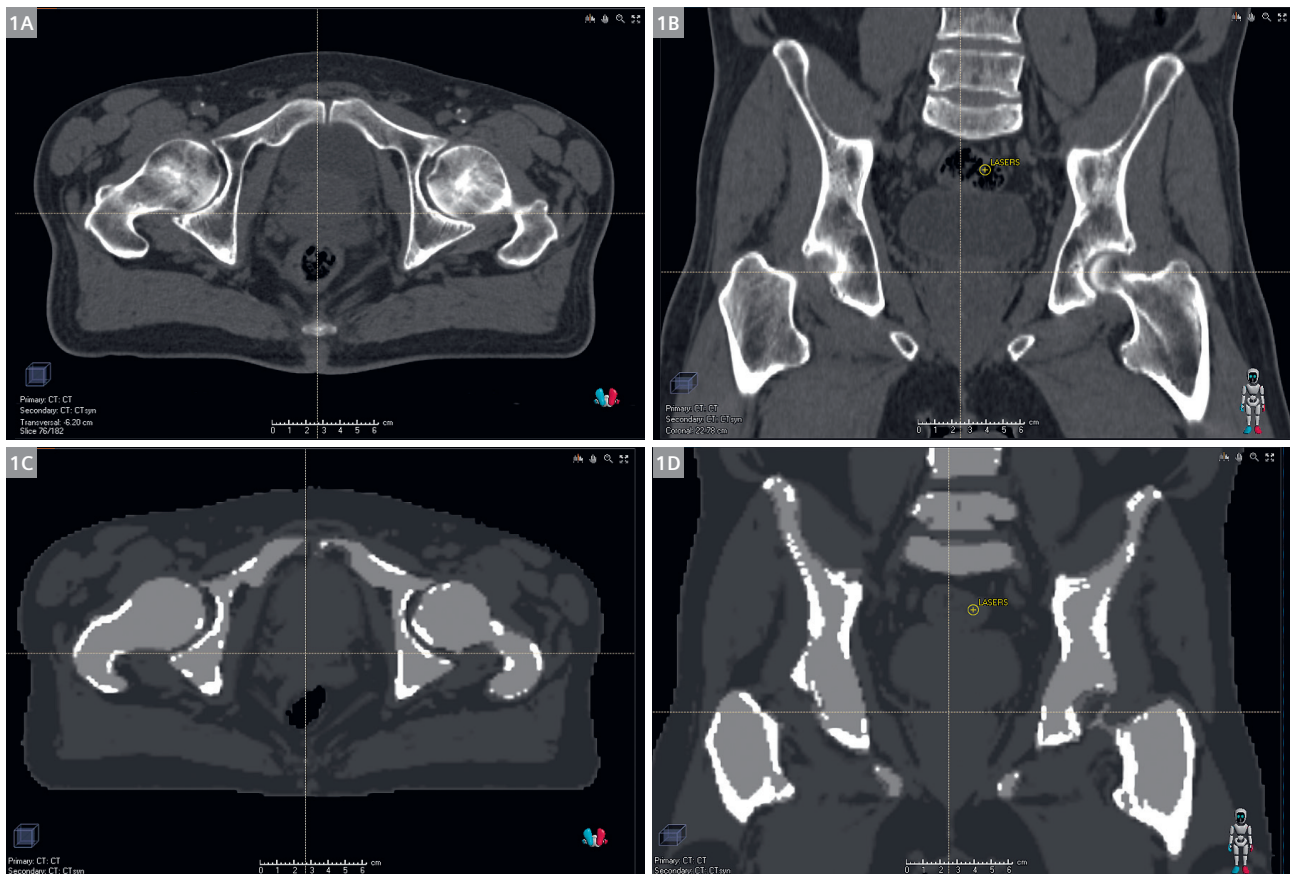
1 Example of a sCT reconstruction. **(1A and 1B)** axial and coronal views of a planning CT; **(1C and 1D)** sCT images for the same patient.

On the other hand, MR imaging (MRI) offers a much better soft tissue contrast, and has the potential to add complementary information such as functional imaging. These advantages can help for more precise visualization and contouring of targets and organs at risk (OAR). MRI also does not use ionizing radiation, so no additional dose is given to the patient when using this imaging modality.

Working with the two imaging modalities in a complementary manner allows taking advantage of the strengths of both CT and MR, however, it does pose additional challenges. Registration of MRI to CT must be as accurate as possible to allow contouring on both image sets. Patient positioning must thus be reproducible in both CT and MR rooms. To do so, it is preferable to have a dedicated RT planning MR setup, including an RT table top overlay (i.e., a flat and indexable table top), MR compatible immobilization devices, an external laser bridge, and coil bridges to avoid direct contact with the patient which can deform patient anatomy. Despite compatible setups and proper patient positioning, registration can still be difficult, as there may exist residual differences in patient positioning between CT and MR sessions. In addition to this, CT and MR present completely different contrasts. Indeed, a structure perfectly visible on one image might not be easily seen on the other, making the visual registration difficult. Finally, there are often differences in the position and shape of internal organs as, for example, rectum and bladder filling can change between CT and MR image acquisitions. This all contributes to making it difficult in having an MR image that perfectly matches the CT image, and affect the overall geometric precision of the radiation therapy treatment to be administered. Using two imaging modalities also implies a heavier workload for the patient and department staff, as two examination sessions are needed.

Synthetic CT

Recently, there has been increased interest in opting for MRI-only based treatment planning, particularly for prostate RT (see Bird et al. [1] for a publications review of clinical implementation of pelvic MRI-only planning). Planning on MR alone would mean that no registration is needed, while also allowing for a lighter workload for the patient. Because CT is required by TPS for dose calculation and during treatment for IGRT, one needs to replace the traditional CT image with something else to be able to perform RT planning without it. A potential solution is to generate a synthetic CT (sCT) image from the MRI. The idea is to use MRI to generate an image that has a contrast similar to CT, where pixel values are given in HU. Several strategies can be used to generate the sCT, and some commercial products are starting to become available.

Our clinic uses the synthetic CT product from Siemens Healthineers, which is available in their *syngo*.via software. The product is described in more details in the White paper [2]. In summary, this software uses specific MR sequences for sCT computation, which are available for the head and pelvic regions. For pelvic cases, a fast large field-of-view VIBE Dixon sequence is acquired (acquisition time around 2:30 minutes @ 1.5T), from which four images are output (in-phase, opposed-phase, water and fat). From these four images, soft tissue is segmented as water/fat/air using a classifier, while bones (2 densities) are rendered using a multi-atlas-based model. The result is a 5-compartment segmented sCT image, which is then imported in the TPS and recognized as a regular CT.

Prostate EBRT at our center

The current workflow at our center for prostate EBRT planning is as follows. First, the patient is scanned at the MR (MAGNETOM Aera 1.5T, Siemens Healthcare, Erlangen, Germany) in treatment position. Our current prostate MR protocol consists of a single T2 3D sequence (T2-SPACE @ 0.8 mm isotropic resolution, acquisition time around 9 minutes). Then, treatment simulation is performed in the CT room (SOMATOM Confidence, Siemens Healthcare, Forchheim, Germany). CT and MR images are then imported into our TPS (RayStation 7, RaySearch Laboratories, Stockholm, Sweden), where registration between MR and CT is performed (with focus on the prostate). OAR are contoured by radiation therapists on the CT image, using the registered MRI as reference. These contours are verified by the radiation oncologist, who then contours the prostate and seminal vesicles on the CT, again using the MRI as reference. The treatment plan optimization, using a single full arc VMAT 6MV beam, is then performed on the planning CT image. Before each treatment session, a CBCT is acquired at the linac (Elekta Versa HD, Elekta AB, Stockholm, Sweden) and registration is made against the planning CT using Elekta XVI software.

Project scope

Switching to an MRI-only workflow is a major change and we should expect it to come with some challenges along the way. The scope of the project presented here was thus to perform a preliminary evaluation of the workflow and clinical impacts of using an MRI-only process for prostate EBRT planning. The MR sequence for pelvic sCT reconstruction was added to our regular prostate protocol. This additional sequence was run only after obtaining patients' consent after the regular protocol was completed. We selected the first 12 patients for whom the sCT sequence was successfully acquired.

The goal was not to perform a full commissioning of the MRI-only workflow, but to identify:

(1) pitfalls and challenges at each step of the treatment chain;

(2) questions which still need answers, and

(3) the next steps required before making the transition.

To keep things simpler to start with, we focused on the treatment of prostate with seminal vesicles (SV) only (no treatment of pelvic nodes included).

The project was a collaborative effort between medical physicists, radiation oncologists, and radiation therapists. It is important to note that the observations made here are relevant to the workflow we use at our own center. It is advisable that each center performs their own evaluation to identify challenges specific to their clinic. The following sections present a brief summary of the methods used and results obtained for each of these steps.

Imaging

Method

Images from the 12 patients included in this study were qualitatively analyzed to evaluate image quality and sCT reconstruction accuracy. First, the general appearance of the reconstructed sCT was evaluated, then each sCT was compared to the actual planning CT. Bone registration between sCT and CT was performed first, followed by registration with respect to the prostate, as is done in our current CT+MR workflow.

Results

First results showed that sCT reconstruction generally works quite well. See Figure 1 for a comparison between sCT and planning CT for one patient. A good agreement overall is seen for all tissue compartments between sCT and CT. sCT shows a clear difference between muscle and fat, and air pockets inside the rectum or bowels are well reconstructed. The two-density bone structures are clearly visible on the sCT, and agree with what is seen on the CT. Compared to the planning CT, sCT has a lower resolution, and only 5 HU levels. These characteristics combine to give an appearance that looks unnatural when compared with the planning CT.

Registration between sCT and planning CT confirmed that obtaining a reproducible patient positioning between MR and CT modalities could be difficult. Differences in external contours of up to 1 cm were not uncommon; rotation of pelvis/hips was sometimes seen, as well as differences in leg positions; changes in bladder and rectum filling were also seen for most patients. Registration with respect to the prostate required translations of up to 1 cm compared to bone registration. These observations confirm
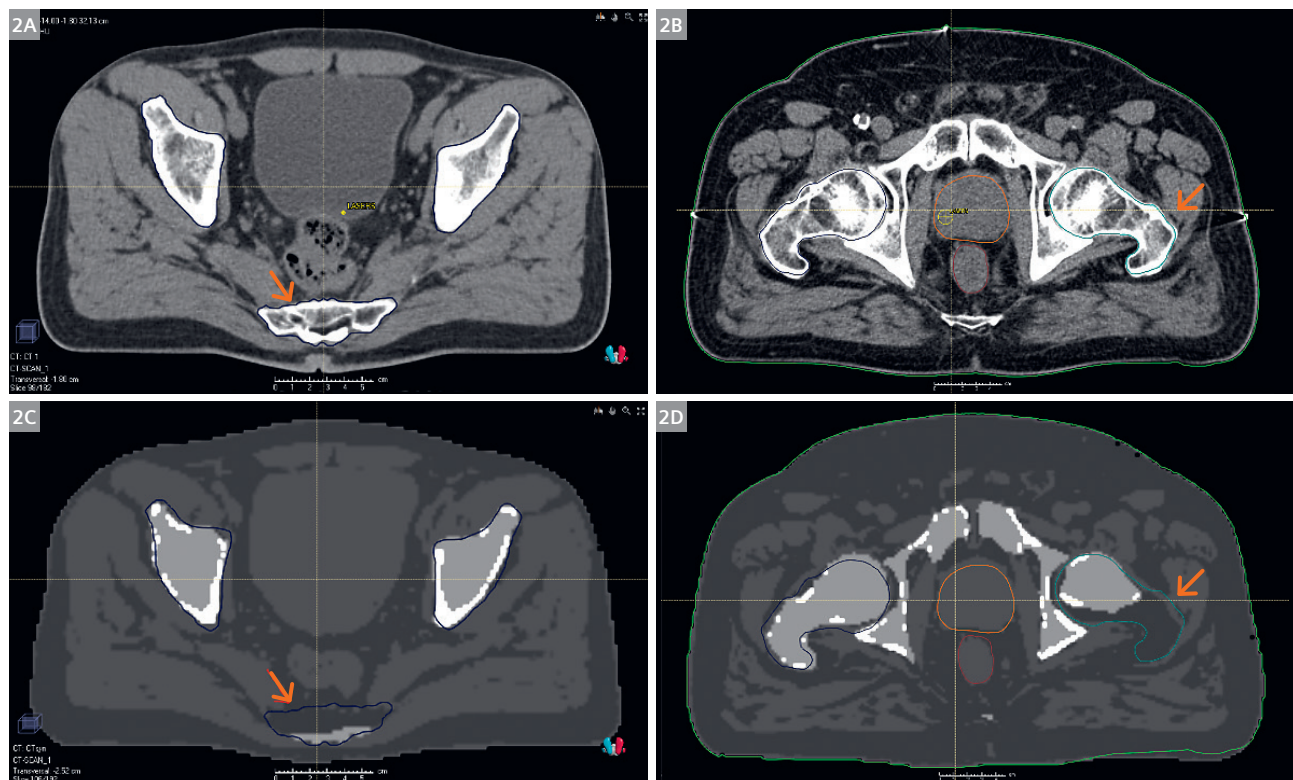
2 Misreconstruction of some bone structures. **(2A and 2B)** planning CT images; **(2C and 2D)** sCT images for the same patient. Arrows point to bone structures that are incorrectly rendered on the sCT.

an advantage of using an MRI-only workflow, as the sCT is intrinsically registered to the MR images.

Careful inspection of sCT images also showed some limitations of the reconstruction. Nine out of 12 patients had some sort of misreconstructions in bone structures (see Figure 2). Most of these misreconstructions were limited to a small missing portion at the tip of the sacrum. However, one of these patients had a larger part of the sacrum missing. For another patient, some parts of the femoral heads were also missing. Another limitation is that calcifications are not reconstructed. Those calcifications are oftentimes useful for the registration during treatment, as they usually provide good contrast on the CBCT.

Some patients external contour was not fully included in the FoV, which showed the importance of proper placement of scan limits, and screening of patients that might be too large to be included fully in the MR FoV (50 cm FoV on the MR, vs. 70 cm for the CT).

Other artifacts which sometimes occurred included breathing artifacts on the abdomen (six out of 12 patients) getting incorrectly reconstructed as tissue, and air pockets at unusual places (e.g, in the bladder) for two patients (see Figure 3).

Discussion

Our first contact with sCT reconstruction showed a good overall agreement with planning CT. Fat and muscle compartments were well represented, despite some misreconstructions in the bones. A more thorough investigation would be needed to identify what could have caused the problems which we have encountered. As the bones are rendered using a multi-atlas-based model, it is possible that their proper reconstruction is sensitive to differences in patient positioning or scan limit placement.

Other artifacts were also seen, such as breathing artifacts on the abdomen, and tissue incorrectly assigned to air density. It is important to mention however, that most of these artifacts were easily identified when looking at source MR images. In these cases, they could be corrected inside the TPS by contouring on the MR images and assigning the correct density to those structures. Moreover, in most cases artifacts appeared outside of the region intercepting the beam, and would have no clinical impact on the treatment plan.

These early results showed the need to establish image quality checklists before we can start using these images alone for treatment planning. MR and sCT images should be reconstructed and inspected immediately following the MR session to assess image quality before the patient can leave the clinic. Acceptance criterion
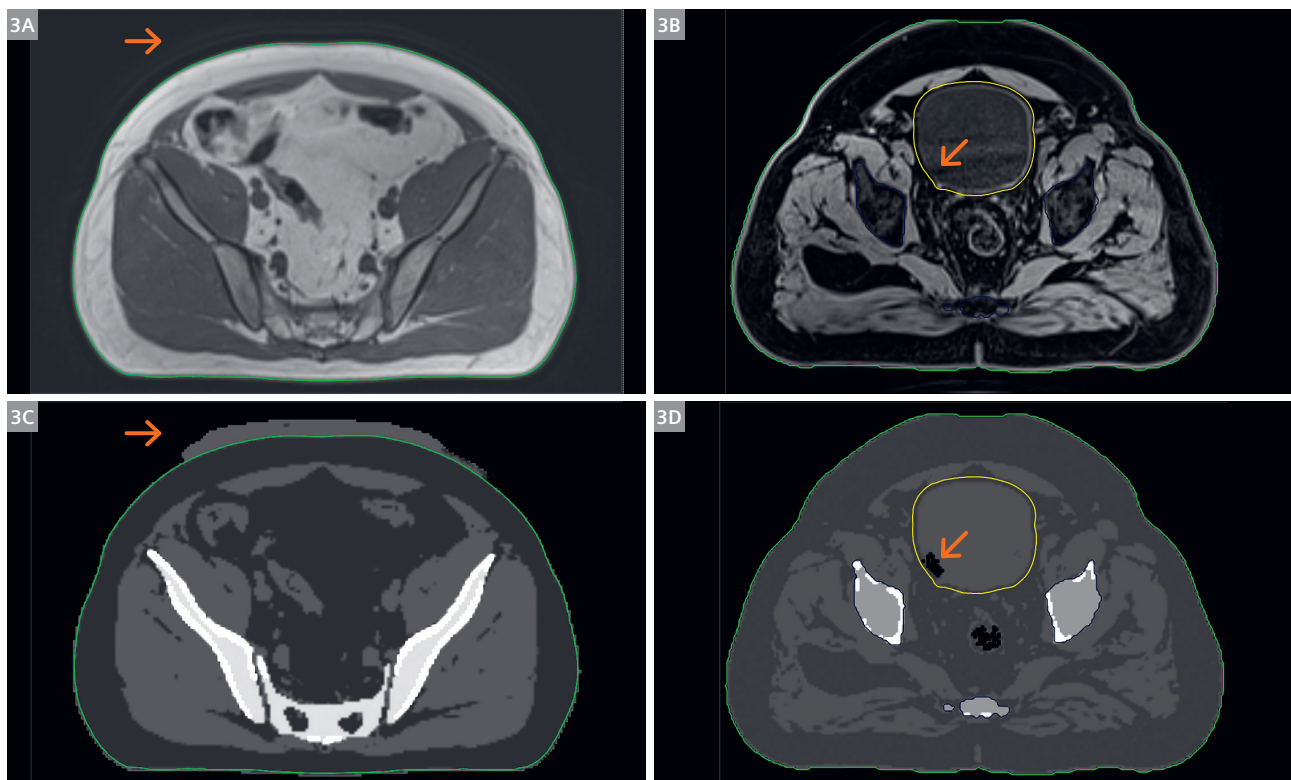
3 Other sCT artifacts. **(3A and 3C)** the arrow shows where ghosting, caused by respiratory movement on the abdomen, was incorrectly rendered as muscle on the sCT. **(3B and 3D)** ghosting inside the bladder is incorrectly rendered as air.

should be established, and therapists should be ready to have the patient undergo a regular planning CT in case images are of poor quality or the sCT reconstruction fails.

Imaging – geometric distortions in MR

CT images can be considered to be spatially accurate, but MR images are affected by geometrical distortions due to main magnetic field inhomogeneities, patient-induced susceptibility effects, gradient non-linearity, and eddy currents. These distortions must be small enough to ensure accurate OAR and target contouring. The goal of this part of the study was to quantify the distortions on MR images used in prostate planning and evaluate the impacts on the MRI-only workflow.

Method

We used a custom MRI distortion evaluation phantom, based on the work from Walker et al. [3]. The phantom consists of a stack of PVC foam panels holding arrays of markers (fish oil capsules) visible on CT and MR images arranged over a polar grid, centered on the MR axis. A CT scan and an MR scan were both performed on the phantom. Images were imported in RayStation, where a rigid registration was first performed on the central region of the phantom (a 5-cm radius sphere around magnet isocenter), where distortion is assumed to be lowest. A deformable registration from MR images to CT was then performed over the whole phantom. This deformation is represented by a deformation vector field. The magnitude of the deformation vector at each point gave an indication of the geometric distortion induced in the MR image.

Distortion assessment was done for the T2 SPACE and the VIBE Dixon in-phase image. All patients' sCT images were registered to the phantom using the MR scanner isocenter position. Patient regions of interest (targets and OAR) were copied over on the phantom CT image. Displacement vector field statistics were obtained in those volumes to assess maximum distortion inside a subset of relevant anatomical structures: prostate (CTV), rectum, femoral heads, and complete external contour. From previous analyses, we know that distortion becomes greater at the edges of a very large FoV image. In this study, distortion was only relevant in the region intercepting the treatment beams. Thus, for the external contour, distortion was analyzed only over a section of 15 cm in the superior-inferior direction. This section covered all patient targets + 4 cm on each side in this direction, so the whole VMAT beam is entirely comprised in this region. For each ROI, distortion was analyzed on the image on which it had been contoured: T2 SPACE for CTV and rectum, and VIBE Dixon in-phase image for femoral heads and external. The maximum and the 95th percentile displacement values were analyzed.

Results

Table 1 shows the patient-averaged maximum and 95th percentile distortion, as well as overall maximum displacement over all patients, for some regions of interest.

Inside the CTV and OAR, the global maximum distortion over all patients was less than 0.2 cm, while the 95th percentile was 0.1 cm or less. Inside the patients' external contour, the global maximum was close to 0.5 cm, with a 95th percentile of less than 0.15 cm.

Discussion

Based on the results above, it appears that geometric distortion for our MRI sequences can be kept reasonably low inside the target and OAR (maximum of 0.18 cm, and a 95th percentile of 0.1 cm or less). This level of uncertainty seems acceptable for prostate treatment planning. Moving further away from the magnet isocenter, distortion becomes greater, and can reach close to 0.5 cm overall within the patient's body outline. This again seems reasonable as the effect of

---

[1]Distortion values depend on field strength and acquisition protocol (e.g. in-plane acquisition pixel size or acquisition readout pixel bandwidth), therefore, measured values may differ at various sites.

Deformation statistics – Average and global maximum for all 12 patients[1]				
ROI	Image	Maximum distortion (patient average) [cm]	95th percentile distortion (patient average) [cm]	Maximum distortion (overall) [cm]
CTV	T2-SPACE	0.14	0.09	0.16
Rectum	T2-SPACE	0.13	0.08	0.16
Left femoral head	Dixon in-phase	0.18	0.10	0.18
Right femoral head	Dixon in-phase	0.16	0.10	0.18
External body contour	Dixon in-phase	0.39	0.14	0.47

Table 1: Overall distortion[1] statistics inside patients' target and OAR volumes.

the difference in external contour will be spread out over a complete VMAT arc, and should have no significant impact on the dose delivered to the target volume or OAR. There are some limitations worth mentioning in this analysis. First, the method employed is limited by the accuracy of the deformable registration algorithm. It was observed in this study that the choice of deformation grid size had an impact on registration. The grid size was chosen empirically to obtain the best possible visual match between the two images after registration. Another limitation of the method is that there is no image information in empty spaces between the markers in our phantom. The choice of distance between markers could have an impact on the deformation vector field, although this field is expected to be spatially slowly varying.

To evaluate the reproducibility of the method, the phantom was scanned at the CT using the same imaging parameters on two separate sessions. Ideally, performing the rigid and deformable registration analysis should result in no displacement between the two image sets. Results showed a maximum displacement of 0.07 cm within the CTV, and 0.085 cm inside the patients' external contour. This displacement is indeed very low, but not zero, which demonstrates some uncertainty of the results.

Finally, one important limitation of distortion evaluation using a phantom is that it does not take into account specific patient-induced susceptibility distortions. The phantom used in this study is very large to cover a larger FoV, and was not made to be representative of a patient anatomy. It is likely that results would be slightly different for each individual patient.

Target volume contours

In our current workflow, MRI is registered to CT, with emphasis on the prostate. A radiation oncologist then contours the prostate and seminal vesicles (SV) on the CT image, with the MR T2-SPACE image to assist, as the MR gives a better visibility for the base, apex, and anterior wall of the prostate. In an MR-only workflow, no CT would be available for contouring. The question is then to determine whether using only MRI for contours will change how the prostate is delineated.

Method

A radiation oncologist was asked to contour the prostate and SV for the 12 patients using T2-SPACE images only. These patients had already been treated, so a prostate contour made using CT was already available. Total volume of these structures were compared between CT+MR and MR-only contours. Automatic segmentation was also performed on the prostate to divide it in 6 subregions (superior, inferior, left, right, anterior, and posterior). Differences in contours between CT+MR and MR-only in these subregions were compared separately to determine if there were differences in some preferable directions.

Results

Table 2 shows results for the overall target volumes. These results show that both the prostate and SV have smaller volume when contoured on MRI alone vs. CT+MRI. On average, the prostate was 2.7 cc smaller (-7%; p-value = 0.038), and the SV 1.7 cc smaller (-14%; p-value = 0.007). The maximum absolute difference for a single patient was -11.6 cc for prostate and -4.5 cc for SV.

Differences in volumes were also analyzed separately for 6 regions (left, right, ant, post, sup, inf). Table 3 shows the results of this analysis. Intersubject variability was high, but statistically significant differences were observed in anterior and superior regions, where the volume was found to be smaller for MRI. The mean volume difference was of -1.33 cc (p = 0.048) and -1.59 cc (p = 0.015) for the anterior and superior regions, respectively.

Discussion

Contouring targets on MRI alone vs. CT+MRI has an impact on the volume contoured. Overall volume was smaller for prostate and SV when contoured on MRI alone. On average,

ID	Prostate				Seminal vesicles			
	CT+MR volume [cc]	MRI volume [cc]	Difference [cc]	Relative difference [%]	CT+MR volume [cc]	MRI Volume [cc]	Difference [cc]	Relative difference [%]
Min	22.6	21.4	-11.6	-23%	6.6	4.3	-4.5	-34%
Max	72.6	75.9	3.3	8%	18.0	19.9	2.0	11%
Mean	43.0	40.3	-2.7	-7%	12.8	11.2	-1.7	-14%
p-value	0.038				0.007			

Table 2: Overall volume comparison of the prostate and seminal vesicles.

ID	Left [cc]	Right [cc]	Ant [cc]	Post [cc]	Sup [cc]	Inf [cc]
Min	-2.69	-1.50	-3.90	-3.05	-3.74	-4.60
Max	1.09	1.49	1.87	3.04	3.26	2.46
Mean	-0.18	-0.08	-1.33	0.56	-1.59	-0.74
p-value	0.547	0.723	0.048	0.291	0.015	0.192

Table 3: Directional volume difference (+: MRI larger).

the differences were found to be small, but they can be large on an individual basis. For the SV, the difference was considered to have no clinical impact, as only 1 cm proximal to the prostate is included in the treatment.

We found that prostate volume was slightly smaller in anterior and superior regions, but again the difference was small on average. Because prostate boundaries are better visualized on MRI, it is more likely that contours on CT are slightly larger than they need to be, instead of the other way around. Based on these results, we felt confident going forward with contouring on MRI alone.

OAR contours

Not having an actual CT image to perform OAR contours implies that these contours would need to be done using only MR images and possibly the sCT image. The evaluation for this step of the workflow aimed to identify pitfalls and areas needing improvement in our imaging protocol.

Method

Therapists contoured OAR on five selected patients using all MR images available (T2-SPACE and all four Dixon images from the sCT sequence) as well as the sCT itself (see Figure 4). They were instructed to use any images that they found to work best for each OAR and to take note of their observations. OAR contoured for prostate planning include rectum, bladder, small bowel, penile bulb, pelvis, femoral heads, external genital organs, and cauda equina.

Results

Qualitative observations were made regarding image quality and OAR visibility. For the rectum, T2-SPACE, Dixon in-phase and sCT were found to be useful. It was noted that visibility was suboptimal in the most inferior section. The bladder was easily seen on all images, but was not fully encompassed on the T2 image due to limited FoV. It was also noted that there could be filling of the bladder between the Dixon and T2 sequences. The small bowel was easily seen as well, and could be drawn directly on the sCT image using the Dixon fat image to remove muscles. The penile bulb was found to be more easily seen on the T2 image. External genital organs were easily seen directly on the sCT, using any other image as a reference if needed. Pelvis and femoral heads were very easy to contour on the sCT using automatic segmentation tools, as the image is comprised of discrete HU levels. Misreconstructions on the sCT could be corrected using other images. The cauda equina was found to be very difficult to see on all MR images, and the quality of the sCT was insufficient in the sacrum region to allow proper contouring of this structure.
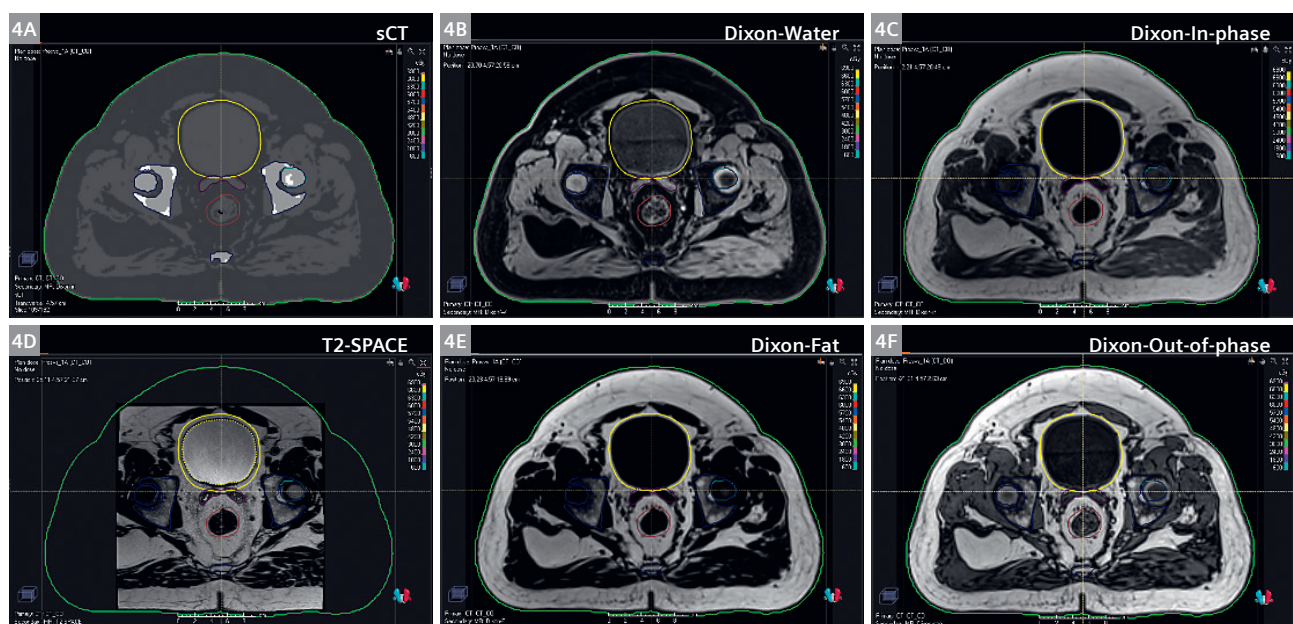
4 An example of all images available from our MR protocol for a single patient.

Discussion

Most OAR could be easily contoured using available images. For the clinic workflow, we would need to standardize which image(s) to use for each OAR. This evaluation allowed identifying areas needing improvement. In particular, it was found that the T2-SPACE sequence could be improved for better visibility of the rectum. We could also try to increase resolution on the Dixon sequence to get better visibility of the cauda equina. However, for treatment of the prostate alone, cauda equina is rarely a critical OAR, so an approximate contour should be sufficient in this case.

Plan optimization and dose accuracy

Following the imaging session as well as OAR and target volume contouring, the next step in the workflow is to optimize the treatment plan itself in the TPS. In this preliminary testing phase, we evaluated if the usage of the sCT would induce changes in the plans that are produced. There are two elements that were evaluated. First, would working on a sCT change how dosimetrists work, and are there pitfalls in the workflow? Second, is the dose calculation in the TPS different when working on the sCT vs. the regular planning CT?

Method

For the workflow and plan optimization evaluation, five therapists worked from scratch on five different cases, planning a regular prostate + SV treatment. The dose prescription was 60 Gy in 30 fractions, using a single-arc 6MV VMAT beam. The instructions given were to optimize the plans just as they normally would and note any relevant observations.

For the dose accuracy evaluation, original treatment plans (planned on regular CT) for all 12 patients were recalculated on the sCT. To mitigate the effect of differences in the patients' external contour (caused by differences in positioning during imaging sessions or geometric distortions on the MR images), areas where body outline was larger on the sCT were overridden with air density, while areas where the outline was smaller on the sCT were overridden with adipose density.

To allow for a direct comparison of dose distributions and eliminate differences in internal organ shapes, contours (targets and OAR) from the planning CT were copied directly on the sCT. Dose difference distributions were then evaluated visually, and dose volume histograms (DVH) were analyzed in some structures of interest (CTV, PTV, rectum, bladder, and femoral heads).

Results

Plan preparation and optimization

Some missing details were observed during the plan preparation and optimization stage. First, it was noted that the localization point, which represents the point of intersection of the lasers, could not be placed on the sCT. It is usually identified on the CT by placing radio-opaque markers on the patient's skin. In our traditional CT+MRI workflow, no markers are used during MRI. As such, the localization point was not identifiable on MR images.

Another difficulty was that the examination table is not visible on the MRI. Usually, a table structure modeled for accurate beam attenuation is predefined in the TPS. This structure is placed manually according to its position visible on the planning CT. As the table is not visible on MR images, it was impossible to position the structure accurately on the sCT.

Similarly, positioning accessories (namely an indexable board placed on the table) are not visible on the MRI. In the traditional workflow, all accessories are included within the patient's body outline, so that beam attenuation is properly taken into account. In this study, as the accessories were not visible, they could not be included.

Some qualitative remarks were also pointed out by dosimetrists, mostly regarding visual appearance of the sCT. Some felt that they were not dealing with a real patient because of the segmented appearance, while others thought that OAR contours looked less accurate because of the lower resolution. No issues were observed with regard to the plan optimization process, and they found that the plans optimized on the sCT were of equal quality to those optimized on a regular CT. Final dose distributions were qualitatively similar.

Dose accuracy

For the reasons mentioned above regarding equipment not visible on MRI, table and accessories were excluded from the regular CT to allow a direct comparison between plan dose calculated on the sCT vs. CT.

Having no specific HU to mass density curve for the sCT, the same curve as the regular planning CT was used in the first phase of this evaluation. Table 4 shows the difference in CTV average dose using this curve. Initial tests showed that CTV average dose on sCT was 1.3% higher (averaged over all patients), with a maximum difference

	"Water" = 1.0 g/cm³	"Water" = 1.05 g/cm³
Min	0.5%	-0.5%
Max	2.1%	0.9%
Mean	1.3%	0.1%

Table 4: CTV average dose difference for different densities of the "water" compartment (sCT dose - CT dose).

of 2.1% for two out of twelve patients. A possible explanation is that the "water" compartment on sCT corresponded mostly to muscles, which has a slightly higher density than water (around 1.05 g/cm³ for muscle instead of 1.0 g/cm³ for water). This compartment was thus segmented on the sCT and assigned muscle density. Using this density, CTV average dose on sCT was 0.1% higher (averaged over all patients), with a maximum difference of 0.9% for one patient.

Having found that the dose difference was lower with muscle density assigned to the water compartment, this density was kept for the following comparison. Dose difference distributions showed that local differences were in general well below 1% of the prescription dose (see Figure 5 for a representative sample). No significant difference was found on the DVH curves of all evaluated contours (targets and OAR).

Table 5 shows average, min, and max differences for some relevant DVH points (sCT - CT) evaluated over all patients. The average maximum difference was found to be 0.31% for the D1% in the PTV. The maximum absolute difference (for a single patient) was of 1.15%, again for the D1% in the PTV.

Discussion
This preliminary evaluation showed that, with proper densities applied to all five sCT segmented compartments, it is possible to obtain a dose distribution that is very similar to that planned with the regular CT. Maximum local differences were less than 1% of the prescription dose, and

DVH curves were visually indistinguishable between CT and sCT. Maximum differences on the DVH indices were for the PTV D1%, which corresponds to the plans' hot spots inside the target volume. These observations suggest that no uncertainties of clinical relevance result from the dose computation on a sCT vs. a regular CT.

A few issues will need to be addressed in the simulation step, before we are able to plan solely on the sCT. First, we will need to test MRI markers (commercial markers or off-the-shelf oil capsules) to identify properly

	Average	Min	Max
Femoral Heads D1%	0.15%	-0.62%	0.75%
Femoral Heads mean	0.00%	-0.25%	0.21%
PTV D1%	0.31%	-0.92%	1.15%
PTV D99%	0.14%	-0.67%	0.80%
PTV mean	0.24%	-0.66%	0.78%
Rectum D1%	0.09%	-1.09%	0.68%
Rectum mean	-0.04%	-0.23%	0.13%
Bladder D1%	0.17%	-0.57%	0.76%
Bladder mean	-0.06%	-0.20%	0.02%

Table 5: Average, min, and max differences between sCT and CT of selected DVH points.
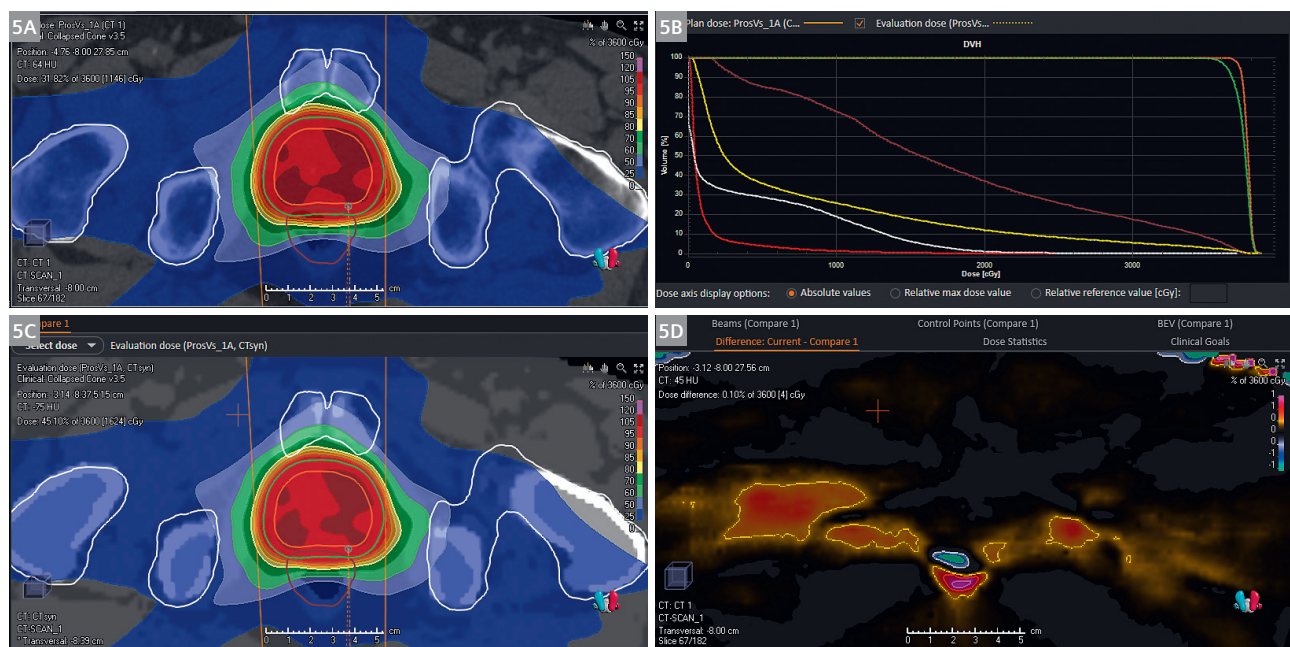
5 Example of a dose distribution computed on planning CT **(5A)**, and the same plan computed on sCT **(5C)**. Dose difference (CT - sCT) is shown at bottom right **(5D)** (scale goes from -1% to +1%). DVH curves are presented at the top right **(5B)** (solid lines = CT, dashed lines = sCT). Green: PTV; Orange: CTV; Brown: Rectum; Yellow: Bladder; White: Pelvic bones; Red: Small bowels

the laser localization point on patients. Second, we should establish a procedure to properly identify table position (not visible on MR images), which could be as simple as measuring the height of the lasers with respect to the table top. Finally, we need to determine how to consider beam attenuation through positioning accessories. For example, a new table structure could be included in the TPS that takes into account the outline and attenuation of standard accessories.

IGRT treatment

Workflow in our clinic for prostate treatment includes a daily CBCT, which is registered on the planning CT. As was noted above, the sCT has quite a different appearance than the CT. The question here was thus to evaluate how using a sCT as a reference would affect the registration.

Methods

Five patients for which sCT and CT images agreed well (with respect to patient positioning and internal organs) were selected, in order to have an accurate reference registration between those two images. Five therapists then performed three registrations each on all five patients: one from sCT to planning CT (sCT→CT), another from CBCT to planning CT (CBCT→CT), and finally from CBCT to sCT (CBCT→sCT). The sCT→CT registration was taken as a "true" reference, to which CBCT registrations were compared. Only translations were allowed and all registrations were done manually (no automatic registration).

For each patient, standard deviation on registration results across therapists is evaluated to assess variability. This variability was compared between CBCT→sCT and CBCT→CT registrations. From the CBCT→sCT and CBCT→CT registrations, an implicit sCT→CT registration was obtained. This implicit registration was then compared to the reference sCT→CT registration.

Results

Table 6 shows the inter-user standard deviations in each direction (average over 5 patients) of the CBCT→CT and CBCT→sCT registrations. In each direction (RL = Right-Left; IS = inferior-superior; PA = posterior anterior), the standard deviation was slightly higher for the CBCT→sCT registration. However, none of those differences was found to be statistically significant (p>0.05).

Table 7 shows average differences in translation between the implicit and the reference sCT→CT registrations. Differences were of 0.042 cm, -0.127 cm and -0.021 cm in the RL, IS, and PA directions respectively. Only the difference in IS was found to be statistically significant, although this difference was small (less than 0.15 cm).

Discussion

From these preliminary results, there does not seem to be major differences using planning CT or sCT for registering CBCT. The only statistically significant difference was found to be a small (<0.15 cm) shift in the IS direction. It can be noted that the registration was performed by using not only a visual match between the images, but also by including target contours as a reference. Therefore, it is possible that differences seen earlier in target volume contours could affect how registration is done.

This part of our preliminary work was limited by a small sample size (5 therapists, 5 patients). Moreover, for simplicity, the registrations were performed in the TPS (RayStation), while registration in a clinical scenario would be made in different software (Elekta XVI). Also, registration in this evaluation were all manual, whereas in the clinical workflow an automatic bone registration is first performed, before manual corrections are applied. To get a clearer picture of the impacts of using sCT for IGRT, next steps would require a larger sample size and using the full clinical treatment workflow.

Conclusion

This study aimed to evaluate the impact on the clinical workflow of prostate EBRT planning when transitioning from a CT+MR to an MR-only workflow. Several steps in the complex treatment chain were examined, namely imaging, target and OAR contouring, plan optimization and dose calculation, and finally CBCT registration for IGRT. This evaluation allowed us to identify areas needing improvements before safely making the transition. While the results presented here are specific to the workflow used in our own center, some observations could be relevant for other centers.

	RL [cm]	IS [cm]	PA [cm]
CBCT→sCT	0.096	0.200	0.170
CBCT→CT	0.069	0.175	0.127
Difference	0.027	0.026	0.043
p-value	0.079	0.498	0.195

Table 6: Average inter-user standard deviation for CBCT registrations.

	RL [cm]	IS [cm]	PA [cm]
Average difference	0.042	-0.147	-0.021
p-value	0.079	0.022	0.635

Table 7: Difference in implicit vs. reference sCT→CT translations.

In particular, we found that image quality should be assessed directly after imaging at the MR, in case a fallback planning CT would be necessary. We discussed the importance of MR image geometric distortion assessment; this is something that should be done in each center at the time of commissioning, and as part of a periodic QA program. Differences in target volumes were observed when contours were made using only MRI. These differences were attributed to better visibility of the anterior wall and base of the prostate as seen on the MRI. Some areas needing improvement were noted for the OAR contours. It was found that the use of a sCT instead of a regular planning CT would have no significant impact on plan optimization and dose calculation in the TPS, as long as an appropriate HU-density curve is determined. Finally, a small difference in inferior/superior direction was found in the registration of the CBCT when matched against the sCT instead of the planning CT. This difference could be attributable to differences in target contours, although a more thorough investigation would be needed.

Next steps in the study would be to make adjustments necessary in each part of the chain as were presented above. We would then need to establish clear guidelines and protocols about the usage of the sCT. In a second phase of the study, we could perform end-to-end testing of the MR-only workflow. Patients could then continue to undergo both MRI and CT as a backup. Treatment plans could be made entirely on sCT, and then recalculated on CT at first for a sanity check.

In conclusion, this study showed that MRI-only based radiation therapy of prostate cancer is possible, with some adjustments needed at each step of the planning process. The transition must be planned very carefully, and impacts should be well understood and documented. As with any major change, we anticipate that workload for physicists and therapists could be increased at first, as everyone gets accustomed to the new workflow. Overall, this study gave our center a clearer picture of what needs to be done to make a safe and optimal transition to an MR-only workflow.

Acknowledgments

Contact

Jean-François Cabana
Physicien médical clinique
Centre Régional Intégré de Cancérologie
de Lévis – Hôtel-Dieu de Lévis
101, rue du Mont-Marie,
Lévis (Québec) G6V 5C2
Canada
Phone: +1 418-835-7121, ext. 14642
jean-francois.cabana.cisssca@ssss.gouv.qc.ca

References

1 Bird, D., Henry, A. M., Sebag-Montefiore, D., Buckley, D. L., Al-Qaisieh, B., & Speight, R. (2019, November 1). A Systematic Review of the Clinical Implementation of Pelvic Magnetic Resonance Imaging–Only Planning for External Beam Radiation Therapy. International Journal of Radiation Oncology Biology Physics. Elsevier Inc. https://doi.org/10.1016/j.ijrobp.2019.06.2530
2 Siemens Healthcare GmbH. (2019). MR-only RT planning for the brain and pelvis with Synthetic CT.
3 Walker, A., Liney, G., Holloway, L., Dowling, J., Rivest-Henault, D., & Metcalfe, P. (2015). Continuous table acquisition MRI for radiotherapy treatment planning: Distortion assessment with a new extended 3D volumetric phantom. Medical Physics, 42(4), 1982–1991. https://doi.org/10.1118/1.4915920

Optimization of MR Acquisition for Brain Irradiation

Veit Mengling, M.Sc.[1]; Christoph Bert, Ph.D.[1]; Rosalind Perrin, Ph.D.[1]; Siti Masitho, M.Sc.[1]; Johanna Grigo[1];
Thomas Weissmann, M.D.[1]; Sina Mansoorian, M.D.[1]; Hadi Siavooshhaghighi[1]; Rolf Janka, M.D.[2];
Sylvain Doussin, Ph.D.[3]; Melanie Habatsch[3]; Rainer Fietkau, M.D.[1]; Florian Putz, M.D.[1]

[1]Department of Radiation Oncology, University Hospital Erlangen, Friedrich-Alexander-University Erlangen-Nuremberg,
 Erlangen, Germany
[2]Institute of Radiology, University Hospital Erlangen, Friedrich-Alexander-University Erlangen-Nuremberg,
 Erlangen, Germany
[3]Siemens Healthineers, Erlangen, Germany

Abstract

MRI is a crucial factor for accurate treatment planning
for brain irradiation. Currently, most sites use MR images
acquired by radiologists. Although these images provide
excellent diagnostic information, they often lack the
level of geometric precision required for treatments like
stereotactic radiosurgery. In this work, we summarize and
discuss our advances in optimizing MR image acquisition
for treatment planning of brain irradiation.

Introduction

MR images acquired for diagnostic uses aim to detect previ-
ously unknown pathologies and provide information on
differential diagnosis. On the other hand, MR images used
for radiotherapy purposes require a geometrically accurate
and clear depiction of the tumor and organs at risk (OAR)
in three-dimensional space for accurate delineation. Due
to physical limitations, both requirements can only be
met at the same time with excessive measurement times,
which often cannot be realized in clinical workflows.
Therefore, a tradeoff between image quality and geometric
precision has to be found.

Positioning of the patient is also different in diagnostic
radiology and during radiotherapy. One of the main
reasons is that most positioning and immobilization aids
used in radiotherapy are either not MR-compatible, or do
not fit inside the bore of the MR scanner. The different
position of the patient during MRI and planning-CT acquisi-
tion can lead to registration problems because of different
anatomies shown in the images.

In this article, we present our advances in the optimi-
zation of MR imaging for brain radiotherapy. For that, MR
acquisition protocols optimized for radiotherapy purposes,
and a novel coil setup for image acquisition in treatment
position will be introduced and discussed.
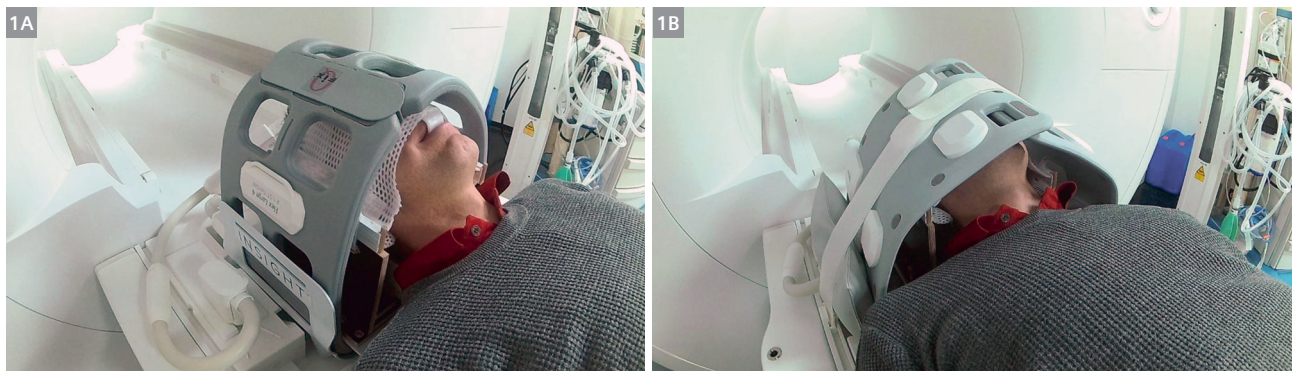
1 Setup for MR imaging in treatment position for brain tumor patients. **(1A)** shows the commercially available setup with two 4-channel Flex coils, **(1B)** shows our novel proposed setup with two 18-channel UltraFlex coils. In both setups, the coils are wrapped around the head of the patient, closing under the tabletop and above the nose of the patient. The most notable differences are the fixation and connection of the coils. The mask holder is a self-built wooden replica of the metallic one used during irradiation.

Material and methods

Setup

A 1.5T MAGNETOM Sola with the MAGNETOM RT Pro Edition (Siemens Healthcare, Erlangen, Germany) was installed in December 2018 and has been used for radiotherapy planning since March 2019. It has a 70 cm bore size, second-order active shimming, and a maximal field of view (FOV) of 50 x 50 x 50 cm^3. The maximum gradient amplitude is 45 mT/m and the maximum slew rate is 200 T/m/s.

It is equipped with the INSIGHT system (Qfix, Avondale, PA, USA) including an MR-compatible flat tabletop with indexing capability. The flat tabletop allows imaging with the spine coil. The system also comes with coil holders (Qfix) for the 18-channel body coil and two 4-channel flexible coils (Siemens Healthineers) that can be used to form a head coil. The body coil holder allows for reliable coil positioning without the coil touching the patient. An MR-compatible Lok-Bar (CIVCO Medical Solutions, Kalona, IA, USA) with three pins enables consistent positioning of immobilization devices.

Two laser systems are available for patient positioning. Aside from the standard internal MR laser, an additional MR-compatible external laser bridge (DORADOnova MR3T, LAP of America Laser Applications, Boynton Beach, FL, USA) was installed. It consists of six sagittal, transverse, and coronal lasers, and allows patient localization, isocenter marking, and direct laser steering to set skin marks.

For head acquisitions intended to guide stereotactic radiosurgery (SRS), patients were positioned with stereo-tactic mask immobilization (Brainlab, Munich, Germany). As the mask manufacturer did not provide MR-compatible mask holders at the time of implementation, an in-house built wooden mask holder was constructed that is compatible with the flat tabletop. Two surface-coil setups with, respectively, 8 and 36 receiving channels were investigated (see Figs. 1 and 2): 1) A commercially available setup consisting of two receiving coils (4-channel Flex Large) and the respective coil holder, and 2) our novel setup, which also consists of two receiving coils (18-channel UltraFlex Large, Siemens Healthcare) but significantly more receiving channels. The intention was to increase the signal to noise ratio (SNR) as well as image quality for target and OAR delineation, as the wooden mask holder induced an additional distance between the coils and the patient compared to the standard setup. As the UltraFlex coils are larger than the Flex coils, the coil holder could not be used in the novel setup. Reproducible positioning was instead achieved by placing cushions under the UltraFlex coils and fixing them with two Velcro straps at the top (see Fig. 1B).

Image-quality evaluation

As part of routine clinical practice, most patients received MR imaging in one of the above-described surface-coil setups in treatment position as well as in a standard diagnostic setup (Head/Neck 20-channel coil) in the same session to enable optimal diagnostic assessment as well as dedicated imaging for treatment planning. To evaluate the image quality of the two setups in treatment position, the SNR of each setup was compared with the SNR in the standard diagnostic radiology setup (Head/Neck
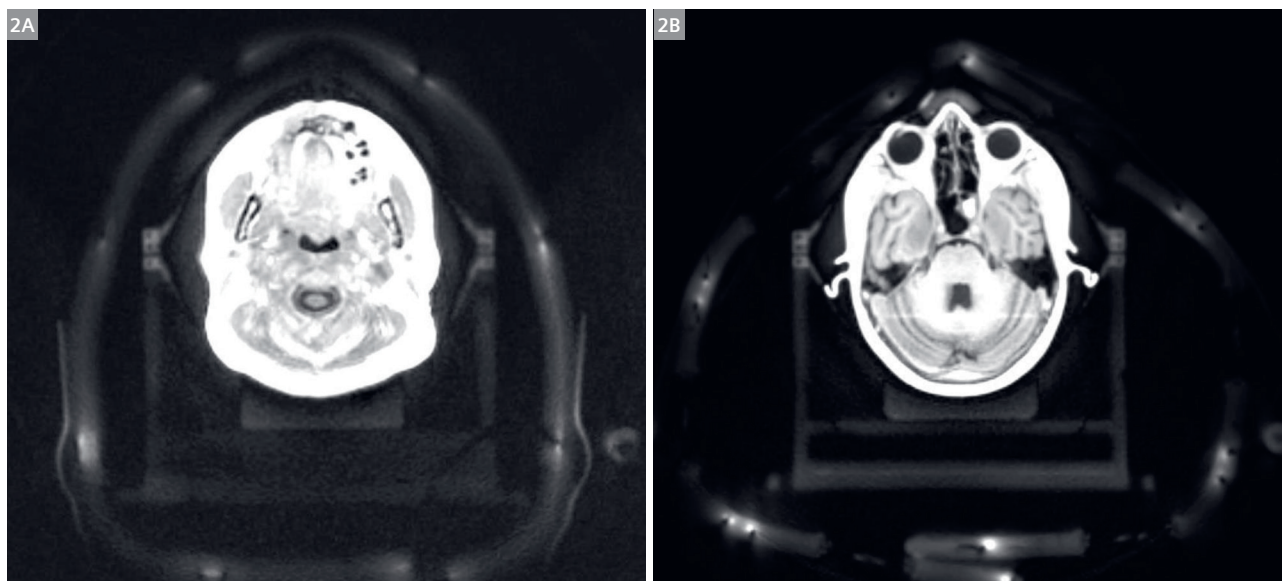
2 Axial view of the **(2A)** 4-channel Flex coil setup and the **(2B)** 18-channel UltraFlex coil setup. As the image quality was worse in 2A and the coils have fewer visible elements, different windowing and slice positioning was chosen for the two images.

20-channel coil). As the SNR was not homogeneous along the anterior-posterior direction, the evaluation was split into the anterior, the central, and the posterior part of the head. To calculate the SNR, the mean intensity in a circular region of interest (ROI) in white matter was divided by the standard deviation of a circular ROI in the background in the corresponding section. To ensure a homogeneous signal and that the coil profile did not affect SNR calculation, the circular ROIs were at least 0.5 cm^2 in the white matter and between 4 and 5 cm^2 in the background. The SNR was calculated on both the transversal T1w-MPRAGE sequence after contrast-agent injection and on the T2w-FLAIR (for detailed parameters see Table 1).

The suitability for contouring was assessed by three experienced radiation oncologists (FP, TW, SM). Images of the three setups (154 in total) were blinded, loaded into 3DSlicer (v. 4.10.2) [1], and presented to the physicians in randomized order. The radiation oncologists then graded each image on a scale of 1 (not suitable for contouring) to 4 (excellent suitability for contouring), based on the image quality and the distinguishability of the lesions from the surrounding tissue using a custom-made software module in randomized order. Additionally, the radiation oncologists counted the number of metastases for every data set with a similar software module in randomized order and in a blinded fashion.

	T2w-TSE-FLAIR	T2w-SPACE-Dark-Fluid	T1w-MPRAGE	T1w-SPACE	EPI with shaped excitation (ZOOMit)
Voxel size [mm x mm x mm]	0.7 x 0.7 x 5.0	**0.5 x 0.5 x 1.0**	1.0 x 1.0 x 1.0	**0.5 x 0.5 x 1.0**	0.8 x 0.8 x 3.0
Orientation	Transversal	**Transversal**	Transversal	**Transversal**	Coronal
Dimension	2D	3D	3D	3D	2D
Contrast agent	yes	yes	yes	yes	yes
Flip angle [°]	150	120 (T2 Var)	8	120 (T1 Var)	90
TR [ms]	9000	**7000**	2200	700	**4000**
TE [ms]	93	**374**	3.02	22 **19**	**65**
TI [ms]	2500	**2050**	900		
Fat-saturation	yes	yes	no	yes	yes
Bandwidth [Hz/Px]	130	**751**	**160**	**399**	**1221**

Table 1A: Detailed sequence parameters of the protocols used for head imaging.

	T2w-SPACE	Dixon	T2w-BLADE	RESOLVE ok	EPI with shaped excitation (ZOOMit)
Voxel size [mm x mm x mm]	0.9 x 0.9 x 1.0	1.6 x 1.6 x 2.0	0.6 x 0.6 x 3.0	0.9 x 0.9 x 4.8	0.8 x 0.8 x 3.0
Orientation	Transversal	Transversal	Sagittal	Transversal	Transversal
Dimension	3D	3D	2D	2D	2D
Contrast agent	no	no	no	no	no
Flip angle [°]	**155**	15	160	180	**90**
TR [ms]	1200	6.2	5820	8060	4000
TE [ms]	**138**	2.39/4.77	117	60/98	70
Fat-saturation	no	no	no	yes	yes
Bandwidth [Hz/Px]	651	**1015**	**178**	994	**1221**

Table 1B: Detailed sequence parameters of the protocols used for prostate imaging.

Significance of the qualitative grading results was tested using a Welch two-sample t-test. To compare the number of counted metastases between the diagnostic setup and the novel UltraFlex setup in treatment position, a paired t-test was used. Calculations were performed using R and SPSS v.21. The level of significance was set at P < 0.05.

As the positioning in a thermoplastic mask was hypothesized to enable better immobilization than the standard diagnostic setup, motion artifacts in T1w-MPRAGE images of patients who received scans both in the treatment position and in the radiologic setup were compared. If motion artifacts were clearly identifiable in either OAR or target volumes, the image was classified as motion-corrupted.

Sequence protocols

MRI sequences for radiotherapy planning should depict the three-dimensional boundaries of target volumes and organs at risk with the highest geometric accuracy and as clearly as possible. As the main emphasis of diagnostic imaging lies on the identification and characterization of diseases, dedicated sequence optimization for the purpose of RT planning is needed.

Whenever possible, isotropic 3D sequences should be used, as they reduce distortions and enable accurate multiplanar reconstructions. [2] Slice thickness should be as low as possible, with the exact value depending on site- and treatment-specific considerations and a general rule of thumb is that structures should be visualized on at least 5 slices to minimize over- or underestimation of volumes due to partial-volume effects [2, 3]. As geometric precision is affected by various mechanisms in MR imaging, specific methods should be applied to counteract these effects. To decrease the geometric distortions caused by gradient nonlinearities, vendor-provided 3D distortion correction should always be applied as a minimum [2]. As susceptibility-induced distortions can lead to errors in frequency-encoding-direction, active shimming on a per-patient basis should be used and the receiver bandwidth should be set as high as possible [2, 4, 5].

Before creating the core protocols, we formulated the following site- and disease-specific clinical objectives.

Brain metastases

MRI sequences in brain metastases should be able to depict the three-dimensional contrast-enhancing tumor volumes as accurately as possible without gaps. As brain metastases frequently measure 5 mm or less in diameter, resolution should be high in every image dimension to minimize partial-volume effects. Contrast ratio between lesions and surrounding brain parenchyma should be optimized to allow accurate delineation and minimize interobserver variability.

Gliomas

Similar considerations were applied for gliomas. However, emphasis on the most accurate depiction of the contrast enhancement was lower than in metastases, as the volume of contrast enhancement – if present – and clinically employed margins usually are much larger in gliomas than in metastases. In addition, the volume of contrast enhancement in malignant gliomas only represents a fraction of all tumor cells, with glioma cells extending far beyond the boundaries of the contrast enhancing area. Therefore, more emphasis was put on accurate depiction of the surrounding T2w-FLAIR hyperintensity, which may represent non-enhancing tumor or microscopic disease extension. T2w-FLAIR hyperintensity should be depicted in high-resolution and continuously without slice gaps.

As contrast-enhancing tumor and post-therapeutic changes are frequently difficult to differentiate in recurrent gliomas, additional information for contouring should be provided by a high resolution diffusion-weighted sequence.

Results

Patients

The data in this study results from patients who received an MRI scan within the first year after installation of the scanner. A total of 89 patients were included, with 19 patients receiving multiple scans. As the images were taken as part of standard clinical care, not all patients received imaging in a mask setup and the radiology setup. Additionally, not all patients received a T2w-FLAIR, as it was not needed for therapy in every case. In total, 11 T1w-MPRAGE images were acquired in the Flex coil setup, 83 in the UltraFlex coil setup, and 60 in the radiology setup. 10 T2w-FLAIR images were acquired in the Flex coil setup,

	Head coil	Flex coil	UltraFlex coil
	T1w MPRAGE		
Anterior	102±22	84±8	163±28
Central	95±20	68±6	104±23
Posterior	119±23	56±7	78±14
	T2w FLAIR		
Anterior	91±11	62±7	107±13
Central	87±9	58±7	86±11
Posterior	98±16	51±10	64±8

Table 2: Mean SNR (± standard deviation) of the radiology setup (Head coil, n = 60), the vendor-provided setup (Flex coil, n = 83) and our novel setup (UltraFlex coil, n = 11).

65 in the UltraFlex coil setup, and 37 in the radiology setup. For more details on the patients, see Table 2.

Motion artifacts
Of the 60 patients imaged in the diagnostic setup, eight showed severe motion artifacts in the radiology setup that were visible in treatment relevant regions. In contrast, no relevant motion artifacts could be detected in both the novel setup and the commercially available setup, in which patients were imaged in treatment position with mask immobilization.

SNR
The mean SNR for the three setups is shown in Table 2. In the novel setup, it decreased from anterior to central and from central to posterior for both investigated sequences. The SNR in the commercially available setup also decreased from anterior to central and from central to posterior for both sequences. The anterior and central SNR in the radiology setup showed no significant difference, while the SNR in the posterior part of the head was higher than in the anterior and the central part of the head for both sequences.

The SNR of the novel setup for both sequences was higher than the SNR in the radiology setup anteriorly, but lower posteriorly. Centrally, it was higher than in the radiology setup for the T1w-MPRAGE. For the T2w-FLAIR, no significant difference was found centrally. In contrast, the SNR of the commercially available setup was lower

anteriorly, centrally, and posteriorly. For more details of the distribution, see Figure 3.

Blinded expert-based assessment of image quality
The qualitative grading of the image quality showed a median score of 2 ("suitable for contouring") for all three setups in a randomized and blinded assessment. No significant difference could be found between the setups ($0.1 < P < 0.4$). Furthermore, in a randomized and blinded comparison, there was no significant difference in the number of identified brain metastases between the diagnostic setup and the novel high-channel UltraFlex setup (mean number of identified brain metastases 3.4 vs. 3.2, $P = 0.369$). Figure 4 shows images of a patient who received imaging in all three setups.

Sequences used
According to the requirements and objectives defined in the previous section, the following core protocols were established. Detailed sequence parameters can be found in Table 1. Brain measurements are mostly taken with the novel high-channel UltraFlex setup. All sequences use active shimming to reduce patient-induced distortions as well as 3D distortion correction to reduce system-induced distortions. To further reduce the effect of patient-induced distortions, the bandwidth was set to the highest value possible while keeping acceptable SNR and acquisition time.
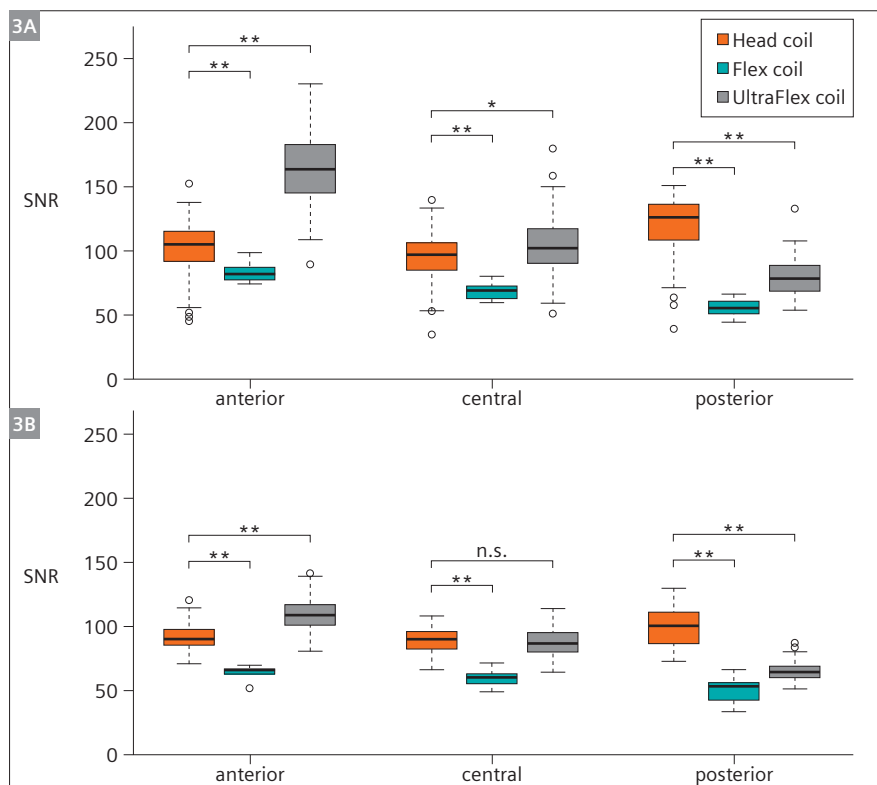
3 Boxplot of the SNR of the different coil setups in the anterior, central, and posterior part of the head measured on **(3A)** the contrast enhanced T1w-MPRAGE and **(3B)** the T2w-FLAIR.
* indicates a significance level of $P < 0.05$,
** indicates a significance level of $P < 0.01$.

Brain metastases

Gadolinium-based contrast agent is injected immediately after completing the localizer. To ensure sufficient contrast uptake, a transversal T2w-FLAIR is acquired. After that, a high-resolution 0.5 x 0.5 x 1.0 mm³ transversal T1w-SPACE is acquired. The total acquisition time was 14:29 min.

Gliomas

The core protocol also starts with contrast agent injection right after completing the localizer. A 0.5 x 0.5 x 1 mm³ transversal T2w Dark Fluid is acquired next, followed by a 1.0 x 1.0 x 1.0 mm³ isotropic transversal T1w-MPRAGE. For the diffusion sequence, an EPI-ZOOMit with 0.8 x 0.8 x 3.0 mm³ resolution was chosen to enable a high-resolution assessment of diffusion-weighted image changes. The total acquisition time was 26:42 min.

Discussion

Both tested coil setups in treatment position are suited for use in treatment planning of brain irradiation. Compared to the diagnostic gold standard, the mean SNR of the novel setup on both the T1w-MPRAGE and the T2w-FLAIR was better in the anterior part of the head, slightly better in the central part of the head (no significant difference for the T2w-FLAIR), and worse in the posterior part of the head. The variance of the SNR in anterior-posterior direction of our novel setup was higher than in the radiology setup. The SNR in the novel setup was significantly higher in all parts of the head compared to the commercially available Flex coil setup. The anterior-posterior distribution was comparable. This can be explained by the distance of the receive coils to the imaged volume. In the radiology setup, the SNR is highest in the posterior part of the head, where the head lies directly over the receive element. The anteri-

or and the central part of the head are further away from the coil, resulting in lower SNR. The same reasoning leads to the non-uniform distribution for the UltraFlex and Flex coil setup. While the anterior part of the head is in direct contact with the coil, the head rest and flat tabletop overlay led to a distance of about 9 cm between the receive coils and the back of the head. The lower SNR in the posterior part of the head might be improved by adding a small coil in the back of the mask holder. While the combination of coils would need to be tested, a superior SNR with our novel setup may likely be achievable in all parts of the head compared to the radiology set up in the Head/Neck 20 coil. However, this would mean that mask systems without additional elevation on top of the tabletop would show a more homogeneous SNR.

The median qualitative grading of the image quality showed no difference between the three tested setups. This means that the novel setup is not inferior to the diagnostic radiology gold standard, while allowing imaging in treatment position. However, this also means that it is not significantly better than the setup with the smaller Flex coils. One possible explanation is the small sample size (n = 11) for the Flex coil setup compared to the novel UltraFlex setup (n = 83). Another explanation is that the image quality of the two flexible coil setups highly depends on the inspected part of the head. This results in lower scores for posterior lesions compared to anterior lesions. The mean SNR in the posterior part of the head is also more similar between the setups than in the anterior part of the head, which could explain the similar ratings. Most images rated in this work had their lesions in the posterior part of the head. As no significant difference in the number of detected metastases was found between the setups, the SNR is still high enough to reliably detect the lesions.
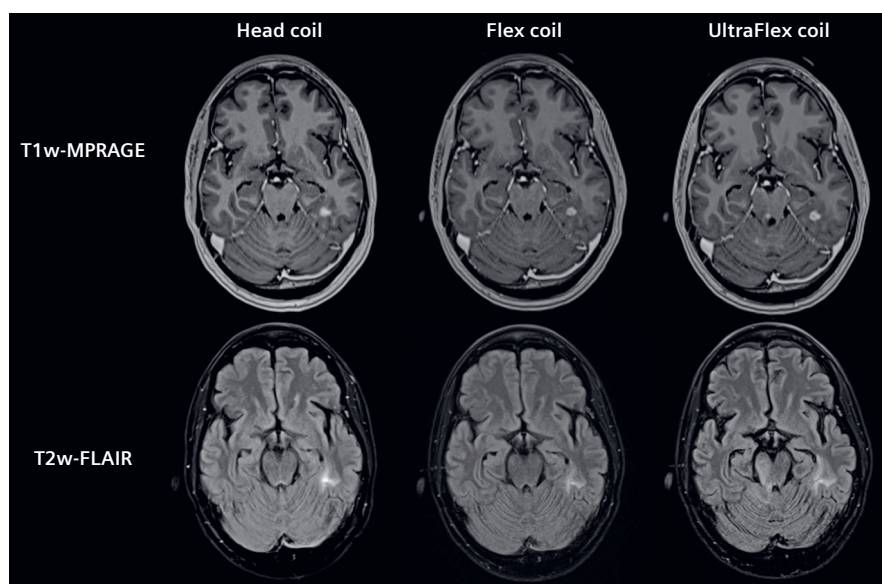
4 Images of a patient in all three investigated setups. The top row shows images of the contrast-enhanced T1w-MPRAGE, while the bottom row shows images of the T2w-FLAIR. The images in the left and middle column were acquired on the same day, the images in the right column were acquired 77 days later. The contrast-enhancing lesion and the FLAIR hyperintensity can be seen clearly in all three setups. While the head coil shows relatively homogeneous SNR, the noise in both mask setups increases significantly in anterior-posterior direction.

All coil setups produced images that were suitable for contouring. Our novel setup, however, combines the advantages of the commercially available setup and the standard radiology setup as it allows for high-quality imaging in RT treatment position. Additionally, positioning in a thermoplastic mask leads to reduced motion artifacts. In our case, no motion artifacts were observed in the mask setups, while some groups report movement to be less than 1.5 mm [6].

The current state of the art coil setup for RT treatment planning consists mainly of flexible surface loop coils with a low number of channels [7–9]. They have been reported to have a significantly worse SNR than diagnostic coils [8]. In comparison, the SNR of our novel setup is significantly higher both anteriorly and centrally, and lower posteriorly compared to the diagnostic coil setup, while having the same suitability for contouring. Therefore, our novel setup can be seen as an improvement over the state-of-the-art setup. The setup is also less prone to setup errors, as the coils only fit under the tabletop in a specific way. This reduces the influence of technician dependent coil positioning, which can be a problem for surface flexible loop coils [10].

Another advantage of our setup is the possibility to use almost all mask immobilization systems, which usually don't fit into the diagnostic head coil. For example, our set-up can be extended for head-neck examinations by adding the Body Long coil with the body coil holder to cover the neck area. Different mask systems will most likely need adapters to attach the masks to the tabletop. If not commercially available, these can be built relatively easily, as demonstrated by our in-house built wooden mask holder.

The protocols we developed are in accordance with a recently published consensus paper on MRI simulation [2]. Active shimming, 3D acquisition, and distortion correction were applied whenever possible.

In our brain metastases protocol, we acquire two high-resolution, contrast-enhanced T1w images. Currently, the T1w-MPRAGE is still the most widely used sequence for imaging of brain tumors [11, 12]. However, there is growing evidence that the T1w-SPACE could be superior to the T1w-MPRAGE for intracranial target volume delineation [11, 13, 14]. Therefore, we performed both sequences for brain metastases. While we could see the target volumes better on the T1w-SPACE in most cases, the T1w-MPRAGE still sometimes provided better contrast. The generally superior conspicuity of lesions in the T1w-SPACE in our experience can be largely attributed to the lower contrast between white matter and gray matter. Often it is beneficial to acquire diffusion-weighted images of the whole brain to aid tumor visualization, especially if treatment-related contrast enhancement is present following surgery or radiation. This can be achieved by an EPI-sequence. For a limited field-of-view an additional EPI-ZOOMit can be useful, as it provides better resolution.

The glioma protocol features a high-resolution T2w Dark Fluid that allows high-resolution imaging of the T2w-FLAIR hyperintensity. As this sequence is significantly longer than a standard T2w-FLAIR, we decided to only include one contrast-enhanced T1w sequence. Ideally the T1w-SPACE should be chosen because it has been shown to provide favorable conspicuity and contrast ratio in comparison to the T1w-MPRAGE in patients with gliomas [11]. However, since mostly the acquisition time slot is limited, we chose the T1w-MPRAGE. The EPI-ZOOMit allows high-resolution diffusion imaging of the investigated volume.

Our experiences in fine-tuning the protocols from the starting point of the diagnostic sequence settings showed that standard parameters like TE, TR, or TI are almost always adjusted optimally for radiotherapy uses, too. The voxel resolution in diagnostic sequences, however, can be slightly non-isotropic, which is undesirable for RT purposes. Additional, standard diagnostic sequences often only employ 2D-distortion correction, if any, which is potentially a relic from times when 3D-distortion correction was relatively computationally demanding. Although most sequences come with active shimming enabled by default, the shimming type should be checked for every sequence. As we only changed parameters that could diminish the quality of the imaging and the sequences, we optimized for precision based on diagnostic sequences, the resulting precision should be at least equal to that of the well-established diagnostic sequences. Protocol time is also a major factor in protocol development. Therefore, it is important to get a feeling for which acceleration techniques yield the optimal results for each sequence type. While most sequences in our protocols are accelerated by parallel imaging techniques such as GRAPPA [15], we also tested compressed sensing. The success of this technique highly depends on the sequence it is used on. For the T2w-SPACE used in the prostate protocol, an acceleration factor of 8 with compressed sensing produced high quality images with significantly reduced acquisition time. Compressed sensing resulted in blurred contours of the metastases when applied to the T1w-SPACE in our brain protocols with large acceleration factors and automatic noise reduction. However, using a low compressed sensing acceleration factor of 2.5 with subtle manual noise reduction provided good image quality and reduced scan duration, thereby further improving our RT planning protocol.

The setup presented in this work is optimally suited for an MR-only workflow, where imaging has to be performed in treatment position. The diagnostic image quality that can be achieved with our setup, as well as the possibility to generate head pseudo-CTs based on these images for dose calculation [16–19], make it an optimal choice for MR-only workflows in head treatments. Head-Neck MR-only workflows may be realized by adding the body coil to our setup to produce high quality head-neck images. A prostate

MR-only workflow can also be realized by calculating a pseudo-CT based on the MRI images. This leads to a more efficient workflow, reducing the number of examinations for a patient and therefore avoiding additional ionizing radiation [20]. Vendor-provided automated algorithms to calculate pseudo-CTs are available on our MR scanner that enable MR-only workflows without the need for additional planning CTs and image coregistration [21]. We are currently evaluating the dosimetric accuracy of the pseudo-CTs; while in our experience problems may arise in post-operative situations, other groups have found excellent agreement for focal brain VMAT radiotherapy with $D_{95\%}$ differences of 0.0% [22].

Conclusion

In this work, we presented a novel setup for brain imaging in treatment position with mask immobilization. We showed that with two UltraFlex coils diagnostic image quality in treatment position with mask immobilization can be achieved. By building a mask holder that fits the specific immobilization system, our coil setup could be used for a range of mask systems. We also shared our initial experiences with implementing dedicated RT-planning protocols and presented the core protocols we employed for radiotherapy treatment planning. For the interested reader, a more detailed discussion of the results can be found in our original publication [23].

References

1   Kikinis, R., S.D. Pieper, and K.G. Vosburgh, 3D Slicer: A Platform for Subject-Specific Image Analysis, Visualization, and Clinical Support, in Intraoperative Imaging and Image-Guided Therapy, F.A. Jolesz, Editor. 2014, Springer New York: New York, NY. p. 277-289.
2   Paulson, E.S., et al., Consensus opinion on MRI simulation for external beam radiation treatment planning. Radiother Oncol, 2016. 121(2): p. 187-192.
3   Snell, J.W., et al., Assessment of imaging studies used with radiosurgery: a volumetric algorithm and an estimation of its error. Technical note. J Neurosurg, 2006. 104(1): p. 157-62.
4   Emmerich, J., et al., Technical Note: On the size of susceptibility-induced MR image distortions in prostate and cervix in the context of MR-guided radiation therapy. Med Phys, 2018. 45(4): p. 1586-1593.
5   Walker, A., et al., MRI distortion: considerations for MRI based radiotherapy treatment planning. Australas Phys Eng Sci Med, 2014. 37(1): p. 103-13.

Contact

Professor Christoph Bert, Ph.D.
Department of Radiation Oncology
Friedrich-Alexander-University Erlangen-Nuremberg
Universitaetsstraße 27
91054 Erlangen
Germany
Phone: +49 (0)9131 85-44213
Christoph.bert@uk-erlangen.de

6   Mandija, S., et al., Brain and Head-and-Neck MRI in Immobilization Mask: A Practical Solution for MR-Only Radiotherapy. Front Oncol, 2019. 9(647): p. 647.
7   Liney, G.P., et al., Commissioning of a new wide-bore MRI scanner for radiotherapy planning of head and neck cancer. Br J Radiol, 2013. 86(1027): p. 20130150.
8   Wong, O.L., et al., Image quality assessment of a 1.5T dedicated magnetic resonance-simulator for radiotherapy with a flexible radio frequency coil setting using the standard American College of Radiology magnetic resonance imaging phantom test. Quant Imaging Med Surg, 2017. 7(2): p. 205-214.
9   Winter, R.M., et al., Assessment of image quality of a radiotherapy-specific hardware solution for PET/MRI in head and neck cancer patients. Radiother Oncol, 2018. 128(3): p. 485-491.
10 Ruytenberg, T., et al., Improvements in High Resolution Laryngeal Magnetic Resonance Imaging for Preoperative Transoral Laser Microsurgery and Radiotherapy Considerations in Early Lesions. Front Oncol, 2018. 8: p. 216.
11 Danieli, L., et al., Brain Tumor-Enhancement Visualization and Morphometric Assessment: A Comparison of MPRAGE, SPACE, and VIBE MRI Techniques. AJNR Am J Neuroradiol, 2019. 40(7): p. 1140-1148.
12 Ellingson, B.M., et al., Consensus recommendations for a standardized Brain Tumor Imaging Protocol in clinical trials. Neuro Oncol, 2015. 17(9): p. 1188-98.
13 Reichert, M., et al., Contrast-enhanced 3-dimensional SPACE versus MP-RAGE for the detection of brain metastases: considerations with a 32-channel head coil. Invest Radiol, 2013. 48(1): p. 55-60.
14 Komada, T., et al., Contrast-enhanced MR imaging of metastatic brain tumor at 3 tesla: utility of T(1)-weighted SPACE compared with 2D spin echo and 3D gradient echo sequence. Magn Reson Med Sci, 2008. 7(1): p. 13-21.
15 Griswold, M.A., et al., Generalized autocalibrating partially parallel acquisitions (GRAPPA). Magn Reson Med, 2002. 47(6): p. 1202-10.
16 Maspero, M., et al., Dose evaluation of fast synthetic-CT generation using a generative adversarial network for general pelvis MR-only radiotherapy. Phys Med Biol, 2018. 63(18): p. 185001.
17 Dinkla, A.M., et al., MR-Only Brain Radiation Therapy: Dosimetric Evaluation of Synthetic CTs Generated by a Dilated Convolutional Neural Network. Int J Radiat Oncol Biol Phys, 2018. 102(4): p. 801-812.
18 Dowling, J.A., et al., Automatic Substitute Computed Tomography Generation and Contouring for Magnetic Resonance Imaging (MRI)-Alone External Beam Radiation Therapy From Standard MRI Sequences. Int J Radiat Oncol Biol Phys, 2015. 93(5): p. 1144-53.
19 Koivula, L., et al., Intensity-based dual model method for generation of synthetic CT images from standard T2-weighted MR images - Generalized technique for four different MR scanners. Radiother Oncol, 2017. 125(3): p. 411-419.
20 Hanvey, S., et al., The influence of MRI scan position on patients with oropharyngeal cancer undergoing radical radiotherapy. Radiat Oncol, 2013. 8: p. 129.
21 Hsu, S.H., et al., Investigation of a method for generating synthetic CT models from MRI scans of the head and neck for radiation therapy. Phys Med Biol, 2013. 58(23): p. 8419-35.
22 Paradis, E., et al., Assessing the Dosimetric Accuracy of Magnetic Resonance-Generated Synthetic CT Images for Focal Brain VMAT Radiation Therapy. Int J Radiat Oncol Biol Phys, 2015. 93(5): p. 1154-61.
23 Mengling, V., et al., Implementation of a dedicated 1.5T MR scanner for radiotherapy treatment planning featuring a novel high-channel coil setup for brain imaging in treatment position. Strahlenther Onkol 197, 246 -256 (2021). https://doi.org/10.1007/s00066-020-01703-y

Clinical Evaluation of a Receiver Coil Custom Designed for MR Simulation of Immobilized Patients

James M Balter[1,2]; Dinank Gupta[2]; Michelle M Kim[1]; James A Hayman[1]; Karen Vineberg[1]; Yue Cao[1,2]; Daniel Gareis[3]; Dan Coppens[4]

[1]Department of Radiation Oncology, University of Michigan, Ann Arbor, MI, USA
[2]Department of Biomedical Engineering, University of Michigan, Ann Arbor, MI, USA
[3]NORAS MRI products GmbH, Höchberg, Germany
[4]Qfix, Avondale, PA, USA

Introduction

There has been significant adoption and/or adaptation of MR scanners to support the needs of Radiation Oncology treatment simulation. A plethora of MR-compatible immobilization devices and phantoms have been developed and imaging sequences have been customized to better suit the needs of supporting planning and guidance of precision radiation treatments. In addition, a number of synthetic CT generation tools have been released commercially. To date, however, little has been done to customize RF coils to better suit the needs of scanning patients immobilized for radiation therapy treatment. This issue was noted as one potential concern for maintaining consistent image quality for scanning certain body sites, most notably the head and neck region. Most existing coil combinations suffer from challenges including increased

claustrophobia due to placing coils in high proximity to the patient's eyes, poor SNR due to contributing coil elements being placed distal to the anatomy being scanned, image intensity non-uniformities and technical challenges for reproducibly and conveniently assembling coil combinations around the patient [1].

While a few attempts have been made at customizing existing coil combinations and/or building unique holders for use of existing coils [2], very little effort has been placed in truly optimizing receiver coils for radiation therapy simulation purposes. The introduction of a flexible coil that can be integrated into an immobilization mold has demonstrated the promise of such technology for radiation therapy simulation [3]. To date, however, no such coils have been developed with intracranial radiation
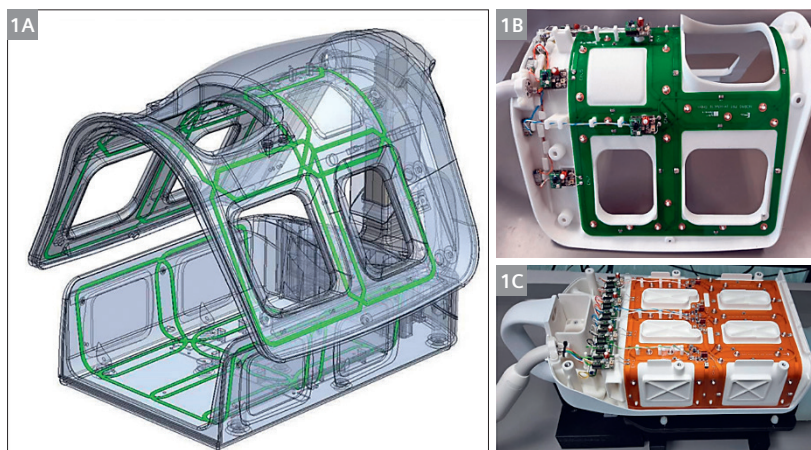
1 Schematic diagram of Encompass receiver coil (1A), as well as pictures of the compositions of the anterior (1B) and posterior (1C) structural elements.

therapy in mind. This report describes a novel coil that was designed to be conveniently integrated with a commonly used commercially available immobilization system. The performance of this coil on phantom as well as patient images, as well as utility to support MR-only simulation for precise treatment of intracranial tumors, is reported.

Methods

The Encompass coil[1] was developed in partnership with two companies (Qfix and NORAS), with specifications developed specifically to support scanning of patients immobilized using the Encompass™ line of cranial immobilization equipment. The coil consists of two separate components, an anterior 7-channel coil and a posterior 8-channel coil. A design diagram and internal images of the coil are shown in Figure 1. The coil was designed to minimize B_0 and B_1 distortions, and incorporate low-noise preamplifiers, active and passive decoupling, and a safety fuse in each channel. The patient is positioned with the posterior component in place, and the anterior section is then attached via a height-adjustable stand. To reduce noise and increase comfort, patients are given ear plugs prior to being placed in their immobilization masks. Figure 2 shows an example image of a patient being positioned in the coil for MR Simulation.

To evaluate the performance of this coil, a series of patient and phantom scans were performed. The ACR standard phantom was scanned using the Encompass coil on a 3T MRI Simulator (MAGNETOM Skyra, Siemens Healthcare, Erlangen, Germany), and resulting images compared to those acquired using a standard 20-channel head and neck coil as well as a combined anterior 18-channel surface coil and 8 elements of a posterior spinal coil in a configuration compatible with scanning

---

[1]While this study has been performed using the prototype coil, the Qfix Encompass 15-channel Head Coil is released and available for sale.

patients immobilized in masks for Radiation Oncology treatment [4], referred to herein as RTCombo.

Under an institutional review board-approved protocol, a series of 10 patients with intracranial tumors who were scheduled for stereotactic treatment were scanned using the Encompass coil following conventional CT-based simulation for intracranial stereotactic treatment planning. Standard T1-weighted post-contrast, T2 FLAIR, diffusion-weighted (using an echo planar sequence), and T1 VIBE Dixon images (in support of synthetic CT generation for MRI-only treatment planning and positioning support) were acquired. A subset of these patients were further scanned, without immobilization, using the 20-channel head and neck coil.

Diffusion-weighted images (at b = 0 s/mm^2) were analyzed to estimate the relative signal to background ratio, which was compared to measurements of equivalent images from other subjects scanned using the 20-channel head and neck coil under different research protocols.

Synthetic CT image volumes were generated using a Unet architecture previously trained on 6500 MR-CT image pairs, from T1-weighted (in-phase) images acquired using the VIBE Dixon sequence [5]. These images were compared to simulation CT scans acquired for radiosurgical treatment planning for intensity similarity, accuracy of dose calculation, and accuracy of supporting alignment to Cone Beam CT (CBCT) scans used for patient positioning. The synthetic CT scans were spatially aligned to the treatment planning CT scans using rigid body transforms. Using a previously reported comparison method [4], treatment plans were generated using the synthetic CT scans for attenuation mapping. These plans were then re-calculated using attenuation mapped from the treatment planning CT scans, and the resulting differences in dose recorded.

The cone beam CT (CBCT) image volumes used to support patient positioning for treatment for these subjects were spatially aligned to the CT as well as synthetic CT scans, and the differences in the transformations were recorded.
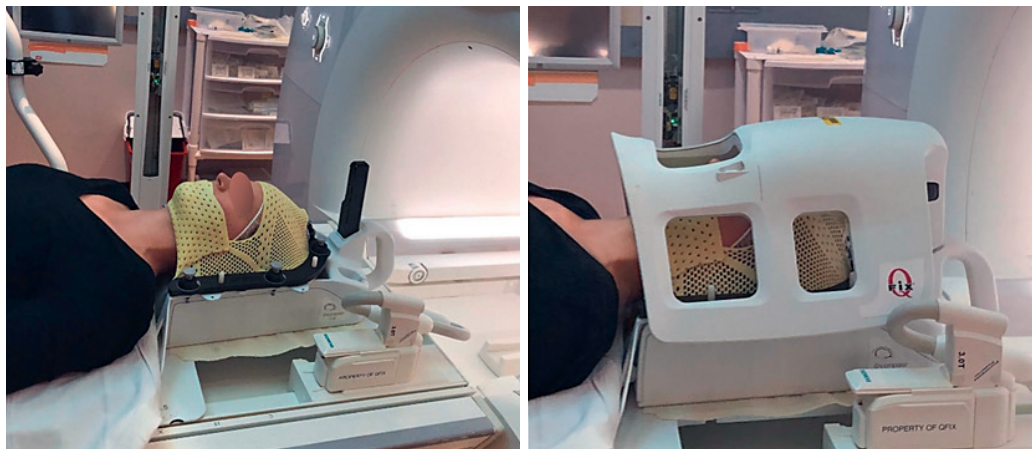
2 Example patient positioning using the Encompass coil. The immobilization frame is indexed to the posterior coil section, and the anterior coil is subsequently attached via a height-adjustable connection.

Results

Figure 3 shows images from the various sections of the ACR phantom from the Encompass coil as well as the 20-channel coil. All tests passed successfully. Figure 4 shows images from the uniform section of the phantom scanned with the Encompass, 20-channel head and neck, as well as combined anterior surface and posterior spine coils. The prototype coil passed all ACR phantom test criteria. SNR values, measured in the center of the uniform section of the phantom, were 88.5, 89.9 and 44.4 for the prototype, 20-channel and RTCombo coils, respectively.

Human subject images (examples shown in Figure 5) were qualitatively reviewed by a physician specializing in intracranial treatment and deemed to be of sufficient quality for clinical use. Analysis of ADC maps from DWI showed higher signal to background ratio for the prototype coil (20.7) versus the 20-channel coil (15.6). Figure 6

shows a comparison of a synthetic CT scan, generated from the T1 VIBE images, to the corresponding clinical CT scan acquired for simulation.

The synthetic CT image volumes compared well with simulation CT scans, with average Mean Absolute Error values of 4.7, 180.5 and 5.7 HU in regions of brain parenchyma, skull, and ventricles across the 10 patients studied, similar to those reported using a 20-channel head and neck coil for non-immobilized patients [5]. Figure 7 shows an example of a treatment plan generated using the synthetic CT from the Encompass coil-acquired VIBE images, as well as that plan with dose re-calculated using the attenuation map generated from the treatment planning CT scan. Treatment plan comparisons across the 10 patients showed dose differences of 2.3 +/-0.9% of the mean dose to the planning target volumes, with the systematic mean dose variation primarily due to the lack of the immobilization frame in the synthetic CT image volumes.
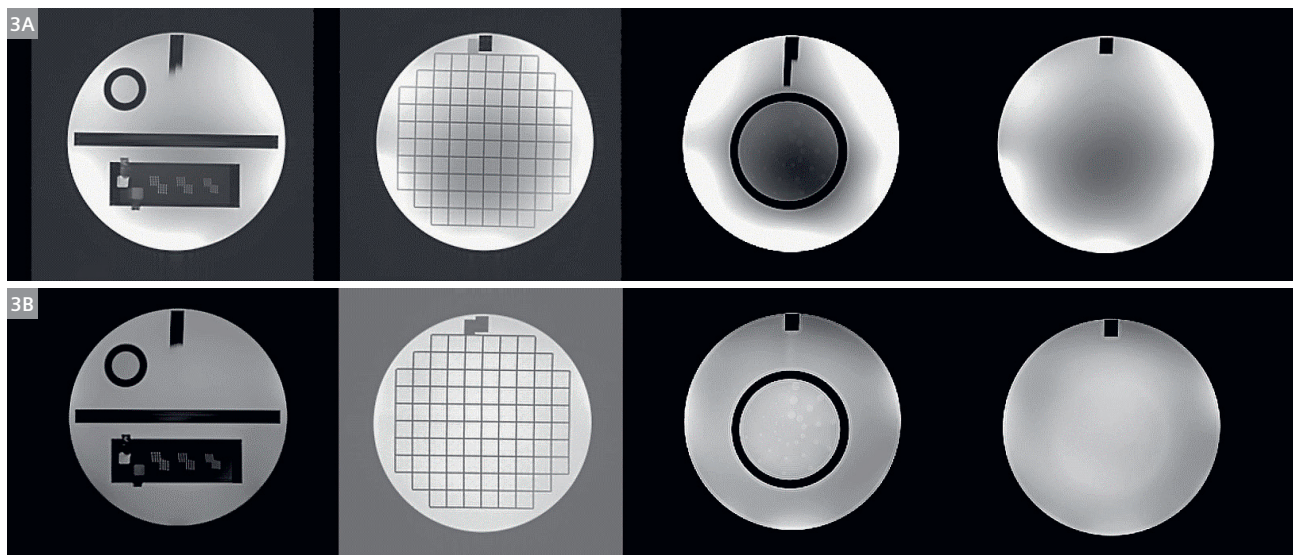
3 Sections of the ACR QA phantom scanned with the Encompass coil **(3A)** and 20-channel conventional Head and Neck coil **(3B)**.
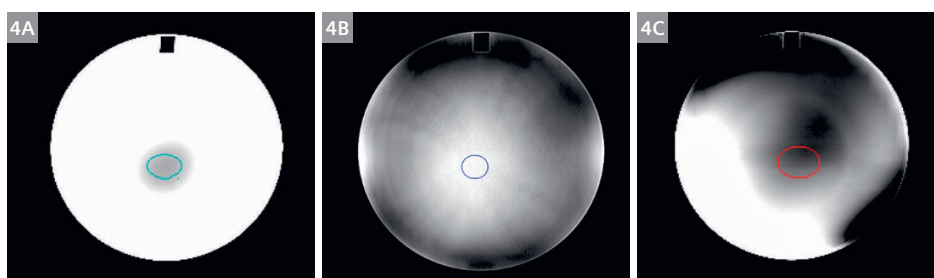
4 Uniform sections of the ACR phantom and regions of interest (contours) used to assess SNR from the **(4A)** Encompass, **(4B)** 20-channel head and neck coil, and **(4C)** RTCombo coil combination.
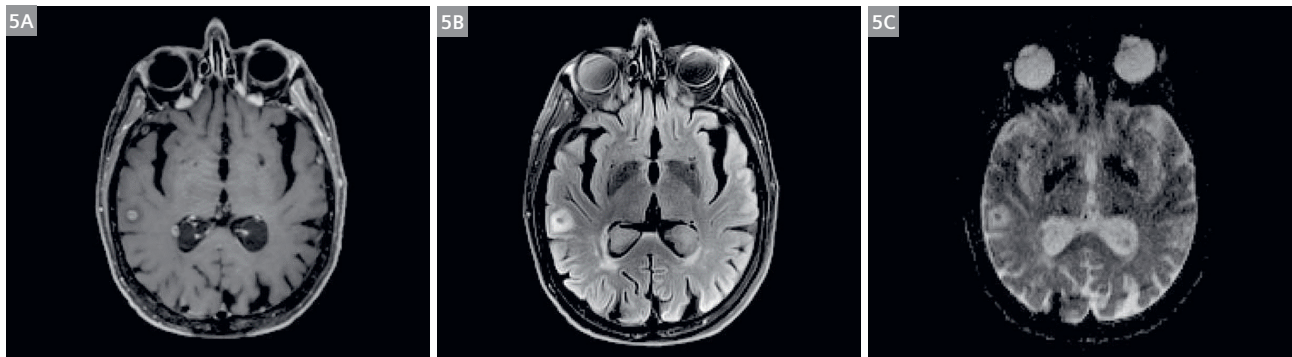
5 Example T1-weighted post contrast **(5A)** and Fluid Attenuated Inversion Recovery **(5B)** images, along with a map of Apparent Diffusion Coefficients **(5C)** for a subject acquired using the Encompass coil.
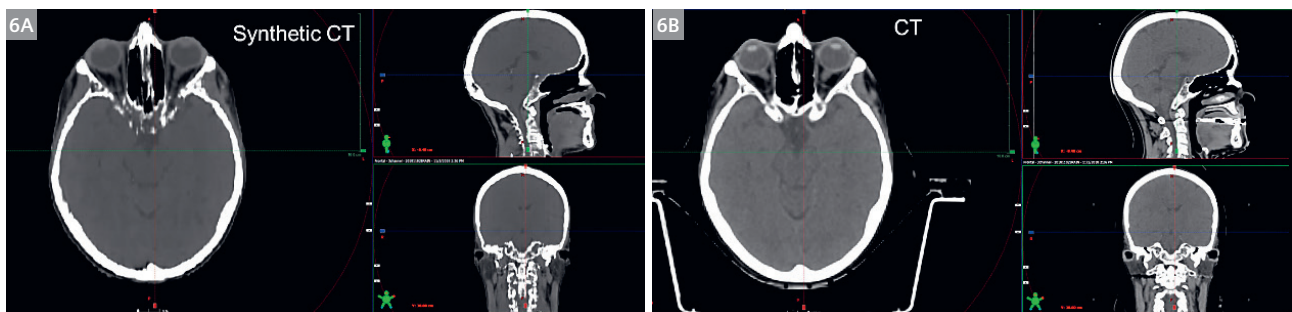
6 Example synthetic CT image volume **(6A)** generated from images acquired with the Encompass coil and actual CT **(6B)** acquired for treatment planning.
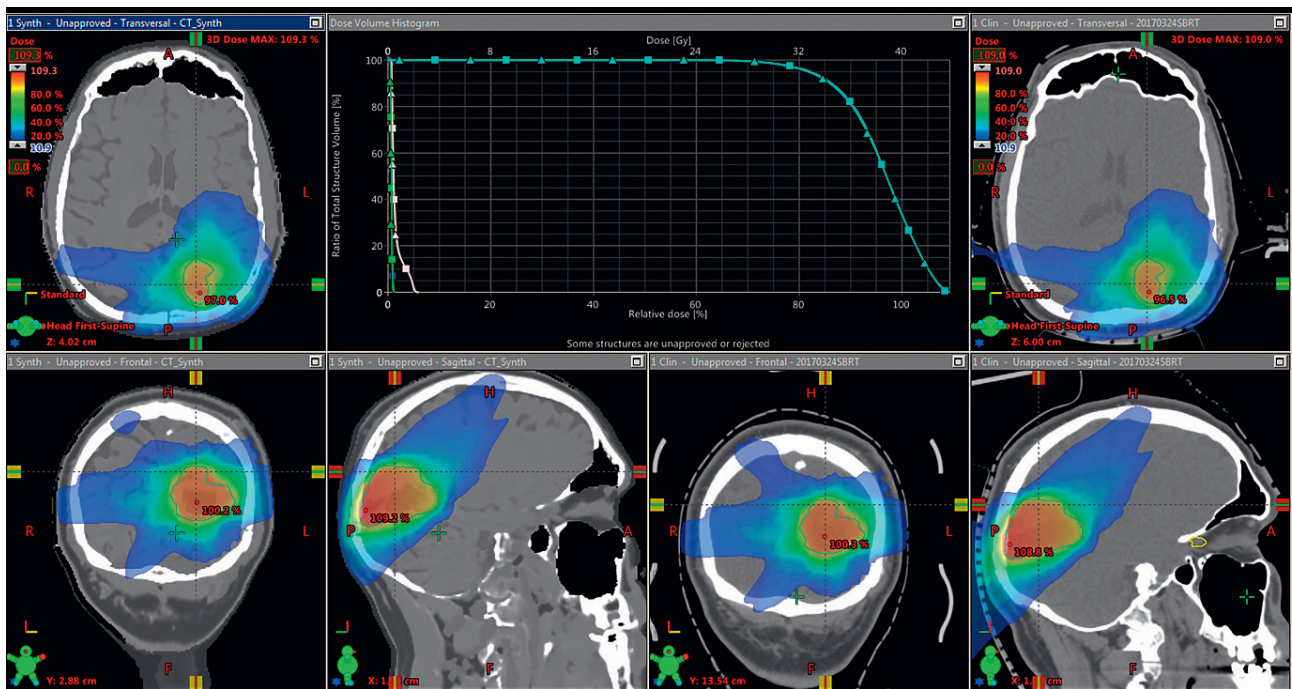
7 Comparison of dose distributions for a plan generated using the synthetic CT from the Encompass coil simulation (left, plan "1 Synth") with that from the treatment fluences used to recalculate dose using the attenuation map from the clinical CT scan (right, plan "1 Clin"). Dose volume histograms are shown for the synthetic CT (squares) and clinical (triangles) plans for the treatment target (blue), brainstem (white) and optic chiasm (green).
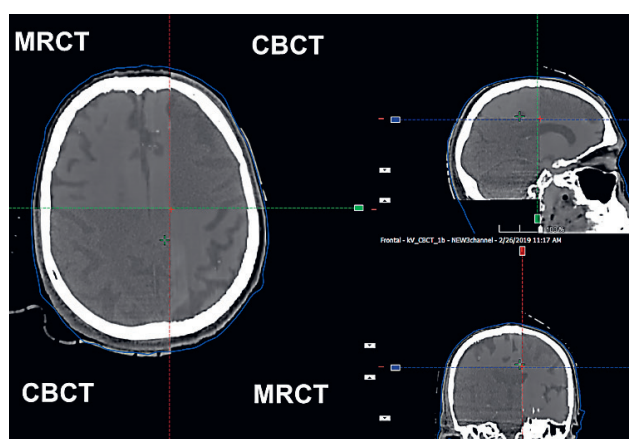
8 Example alignment of a synthetic CT (MRCT) generated from VIBE Dixon images acquired using the Encompass coil with a cone beam CT (CBCT) scan acquired for patient positioning.

	Left-Right	Ant-Post	Inf-Sup
mean	-0.04	0.00	0.07
σ	0.14	0.20	0.23
min	-0.3	-0.5	-0.3
max	0.3	0.4	0.5

Table 1: Differences between CBCT-CT and CBCT-synthetic CT alignments applied to target centers (mm)

Figure 8 shows an example alignment of synthetic CT with CBCT from a treatment. Table 1 summarizes the differences between CBCT-CT and CBCT-synthetic Alignment. A mean difference between CT and Synthetic CT of 0.1 mm (standard deviation of 0.3 mm) was observed across all patients.

Conclusion

Tests performed on the Qfix Encompass coil[1], designed to support MR simulation for immobilized patients, demonstrated image quality comparable to commercial general purpose coils for clinical use for precision radiation therapy of intracranial stereotactic treatment targets. Synthetic CT images generated using this coil are sufficiently similar to CT scans to support MR-only treatment planning and image guided patient positioning for radiosurgery.

Acknowledgments

References

1 Glide-Hurst CK, Paulson ES, McGee K, et al. Task Group 284 Report: Magnetic Resonance Imaging Simulation in Radiotherapy: Considerations for Clinical Implementation, Optimization, and Quality Assurance. Med Phys. 2021.
2 Paulson ES, Erickson B, Schultz C, Allen Li X. Comprehensive MRI simulation methodology using a dedicated MRI scanner in radiation oncology for external beam radiation treatment planning. Med Phys. 2015;42(1):28-39.
3 Tyagi N, Zakian KL, Italiaander M, et al. Technical Note: A custom-designed flexible MR coil array for spine radiotherapy treatment planning. Med Phys. 2020;47(7):3143-3152.
4 Paradis E, Cao Y, Lawrence TS, et al. Assessing the Dosimetric Accuracy of Magnetic Resonance-Generated Synthetic CT Images for Focal Brain VMAT Radiation Therapy. Int J Radiat Oncol Biol Phys. 2015;93(5):1154-1161.
5 Gupta D, Kim M, Vineberg KA, Balter JM. Generation of Synthetic CT Images From MRI for Treatment Planning and Patient Positioning Using a 3-Channel U-Net Trained on Sagittal Images. Front Oncol. 2019;9:964.
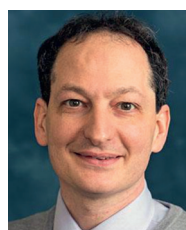
Contact

James M. Balter, Ph.D., FAAPM
Professor and Associate Chair
for Physics Research
Department of Radiation Oncology
University of Michigan
Tel.: +1 (734)936-9486
jbalter@umich.edu

Implementation of a Process for Radiosurgery Incorporating Functional Magnetic Resonance Imaging

Ricardo Ruggeri, MSc.[1]; Elira Lomban, M.D.[2]; Belen Ibañez, M.D.[3]; Marcelo Paolini[4]; Silvia Hansing, M.D.[5]

[1]Medical physics department, Leben Salud, Patagonia, Argentina
[2]Nuclear magnetic resonance department, Leben Salud, Patagonia, Argentina
[3]Neuroradiology department, Leben Salud, Patagonia, Argentina
[4]Multimodal images post-processing department, Leben Salud, Patagonia, Argentina
[5]Radiotherapy department, Leben Salud, Patagonia, Argentina

Introduction

The history of radiosurgery as an option for radiotherapy treatment has its origins in the 1950s, in the work of a Swedish team led by neurosurgeon Lars Leksell. The technique was defined as "the destruction of an intracerebral target, localized stereotactically, without craniotomy, in a single fraction of ionizing radiation, delivered through a system of convergent beams in the target".

Technological advances for radiosurgery in linear accelerators were led by Derechinsky and Betti in Buenos Aires, Argentina. In 1982, they developed and adapted the non-coplanar beams technique using this equipment. In the same period, major advances in computation and in CT and MR imaging occurred, which triggered an explosion in the development and use of radiosurgery, improving and assuring the localization of small lesions and simplifying management.

The incorporation of six-degrees-of-freedom robotic couches, multileaf collimators (MLC), and tridimensional imaging systems like cone beam CT in modern linear accelerators created a need for high-quality medical images that would improve the delineation of the target and organs at risk (OARs).
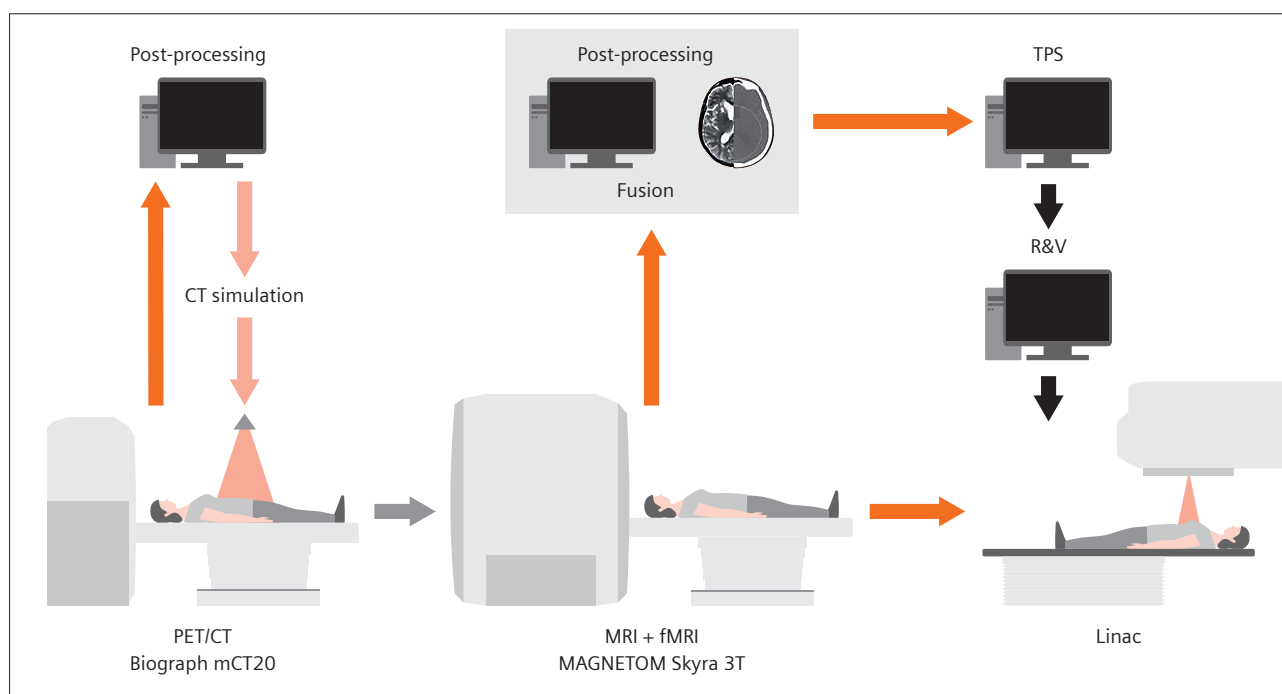
1 The SRS process at COI, integrating fMRI.

Multimodality imaging has been enormously relevant in cutting-edge radiosurgery procedures. Magnetic resonance imaging (MRI) has prevailed over other modalities for its ability to incorporate different acquisition sequences into the same exam. This allows the use of functional magnetic resonance imaging (fMRI), which can be used by radiotherapists to determine dose prescription, and by medical physicists to optimize treatment in the treatment planning system (TPS).

These developments are the result of a clear need not just to preserve the maximum amount of healthy brain parenchyma, but also to know the exact location of eloquent areas related to motor, visual, language, and memory functions. These areas can then be taken into account during treatment planning and patient follow-up.

Enabling our patients to remain active in society, with minimum impact to their quality of life, was our motivation to include cerebral fMRI in our radiotherapy planning protocol.

In the following article, we discuss the benefits of performing fMRI when planning stereotactic radiosurgery (SRS) in patients with primary or secondary brain tumors. We also provide the necessary information regarding implementation protocols.

Problems and challenges

Initially, MRI was used to identify small lesions and to accurately segment these lesions and the surrounding OARs. However, incorporating MRI raised new technical issues that should be taken into account, such as:
- geometrical distortion of the image due to the equipment's characteristic gradients;
- the use of MRI-compatible immobilization devices;
- incorporation of post-processing software that works with multimodality images (CT, PET, etc.), and its corresponding registration and deformable fusion;
- coil configuration for adaptation to SRS immobilization devices;
- sequence and/or acquisition protocol design to achieve a 3D isotropic reconstruction with high resolution and high signal-to-noise ratio.

There are also a number of common obstacles, such as access to an MRI scanner. Indeed, few radiotherapy institutions possess exclusively or even partially dedicated MRI scanners.

Another aspect to consider is the training of MRI technologists, who must understand the image-quality requirements for radiosurgery and how to handle patients when using immobilization devices.

Finally, the issue of reimbursement of MRI must also be considered, as this is an essential factor in deciding whether to use this particular treatment technique.

Technology and general workflow

The radiosurgery process at Centro Oncológico Integral (COI) starts with the patient's CT simulation using a Biograph mCT 20 PET/CT scanner. A CT or PET/CT scan is performed according to the radiotherapist's request, and single or multiple treatment isocenters are located with five mobile lasers, which move in the three Cartesian axes. The CT images and the isocenter location(s) are stored in the *syngo*.via RT Image Suite (RTiS) workflow.

Afterwards, the patient is scanned with the 3T MRI scanner (MAGNETOM Skyra, Siemens Healthcare, Erlangen, Germany). The specific acquisition sequences include fMRI for accurate structure contouring and delineation of eloquent areas or regions.

During post-processing, bioimaging graduates register multimodality images, segment OARs, and obtain fMRI results using *syngo*.via post-processing workflows. The radiotherapists then contour the lesions with their respective margins – gross tumor volume (GTV), clinical target volume (CTV), and planning target volume (PTV) – and decide on the best therapeutic strategy.

All the information is consolidated in the *syngo*.via RTiS workflow and exported to the TPS, where medical physicists perform planning and validation using a patient-specific QA. Once all verifications and relevant controls have been carried out, patient irradiation in the linear accelerator occurs.

The process requires uniform positioning criteria, MRI-compatible immobilization devices, and the availability of flat indexed couches. It also demands connectivity between acquisition software, image post-processing software, treatment planning system, and the record-and-verify system.

Connectivity with the radiosurgery TPS is crucial, especially when image sequences and contoured structures are exported from the post-processing system.

In what follows, we will describe the subprocess of fMRI for SRS, including the acquisition of the fMRI sequence, the results, and their use in the RT workflow with *syngo*.via RTiS.

Physical principles of fMRI

fMRI can help to preserve eloquent areas by locating visual, motor, and language functions. This is done by using specific paradigms for each function and the blood-oxygen-level-dependent (BOLD) technique.

BOLD signal obtained in fMRI uses the endogenous paramagnetic contrast agent, deoxyhemoglobin.

Motor, verbal, or visual stimulation paradigms activate the motor cortex, which increases cerebral blood flow and local oxygen consumption. This causes a rise in deoxy-

hemoglobin concentration in the capillary veins, which leads to a T2* signal loss caused by magnetic susceptibility.

Gradient-echo sequences are most sensitive to the magnetic susceptibility phenomenon. They are typically echo-planar-imaging (EPI) sequences that allow whole-brain coverage with good temporal resolution and minimal risk of motion artifacts.

The fMRI examination includes a stimulation paradigm for each cerebral area of interest. The most frequently used paradigms are motor, verbal, and/or visual.

Each of these paradigms involves a task that must be explained thoroughly to the patient, who then practices it before the acquisition.

During the examination, stimulus periods of 30 seconds are alternated with 30 seconds of rest. This is repeated for a maximum of seven minutes, and constitutes a paradigm.
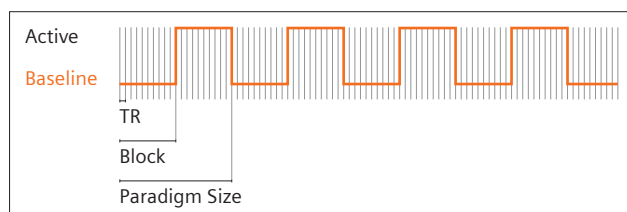
2 Schematic representation of a block design: The orange curve represents active blocks (Task ON) and baseline blocks (Task OFF). The points between the vertical lines represent measurements of cerebral volumes, which take some time to acquire. Here we can see ten measurements per block, with a total of 90 measurements. The size of the paradigm is a vectorial parameter in the BOLD sequence chart, which represents the state OFF+ON. In this example, the size of the paradigm would have ten baseline measurements and ten active measurements (= 20).
Reproduced with permission from MAGNETOM Flash (75) 4/2019 How-I-do-it, Clinical fMRI: Where do I start? Victoria Sherwood and Tina Pavlin, NordicNeuroLab AS, Bergen, Norway.
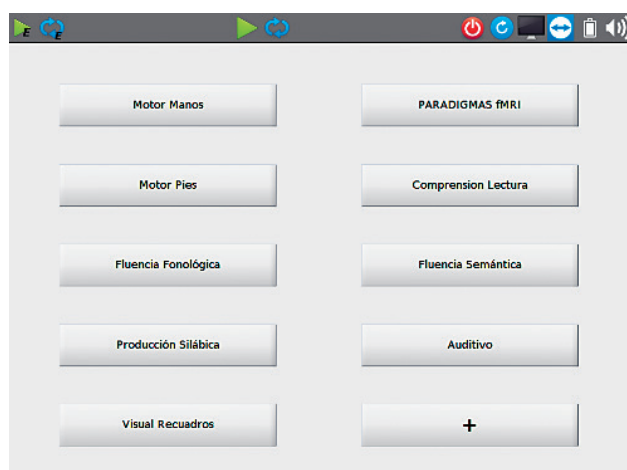
3 Paradigm menu, for study and training.

Exam preparation

Prior to entering the scanner room, the patient spends roughly 15 minutes practicing each of the paradigms to be executed during the exam. This is to ensure that they understand the task so the exam will succeed.

The paradigm must be programmed (Fig. 3) to show the right activity at the moment of the stimulus, according to which part of the brain is to be stimulated: moving the hands and feet for the motor paradigm (this can include opening or closing the fists, flexing and extending the toes, or pressing the thumb against each finger in an exaggerated manner); choosing the correct verb or adjective in a simple sentence for the verbal paradigm; and being exposed to flash-like visual stimuli with a black-and-white grid for the visual paradigm.

Exam protocol

The protocol includes three essential sequences that must be executed at the beginning of the exam to enable correct post-processing:
- ANATOMY t1_mprage_sag_p2_iso
- FIELD MAP gre_field_mapping.
- BOLD ACTIVATIONS ep2d_bold_moco_p2_s2

The paradigms are executed in approximately 30 minutes. The t1_mprage_sag_p2_iso sequence is acquired as an anatomical map that will demonstrate the corresponding activations; a 3D FLAIR isotropic sequence can also be used for the same purpose. The field map (GRE field mapping) contains data for motion correction (MOCO, **Mo**tion**Co**rrection). BOLD activation sequences demonstrate the corresponding function for each paradigm (Fig. 4). BOLD sequences are adapted according to the paradigm. This affects the number of measurements (Fig. 2), which translates into either an increase or decrease in acquisition time.

Acquisition

After the patient has practiced the paradigms, they are positioned in the MRI scanner in a room containing all the necessary equipment. The exam can then begin. We use a 32-channel head coil, shown in Figure 6A, which delivers images with a higher signal-to-noise ratio. The coil is fitted with a mirror (orange arrow) that displays the different paradigms to the patient. Figure 6B shows the MAGNETOM Skyra workstation with software version *syngo*.MR E11.

The paradigms are displayed to the patient on the screen (retro projection). Figures 7A and 7B show the verbal and motor paradigms, respectively. After acquisition of localizer, anatomy, and field map sequences (Fig. 4), the generation of specific BOLD sequence paradigms begins (Fig. 7).
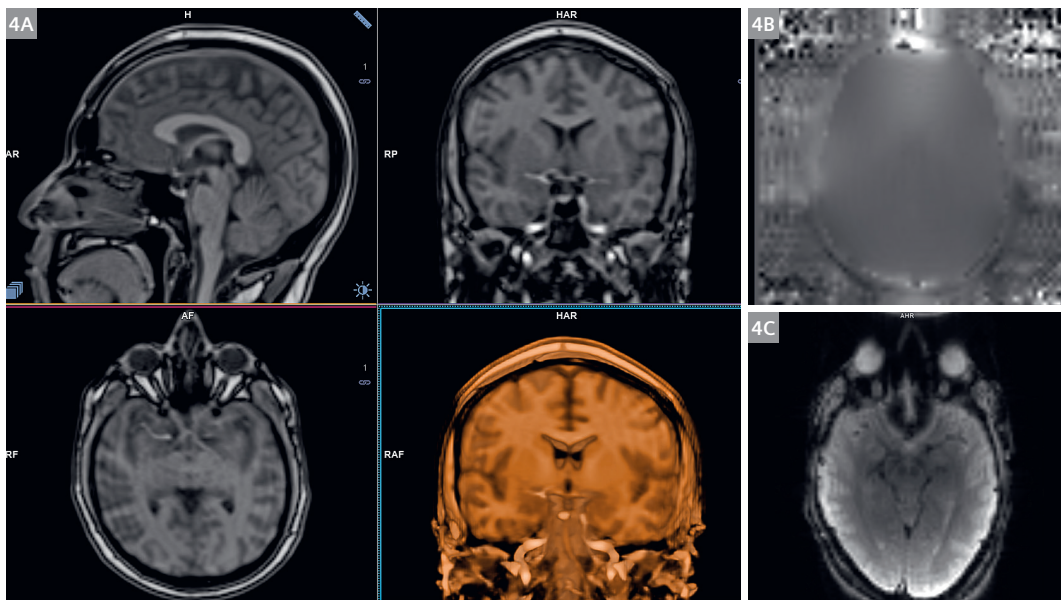
4 Anatomy (4A), field map (4B), and BOLD sequences (4C).
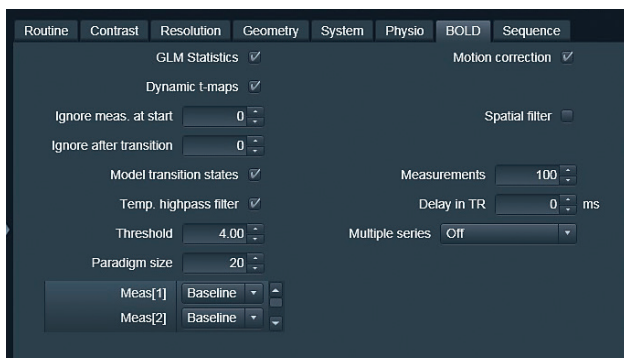
5 BOLD sequence configuration with 100 measurements, a paradigm size of 20, and motion correction.

Sequences and acquisition times

Sequence	Voxel size	Number of slices	FoV	Acquisition time
T1 MPRAGE AXIAL	0.9 x 0.9 x 0.9 mm	176	240	5:00 min.
GRE FIELD MAPPING	3.4 x 3.4 x 3.0 mm	36	220	0.54 min.
BOLD ep2d	2.3 x 2.3 x 3.0 mm	52	220	7:00 min.

Table 1: Essential sequences for an fMRI exam using a MAGNETOM Skyra 3T scanner.
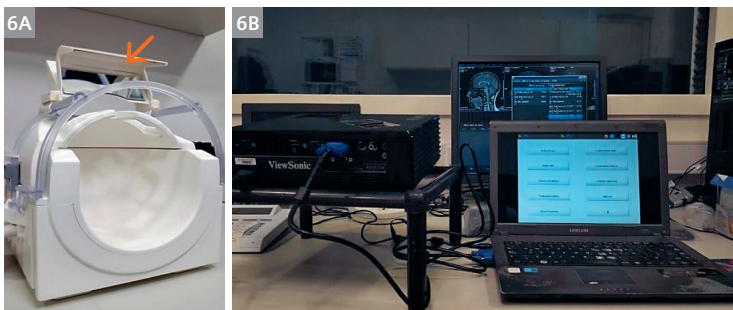
6 (6A) The 32-channel head coil with mirror (orange arrow) for displaying the projected image inside the room. (6B) MAGNETOM Skyra workstation, projector, and laptop for activating the corresponding paradigms.
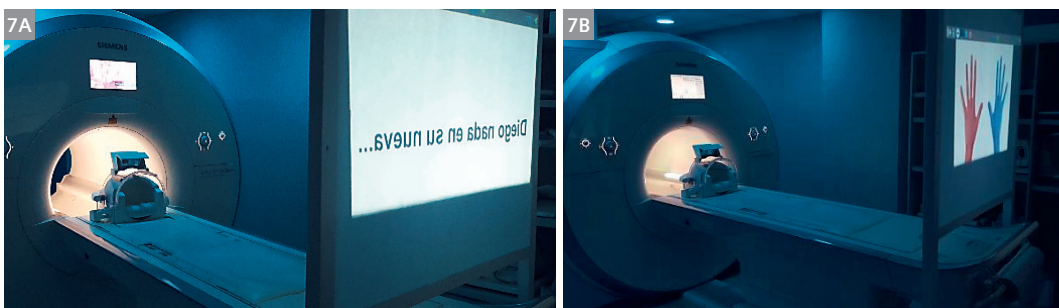
7 Verbal paradigm (7A) and motor paradigm (7B).

syngo.MR Neuro 3D workflow post-processing

After finishing the MRI exam with the paradigms corresponding to the areas of interest, image post-processing begins. This involves loading the images into *syngo*.via (software version VB30) and using *syngo*.MR Neuro 3D (Fig. 8).

The paradigms requiring assessment are then selected – for example, the visual paradigm (Fig. 9).

Activations can be visually evaluated and quantified using the volume of interest (VOI) measurement as seen in the example in Figure 10.

The curve obtained shows consecutive stages of activation and rest during the paradigm.

The paradigms cause brain activations in the association, coordination, and motion-initiation areas. Activations in satellite areas that do not match the study's paradigm also occur. These can be differentiated from activations of interest by assessing the activation-rest curve with adapted VOI (Fig. 11).

Figure 11 shows an area of brain parenchyma where VOI does not indicate activation for the studied paradigm.

Next, two examples (Figure 12) of activations that are useful for contouring eloquent areas.

8 *syngo*.MR Neuro 3D with the visual paradigm loaded.
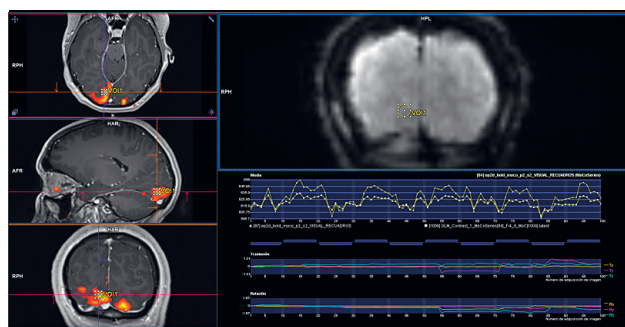
10 VOI measurement for the visual paradigm (VOI used for dynamic evaluation).

9 Sequence selection for post-processing.
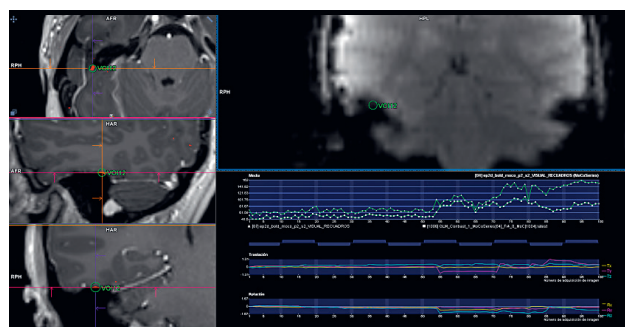
11 VOI showing an uptake area not related to the activation paradigm studied.
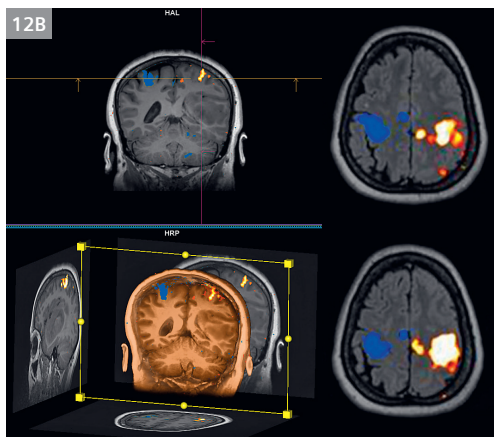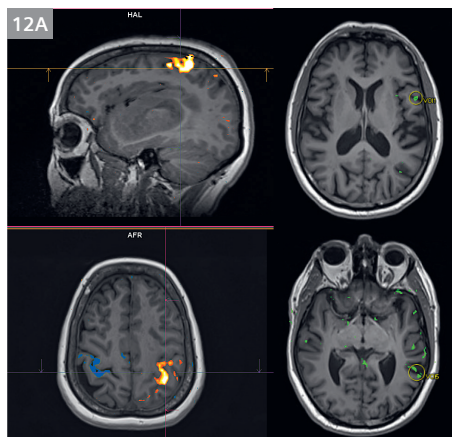
12 **(12A)** Pulmonary secondary tumor; verbal paradigm involving reading comprehension, identifying Broca and Wernicke's areas in the left hemisphere, dominant; **(12B)** Glioma patient, tumor not seen in this slice; motor paradigm activation of both hands; BOLD signal in primary motor areas obtained bilaterally; the activation area of the left hand is represented in blue, and the right hand in yellow.

syngo.via RT Image Suite workflow

Once the images with the activated areas have been obtained, they are transferred in DICOM RGB format from *syngo*.MR Neuro 3D to *syngo*.via RTiS and registered with the patient's CT images acquired during CT simulation. The activated areas can be then contoured and the contours are automatically shown in the planning CT images. After that, the target volume and tumors are also delineated.

In this part of the process, the T1 MPRAGE sequence is fused with CT images and delineates OARs, such as the hippocampus (Fig. 13). Reconstruction (VRT) is also performed for assessment, as shown in Figure 14.

Discussion

For years, radiation oncologists have thoroughly contoured tumors on images, while understanding that OAR contouring is also important for successful treatment. Healthy organs limit the final prescription dose, which is linked to the patient's quality of life.

Progress in the area of MRI has improved the definition and categorization of structures, which has provided the high level of therapeutic certainty required for ablative radiotherapy treatments such as stereotactic radiosurgery (SRS). Nowadays, the ability to explore functional areas of the brain using fMRI is creating great interest for integrat-
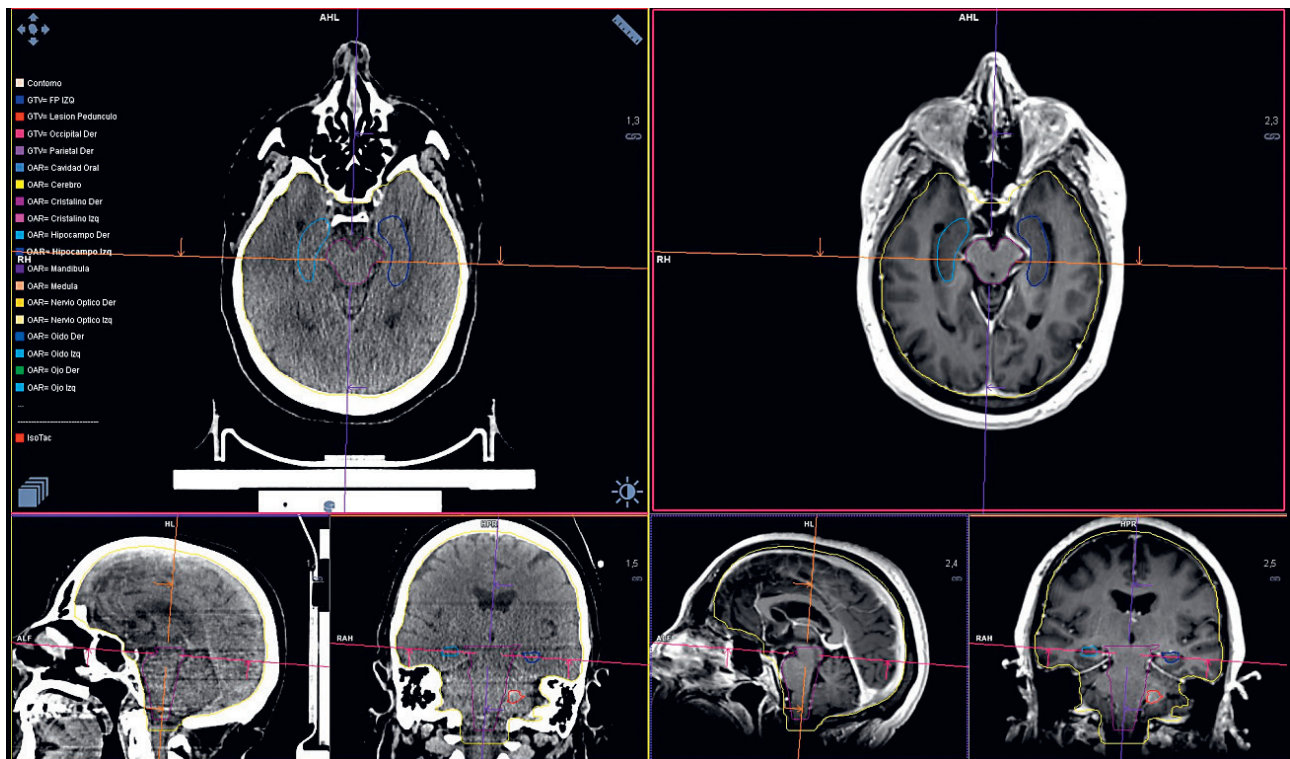
13 *syngo*.via RTiS workflow: the CT images from CT simulation are on the left; the MR T1 MPRAGE images obtained in axial orientation, including the hippocampus registration and delineation, are on the right.
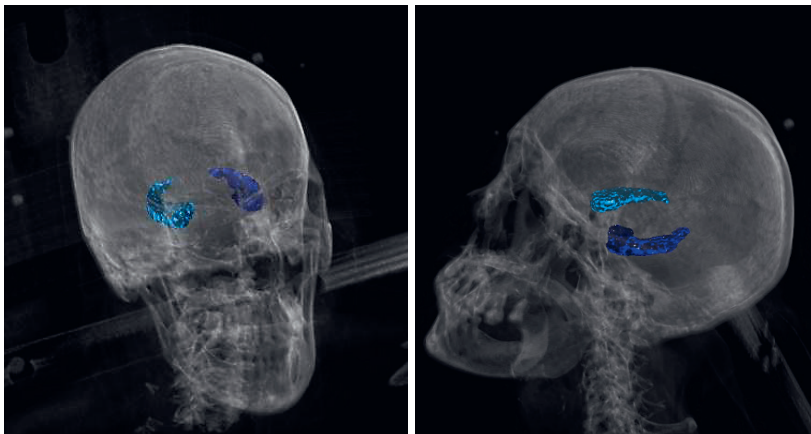
14 Transparent VRT visualization to assess OARs.

ing this type of diagnostic study into precision treatments such as radiosurgery – always with the key objective of improving the patient's quality of life.

By incorporating fMRI into the patient's entire diagnostic and treatment process, medical physicists have more information for radiosurgery and conventional radiotherapy treatment planning. Here at COI, we have been able to perform multimodality image fusion, contour eloquent regions in *syngo*.via RTiS, and export them to the treatment planning system.

It is expected that multimodality contouring platforms will eventually incorporate MRI and other modalities besides CT imaging, with compatible segmentation. Unfortunately, fMRI is rarely used to segment eloquent areas for SRS. This means no applications exist that bring together fMRI reconstruction tools with structure segmentation tools such as *syngo*.via RTiS.

In addition, few centers around the world have the equipment and organizational capacity needed to integrate fMRI into SRS, which is one reason why no relevant protocols exist and why very little work has been done on this topic.

Integrating fMRI into the radiosurgery process has been a great challenge for our radiotherapy and MRI services. Efforts have mainly focused on saving time and associated costs because fMRI has low reimbursement, being a novel technique in the region. Despite the obstacles described, the high level of interest that professionals and Leben Salud's directors have expressed for seeing results and conclusions in this area in the future was the main incentive for incorporating it into standard procedures at our institution.

Contact

Ricardo Ruggeri, MSc.
Technical director and
head of medical physics department
Centro de Oncológico Integral (COI),
a member of the Leben Salud group
Industriales Neuquinos 2800
Neuquén, Patagonia
Argentina
rruggeri@lebensalud.com
Follow me on LinkedIn:
https://www.linkedin.com/in/ricardoruggeri/

Ricardo Ruggeri   Elira Lomban   Belen Ibañez   Marcelo Paolini   Silvia Hansing

The Integration of MRI in Radiation Therapy:

The Power of Multidisciplinary Collaboration
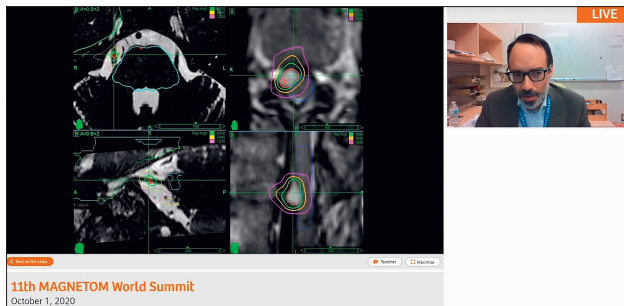
Implementing a Magnet Dedicated to Planning Radiotherapy Treatments

David Roberge
Centre Hospitalier de l'Université de Montréal, Canada
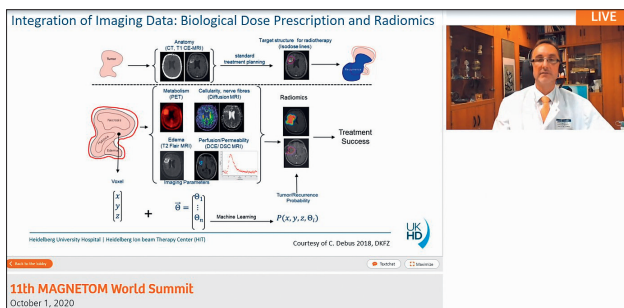
MRI in Radiation Oncology. See what you treat – treat what you see

Juergen Debus
University Hospital Heidelberg, Germany
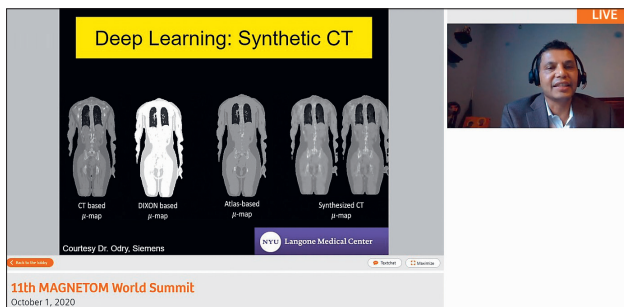
Collaboration between Radiology and Radiation Oncology for MR-guided Radiotherapy

Hersh Chandarana
NYU, New York, NY, USA

Don't miss the talks delivered by experienced and renowned experts at the MAGNETOM World Summit

www.siemens-healthineers.com/MWS2020-recordings

Pushing the Limits of Accuracy in MRI – A Perspective

John E Kirsch, Ph.D.

Athinoula A Martinos Center for Biomedical Imaging, Massachusetts General Hospital, Department of Radiology, Charlestown, MA, USA

Introduction

I am pretty sure that magnetic fields were never intended to be perfectly homogeneous or to vary precisely linearly in space at exactly a certain moment in time. At the very least, it is probably plausible to say that it was not what James Clerk Maxwell was thinking when he formulated his famous equations. Yet in 2021, magnetic resonance imaging (MRI) is used to do just about everything in healthcare, including guiding the placement of an electrode deep into the interior of the human brain at better than 1 mm accuracy to help patients with epilepsy, or producing exquisite anatomical information at 100 micron isotropic resolution (Fig 1).

MRI is based on magnetic fields throughout the entire measurement and imaging process, starting with a static external magnetic field that magnetizes the hydrogen nuclei in the body and ending with producing an image from that magnetization. The accuracy of those fields therefore ultimately determines the precision of the image outcome. The position of a voxel in a digital image representation of the anatomy is based on the singular assumption that the magnetic fields are precisely known everywhere in space and time. Deviation from this and there will be a proportional inaccuracy associated with the position of that voxel.
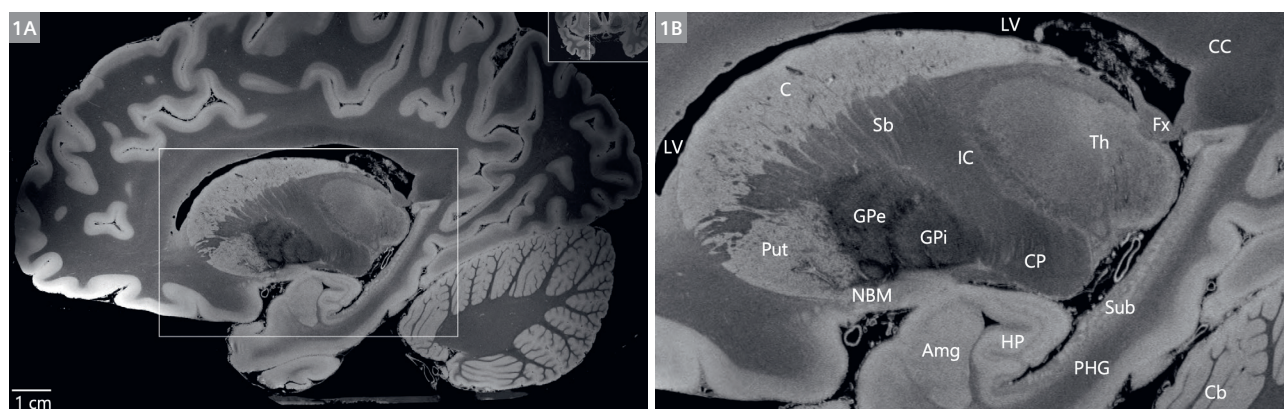
1 100 micron thick sagittal slice through an ex-vivo human brain acquired with the MAGNETOM 7T Classic showing delineation of basal ganglia, diencephalon, and medial temporal neuroanatomy at 100 micron resolution **(1A)**. A zoomed view of the striatum, amygdala (Amg), and hippocampus (HP) (within the white rectangle in 1A) is shown in **(1B)**.
Neuroanatomic abbreviations: C = caudate; Cb =cerebellum; CC = corpus callosum; CP = cerebral peduncle; Fx = fornix; GPe = globus pallidus externa; GPi = globus pallidus interna; IC = internal capsule; LV = lateral ventricle; NBM = nucleus basalis of Neynert; PHG = parahippocampal gyrus; Put = putamen; Sb = striatal bridges; Sub = subicular cortices; Th = thalamus.
With permission: Brian L Edlow, MD, Massachusetts General Hospital. BL Edlow, A Mareyam, A Horn, et al., 7 Tesla MRI of the ex vivo human brain at 100 micron resolution. Sci Data 6, 244 (2019). https://doi.org/10.1038/s41597-019-0254-8.

There are many applications now that rely on the informational accuracy of MRI, whether it be with its signal amplitude, phase, or position in space. Nowhere is this more evident than when using MRI for stereotactic planning, where spatial accuracy is paramount. High resolution isotropic 3D MR imaging has become the modality of choice for radiation treatment planning or surgical implantation procedures. Inaccuracies in the spatial position of the anatomy with respect to external fiducial markers can lead to potentially catastrophic outcomes. Spatial precision is also a requirement for personalized prosthetic modeling, where localized errors in position can cause painful misalignment for the recipient. Tissue morphometry and segmentation are being used more and more for medical and therapeutic evaluation that relies heavily on the volumetric precision not only in a given dataset but also longitudinally over time.

But spatial accuracy is not the only thing that relies on magnetic fields. In recent years, MRI is becoming more quantitative where accuracy in its signal amplitude and phase are necessary as well. Flow quantification in vascular and cardiac applications relies heavily on the precision of the signal phase, as does high-intensity focused ultrasound (HIFU) and other therapeutic procedures that use the phase information for MR thermometry to monitor tissue response. MR elastography requires the phase information to measure tissue stiffness in liver disease. Applications that demand accuracy and reproducibility in the signal amplitude also exist. Quantitative biomarkers such as the Apparent Diffusion Coefficient (ADC) in diffusion-weighted MRI rely on the signal amplitude decay associated with diffusion sensitization of water motion to probe tissues on a microscopic scale. And, fMRI requires extreme temporal stability of the signal magnitude to detect the statistical significance of the blood oxygen level dependence (BOLD) response in brain activity.

In the early days of MRI, we pretty much focused on just trying to maximize the signal-to-noise ratio (SNR) and simply hoped that after a 15-minute acquisition the scan would yield a reasonable facsimile of the human anatomy, whether it be of the brain, a knee, or the liver. But in this age of precision medicine, MRI is becoming much more quantitative, requiring equally greater accuracy. Just getting an image is no longer a reasonable expectation. MRI is now expected to be perfect in every way. Let us take a brief look into just how perfect, or not-so-perfect, it is.

Signal encoding

MRI of course begins with an external static B_0 magnetic field to create the initial magnetization. The MR signal that eventually is generated will possess characteristics of amplitude, phase, and frequency. Essentially, all three of these features are based on magnetic fields as described by the Larmor equation. For them to be accurate, this means that the magnetic fields that they are based on must also be accurate. Note that there are three magnetic fields that we deal with in MRI: B_0, B_1^+, and B_1^-. B_1^+ and B_1^- are the transmission and reception fields, respectively, and are perpendicular to the B_0 field in order to rotate the magnetization and detect it. Although the B_1 fields are clearly important and deserving of discussions about their accuracy, it is the B_0 field that is the focus here since it is ultimately what encodes the MR signal that gets detected and generates the image. Therefore, for the remainder of this paper only the B_0 magnetic fields will be discussed.

The MR experiment can be viewed as having four basic time-sequential elements – preparation, excitation, encoding, and readout. During preparation, the initial state of the magnetization for the experiment becomes defined. This may be an inversion preparation that might be applied for a specific type of tissue contrast, or it might be a type of saturation to suppress the magnetization from a specific tissue such as fat. In this stage, the accuracy of the B_0 field could be argued as playing a lesser role, primarily associated with the spatial uniformity of the outcome.

After the initial preparation, excitation is then carried out to rotate the magnetization out of the B_0 direction to create a transverse component which eventually becomes detected. This process relies on the resonance condition between RF transmission and magnetization, whereby their frequencies must be matched to produce the action of excitation and the rotation of the magnetization. By applying a spatially varying gradient field (G) during excitation one can then selectively excite a specific region in space. Here, the total magnetic field, $B_{0,tot}$ (comprised of the summation of the main magnetic field, B_0, and the gradient field, G) plays a significant role, since a one-to-one relationship will exist between the excitation of a physical location in space that matches the resonance condition according to the Larmor equation. Transmission at a specified frequency and bandwidth will produce excitation anywhere in physical space with a given slice thickness where it matches the Larmor frequency of the magnetization. For this to be accurate requires precision of $B_{0,tot}$ and therefore the main magnetic field, B_0, and the gradient field, G.

The encoding process is facilitated by applying G magnetic fields that spatially vary the B_0 magnetic field in a well-behaving manner so that signal can be mapped uniquely to different points in physical space. Gradient pulses of a given direction, amplitude, and duration encode the signal in k-space, the Fourier counterpart of image space, with the coordinates of k_x, k_y, and k_z. The action of the encoding process is to define the starting point coordinates in k-space for the readout process to follow, and the value of k will be based on the time

integration of the gradient pulsing. That said, the accuracy of the k-space encoding will therefore be defined by the accuracy of the gradient pulsing. In addition, however, since the transverse magnetization experiences the *total* magnetic field $B_{0,tot}$, the uniformity of the main magnetic field B_0 also plays an important role in the accuracy.

The final step of the MR experiment is the signal readout when the magnetization is detected and digitally sampled. k-space gets sampled according to the gradient pulsing that is applied simultaneously during the detection process. The k-space trajectory in readout will be based on the direction, amplitude, and duration of the gradient pulsing. Therefore, the trajectory will be determined by the precision of the gradient pulsing. And, as with the encoding process, the transverse magnetization experiences $B_{0,tot}$, so the readout accuracy will also depend on the uniformity of B_0 as well.

Historical progression

The spatial accuracy and temporal stability of the main static B_0 magnetic field and the pulsed G gradient magnetic fields has gone through different progression through the years. Early magnets were very large and heavy, and their spatial uniformity, or homogeneity, was in general quite poor. As the engineering design and manufacturing improved, magnet homogeneity also improved. However, other factors did not necessarily always allow continual improvement in the homogeneity. For example, a demand existed for wider and shorter bore designs to increase patient comfort, and siting requirements became more challenging for installing magnets in much smaller footprints. As a result, even though magnets progressively have become higher in field strength and more reliable and efficient, attaining the greatest homogeneity across a large imaging volume is not the only factor that is considered in present magnet technology.

Some amount of compensation for this can come from the implementation of active shimming with coils that generate 2nd-order spatial – or more recently even 3rd-order – harmonic correction of the static B_0 field. But it takes space to accommodate these extra shim coils in the bore, and this may be counterproductive with the ever-increasing demand for wider bore systems. For accuracy and precision, magnet homogeneity is what matters. But the final design will ultimately consider these other factors as well.

Probably what has progressed the most in the past decades is the gradient performance (on this point, readers can refer to the recent comprehensive historical summary *"An Attempt to Reconstruct the History of Gradient-System Technology at Siemens"* by Franz Schmitt et al. in the 2020 ISMRM issue of MAGNETOM Flash (77) 2/2020). In the early- to mid-1980s, gradient coils were unshielded, which meant that without compensation the field errors were on the order of 20% of the nominal amplitude of the gradient pulsing. Performance-wise, pulse rise times were typically 1500 μsecs or even longer in duration, and the maximum gradient amplitudes were no greater than about 3 mT/m. Since that time, continual improvements in power amplifiers, gradient coil design, and manufacturing have led to actively shielded configurations that have force compensation to minimize mechanical torque and vibrations, as well as counter windings to minimize higher-spatial-order eddy currents. Errors are reduced by several orders of magnitude or more, and gradient performance on contemporary whole-body clinical systems now have 200 T/m/s slew rates that allow pulse rise times of less than 100 μsecs and amplitudes up to 80 mT/m amplitudes. Digital precision to control arbitrary and complex gradient waveforms and their pre-emphasis to minimize eddy currents has steadily improved over the years, from 12 bits, to 16 bits, and up to 20 bits or higher.

Specialized gradient coil designs have most recently dramatically increased performance to as high as an astonishing 600 T/m/s and 500 mT/m. However, such fantastic improvements have not come without some compromises as well. In order to achieve these levels and stay within safe limits of peripheral nerve stimulation in the human body, the accuracy and extent of the spatial linearity of such gradient fields can be constrained.

The steady improvements in magnet, shim, and gradient coil design over the decades have allowed for rapid expansion of the types of acquisitions and applications that are now achievable with MRI. However, spatial and quantitative accuracy has not necessarily been the only metric by which contemporary systems are judged. Yet it can be considered just as critical and just as important.

Confounding factors (and where things can go wrong)

To have an appreciation for what it actually means to achieve better than 1 mm spatial accuracy or to produce an image with 100 micron resolution is to also have a realistic appreciation for what can go wrong. This became readily apparent to me very early in my career as an MRI scientist. My first role was to develop new applications, and what I found more times than not was that theory rarely behaved the same way in actual practice. And when it comes to the magnetic fields there are many things that can occur to cause these fields to distort in the real world, as shown in Table 1.

The primary objective of the magnet static B_0 magnetic field is to possess perfect uniformity everywhere in space. Since the B_0 field defines the initial state of the magnetization and its encoding, spatial non-uniformities and imperfections are a fundamental source of error. The

magnet itself is of course finite in size. As such, it will possess a nominal field strength in the middle of the bore and zero field strength at some distance far away. Therefore, at some point as you move away from the isocenter yet still are within the imaging field of view of spatial encoding, the B_0 field will taper off and the required homogeneity is lost. There exists a so-called "sweet spot" where the uniformity of the field is the highest.

   One of the most common things that can lead to errors in the static magnetic field are the spatial distributions of the different magnetic susceptibility (χ) that exist in tissues and objects (Fig. 2). This physical property determines the B_0 magnetic field that that medium experiences. Most soft tissues are quite similar, so the distortions of the field are negligible. However, the χ of bone and air are quite different from soft tissue and their presence can cause significant local distortions in B_0. And of course, foreign objects such as surgical or therapeutic implants that might be made of a type of metal possessing very

different properties of χ can produce very large spatial distortions of B_0 near the object.

   The molecular environment that surrounds hydrogen nuclei causes small but observable changes in the microscopic magnetic field environment known as chemical shift. Because fat and water in tissues have a frequency shift that equates to roughly 3.5 ppm of magnetic field difference, this means that the signal from each will originate from different locations in space. The most common example of this is pixel misregistration where fat will be located at slightly different positions in the field-of-view from water. Excitation of fat will also occur at different positions from water.

   These are static B_0 factors. But what about dynamic errors that are caused by external influences or the pulsing of the gradient G fields necessary to encode the MR signal? In urban areas like New York City, the environment can be a "firestorm" of magnetic fields that are constantly fluctuating all around you. A common source are subways, not so much because of the moving metallic trains but because of power lines that can produce strong magnetic fields from surges needed to move the trains. Although Siemens Healthineers has a unique solution for protecting the magnet from such external B_0 perturbations, if an MRI scanner is simply too close it can lead to measurable errors if it occurs when a scan is being done at that time.

   Faraday's law tells us that a magnetic field that changes in time will generate an electric field. When a gradient is pulsed, it changes the total magnetic field $B_{0,tot}$ dynamically over time at a given point in space. This will therefore produce a countering eddy-current induced magnetic field on conductive surfaces that can then distort G and in turn $B_{0,tot}$ dynamically. Such eddy-current fields can come from implants or objects that have conductive components

Static and dynamic B_0 magnetic field	Dynamic G magnetic field
Finite shim volume	Eddy currents
Magnetic susceptibility	Concomitant fields
Chemical shift	Finite spatial linearity
External influences	Calibration and regulation
	Mechanical vibration
	Heating and drift

Table 1: Some of the sources of static B_0 and dynamic G errors.
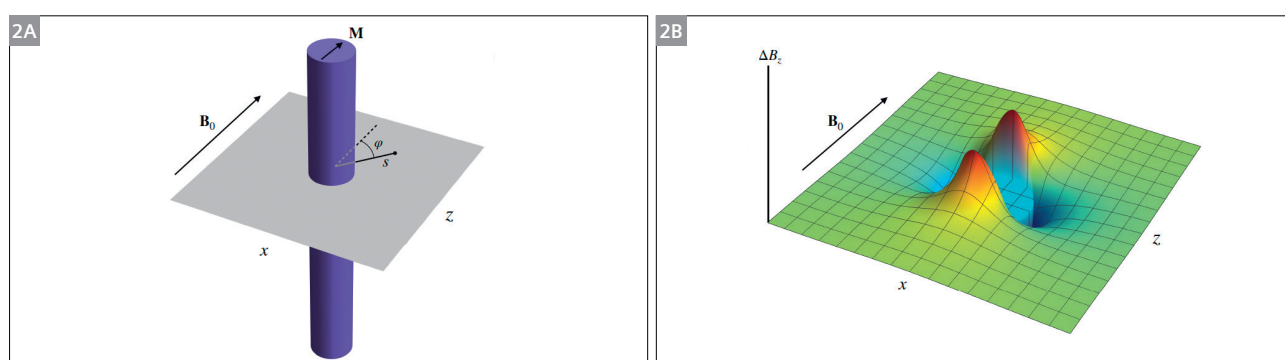
2 Localized magnetic susceptibility induced B_0 distortion in the presence of a cylinder containing uniform susceptibility that is greater than the surrounding external environment. **(2A)**: mathematical model showing the orientation of the cylinder relative to the main static B_0 magnetic field. **(2B)**: theoretical simulation of the distortion of the B_0 field. This model demonstrates the origins of the Blood Oxygen Level Dependent (BOLD) effect in the microvasculature in regions of brain activation.
With permission: Bradley R Buchbinder, MD, Massachusetts General Hospital. BR Buchbinder. Chapter 4: Functional magnetic resonance imaging. Handbook of Clinical Neurology. Vol 135. Neuroimaging, Part I. pp 61-92, JC Masdeu and RG Gonzalez, Editors, Elsevier BV (2016). https://doi.org/10.1016/B978-0-444-53485-9.00004-0

and surfaces, but the dominant source is from the conductive cryoshields within the magnet itself. As previously mentioned, actively shielded gradient coils are designed to minimize this, but the high performance of modern systems will still generate measurable errors within the imaging volume caused by these eddy currents.

Another source of error caused by pulsing the gradients is the additional terms commonly referred to as Maxwell concomitant gradients. According to Maxwell's equations, it can be shown that when producing a spatially varying gradient field, the actual total effect contains higher-spatial-order mathematical terms that are secondary or "concomitant" fields over and above the spatial linear term we wish to produce for encoding purposes. The extent of their contribution to errors are primarily proportional to the square of the magnitude of the gradient strength, the square of the position away from isocenter, and are inversely proportional to the main magnetic field strength. Therefore, large-gradient amplitudes of pulsing such as what are used in diffusion applications can produce appreciable errors from this source.

Aside from these physics-based phenomena, there are also several engineering factors that also can contribute to the overall errors associated with the gradient fields. First, like the magnet, the gradient coil is finite. As such, this will mean that the fields that it generates will eventually fall off away from the isocenter. Additionally, with the increased performance of modern gradients it is necessary to consider peripheral nerve stimulation and other safety constraints that will limit the extent of spatial linearity of the gradient fields. Figure 3 demonstrates how significant the spatial distortion can be if corrections of these errors are not applied.

Calibration and regulation of the amplifier output that drives the production of the gradient field are important aspects of accurate field generation. When a pulse sequence instruction specifies the amplitude and duration of a gradient pulse, this information is sent to the amplifier to convert the digital instruction to an analog electrical current which then drives the gradient coil generating the requested G field. Too much current will produce a G that is higher than what the instruction calls for. Calibrating this is therefore necessary to ensure accurate field generation (Fig. 4). And proper regulation is required to make sure that the baseline current always remains zero when no gradient field is being pulsed.

Rapidly changing magnetic fields associated with gradient pulsing also induce Lorentz forces that in turn produce mechanical vibrations. This of course also leads to the quite familiar knocking sounds associated with all MRI scanners. But it also can produce physical displacement. Although minor in most cases now that modern gradient coils are designed with force compensation to mitigate these vibrations, it cannot be completely ruled out as a potential factor.

The amount of current required to generate the gradient fields can be quite large, which over time produces a lot of heat that must be mitigated with cooling. However, state-of-the-art applications that exploit the maximum gradient performance over longer periods of time can lead
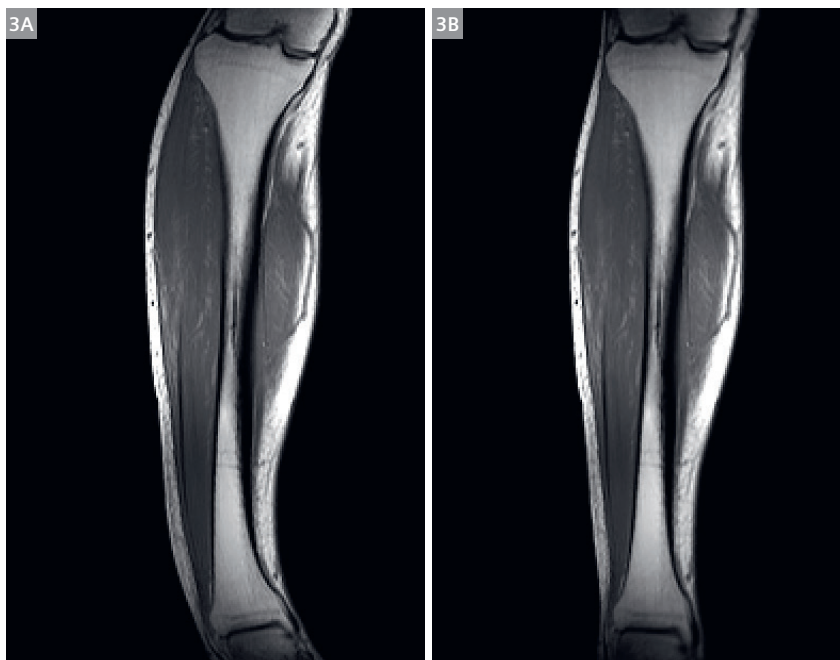
3 Large FOV coronal T1-weighted spin echo slice through the lower leg and calf muscle. Without correcting for the spatial nonlinearity of the gradient field, the image is geometrically distorted **(3A)**. Gradient related nonlinearity distortion is completely predictable if the gradient field is known and can therefore be corrected by pixel reformatting/remapping **(3B)**.

to gradual drifting of the total B_0 field over the duration of the MR experiment.

And finally, with all these things that can go awry, when it is all said and done, Siemens Healthineers continues to strive to improve and perfect things, and we are therefore able to achieve some of the most astounding diagnostic images and remarkable outcomes with MRI, that continues to significantly make a positive impact on healthcare.

MRI applications

Once magnetization is transverse after the excitation process, it becomes vulnerable to all the inaccuracies of the B_0-related magnetic fields, whether from the main static magnetic field or from the pulsing of the gradients. This will be true regardless of the application. However, it is the application and what information it is trying to extract from the human body that ultimately determines whether the errors in $B_{0,tot}$ make a difference or not. For a given B_0 error somewhere in space, the spatial distortion or signal phase deviation may be large or small at that location based on the technique of measurement and its application.

Specific details of the myriad of MRI applications that now exist on modern scanners are beyond the scope of this paper. But there are several basic aspects that can make an application more or less sensitive to the $B_{0,tot}$ field and its errors. One of these is the MR signal readout. How fast one samples the signal and encodes it in k-space

defines the field sensitivity of the MR experiment. The longer this duration, the more time passes for the transverse magnetization to evolve in the $B_{0,tot}$ field that it experiences. Errors in the field increase the magnitude of the error in the signal, as the magnetization continues to evolve during the sampling process.

Single-shot echo-planar-imaging (EPI) applications such as functional MRI (fMRI), diffusion tensor imaging (DTI), and dynamic susceptibility contrast (DSC) are at one extreme of the sensitivity spectrum where the entire readout of the MRI signal and complete sampling of k-space is done with a single magnetization preparation. Ironically, although this provides the ability to produce rapid "freeze-frame" results in a matter of 20 or 40 ms per image, on the scale of evolution of the transverse magnetization this is quite slow. These techniques are therefore extremely sensitive to B_0 errors leading to substantial spatial distortions, and signal magnitude and phase deviations.

In the more traditional steady-state Cartesian sampling used in gradient echo (GRE), spin echo (SE) or turbo spin echo (TSE) techniques, the duration of the readout of a line in k-space, and thus the sensitivity of the scan, is determined by different factors. On the one hand, high-bandwidth sampling associated with short readout durations offers the ability to shorten timing such as echo time (TE) or echo spacing with less sensitivity to B_0 errors, but is accomplished at the expense of increased noise and thus lower SNR. On the other hand, longer durations of lower bandwidth sampling improve the SNR but at the
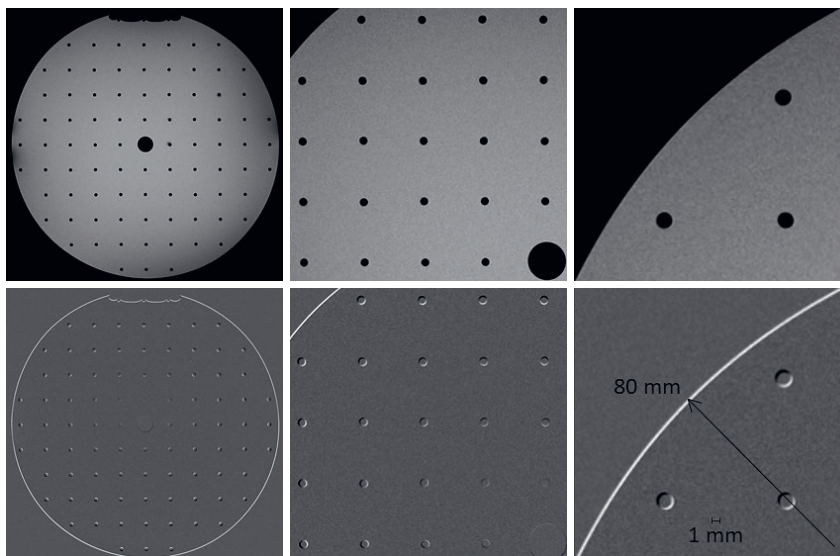
4 Effect of gradient calibration. A high resolution image of a phantom specially designed to assess spatial accuracy is shown in the upper row at various magnifications. The bottom row is a difference map between two slightly different calibrations. Note that since calibration is relative, the absolute spatial error will depend on the distance away from isocenter.

expense of increased sensitivity to B_0 errors. And, what fights against this is that higher spatial resolution necessitates higher k-space sampling of the information requiring larger gradient pulsing which can introduce greater error. So, although one may spatially encode an image with high resolution, the inaccuracy in the spatial position may also be higher.

Cartesian sampling is not the only method used to sample and fill k-space. Depending on the application, spiral or radial sampling trajectories can be of benefit. For example, ultrashort echo times are necessary to catch the MR signal before it rapidly decays away in solids such as cortical bone, or regions of interest that contain large localized susceptibility-based B_0 inhomogeneities, such as lung parenchyma. Each sampled data point in k-space will only be as accurate as the gradient pulsing that is required to encode that sample with the correct k-space coordinates. The more complex the k-space trajectory and the longer the readout of the sampling, the greater the potential for error in the mapping.

And finally, as perfect as we might strive to make the magnetic fields and signal encoding, the cooperation of the subject may end up being the single most important confounding factor. The longer the scan is, the greater the probability that the patient will move during the scan which can compromise the accuracy of the outcome. Navigator signals and tracking devices are prospective strategies used to attempt to mitigate some of these inevitable errors due to motion, but these as well ultimately rely on the accuracy of the B_0 fields to correct things.

On the not-so-distant horizon

As the MRI applications become more sophisticated, so do the ways to produce more accurate and reliable results. Clearly, engineering and manufacturing continues to improve the performance of MRI scanners, and Siemens Healthineers leads the way on this front. The scanner is no longer just a diagnostic device that produces images, but is a quantitative measurement system of biomarkers in the age of precision medicine.

In a different approach that accepts the premise that complicated four-dimensional B_0 errors will always exist, dynamic field cameras are devices that measure these complicated fields and either retrospectively or prospectively correct for such errors so that the result is completely corrected of the deviations that occur during the measurement process.

And of course, artificial intelligence (AI) has made great strides in recent years to become integrated in healthcare, radiology applications, and workflow. MRI is not excluded from this. AI is being assessed across a broad range of applications from improving lesion conspicuity, to increasing SNR without the typical compromise in spatial resolution, and using deep-learning algorithms to correct for B_0-related errors and producing super-resolution results.

Concluding remarks

At the beginning of my career, it was extremely important to me that I never stop learning in whatever field I chose. If I stopped learning, I vowed that I would change my direction. I never anticipated that when I chose to be a scientist in the field of magnetic resonance imaging that I would still be here today 35 years later where never a day passes that I am still fascinated by what can be accomplished with this incredible technology.

James Clerk Maxwell may not have ever expected that magnetic fields would be exploited in this way, but I am pretty sure he would be quite pleased to see what we have done with them.

Contact

John E Kirsch, Ph.D.
Director, Human Imaging Core
Athinoula A Martinos Center for Biomedical Imaging
Massachusetts General Hospital
Department of Radiology
149 Thirteenth Street, Room 2301
Charlestown, MA 02129
USA
jkirsch@mgh.harvard.edu

Meet Siemens Healthineers

Siemens Healthineers: Our brand name embodies the pioneering spirit and engineering expertise that is unique in the healthcare industry. The people working for Siemens Healthineers are totally committed to the company they work for, and are passionate about their technology. In this section we introduce you to colleagues from all over the world – people who put their hearts into what they do.

Melanie Habatsch

Hi, I'm Melanie Habatsch, and I work as an application specialist in the MR Marketing Application Center (MAC) in Erlangen. I grew up in Siegen, Germany, but spent several years working as a radiographer in the radiotherapy department at Kantonspital Münsterlingen in Switzerland. After spending five years in radiotherapy in a hospital, I decided to take the next step and switch from being a customer to working for customers as an application specialist in Particle Therapy (PT). This field of business was new, and it was exciting to feel like we were part of a startup culture. I was mainly involved in developing and implementing training concepts for PT projects, and in evaluating and optimizing clinical workflows. More changes came in 2009 and 2011, with the birth of my two children. When PT closed down, I found new opportunities in MR at the MAC, where I'm responsible for the MR in RT data.

Erlangen, Germany
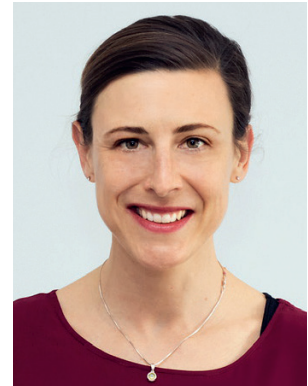
How did you first come into contact with MRI?
My first contact with MR was during my apprenticeship in 1998. As a student, MRI felt like a huge mystery. However, when I began working in radiotherapy planning, I became increasingly inspired by the technology. Back then, the capabilities for registering datasets from different modalities were fewer, but we still tried to use the brilliant soft-tissue contrast to determine the target volume and plan the best therapy for the cancer patients.

What do you find most fascinating about MRI in RT?
That's easy: everything! The developments and innovations within MRI never stop. For me, the cross-modality topics are really fascinating. We can give medical answers to patients and make our customers' daily tasks in hospital easier with our wide range of MRI sequences and features. The combination of different hospital departments and my work "beyond" the scanner itself makes the role extremely interesting.

How does your work support the use of MRI in RT?
With my hospital background and my experience in particle therapy, I'm familiar with the needs of our customers in radiotherapy – and those of their customers, the patients.

We try to close gaps and reduce their daily challenges by using the advantages of MRI and embedding it into the RT workflow. We are a great team and we're always looking for ways to bring our customers value and solutions that go beyond the department.

What do you find motivating about your job?
I love working with people who come from so many different cultural and professional backgrounds and have such a wide range of experiences. It's fascinating and extremely motivating. At first it can feel as if everyone's aims and mentalities are different – but these differences turn into inspiration and open up new ways of doing things. It's like a jigsaw puzzle: The beauty of the whole picture only becomes visible if you have all the differently shaped pieces in place.

What would you do if you could spend a month doing whatever you wanted?
Professionally, I would like to spend time with our new colleagues from Varian, as I see a lot of potential in our collaboration. Personally, I have to say that after a year of social distancing, I'm really looking forward to simply enjoying quality time with family and friends.

Sylvain Doussin, Ph.D.

After earning an engineering degree in green chemistry in 2003, I went on to complete a doctorate in MR physics at the French Alternative Energies and Atomic Energy Commission (CEA) in Paris-Saclay. My thesis focused on the T2 relaxation properties of encapsulated proteins in reverse micelles in a low-viscosity medium under high pressure. While finishing my thesis in 2007, I joined Siemens Healthineers France as an application specialist. I spent five years covering almost all anatomies and MRI specialties throughout France. In Lyon, I also spent several years organizing and supporting cardiac MR courses for radiologists and cardiologists with Professor Pierre Croisille. At the start of 2012, I moved to Erlangen, Germany, to take up a position as Application Training Manager at CS MR. I was responsible for the training strategy for MAGNETOM Spectra, Essenza, and Biograph mMR. I loved "creating" the first mMR experts – application specialists from MR and MI with cross-disciplinary knowledge. After three years at CS, I moved to R&D as a protocol developer, which required MR physical and clinical knowledge. I would say that I feel like a Toolbox because giving opinion/advice to other teams about many aspects of the scanner during development that the other teams can use for collecting feedback about image quality, works in progress, use cases, and new applications as we try to mimic user behavior at the scanner when developing robust solutions. For six years now, I have mainly been responsible for clinical protocol and application development for Biograph mMR, and all release scanners in various regions and specialties. Radiotherapy has been central to my tasks for the past four years.

Erlangen, Germany

How did you first come into contact with MRI?
Before working with MAGNETOM Avanto and the *syngo* MR VB13 software, during my doctorate I had my first MRI experience when imaging a poor spider we found in the corridor! At that time, I was performing high-resolution nuclear magnetic resonance imaging with a vertical magnet of 21.4T and probes of 0.5 to 1 cm! I put the spider in a tube, and it was my first MR image.

What do you find most fascinating about MRI in RT?
MR is not the leader in this domain: MR serves RT, so I need to understand this new world. I like the interaction between the users and developers because there's so much variety. I get to work with radiation oncologists, physicists, technologists, and pure researchers.

Also, these users are not MR users: They are not addicted to all the great applications we have developed in the last decade, nervertheless they do want the most advanced ones so that they can do things like study radiation response or use MR to adapt their treatment every day if necessary.

How does your work support the use of MRI in RT?
In my role within R&D, I try to be the bridge between pre-development and end users. We have existing solutions we can adapt to MR-in-RT, such as DeepResolve and new workflows, and we need to develop new specific ones. Also, with the relatively small AST THP group, it's easy to discuss a new approach or an issue we need to solve. Our colleagues in Cancer Therapy (CTH) need support for MR topics within a sales or collaboration context. And we appreciate their input – descriptions of hardware and software solutions, and entire radiotherapy workflows including imaging, contouring, dose planning, planning adaption, treatment, follow up, and re-imaging – to help us refine our developments.

What do you find motivating about your job?
All potential solutions or proposals have to be tested in real conditions, more so than for any specialty I have encountered so far. Every tiny detail counts because MR-in-RT is heavily influenced by patient positioning with the mask, by compression, by hardware such as the coil framework, and by software such as synthetic CT or a distortion-correction algorithm. It's important to also understand the other treatment modality or imaging modality (e.g. CT), and its strengths and limitations. Every discussion with colleagues and customers is valuable because it helps to expand my existing knowledge.

I would like to encourage RT users to move to MR now, even if their behavior is quite conservative since they have to guarantee the safety of their patients and deliver the

best treatment at all times. On the other hand, RT users have been following the motto of Siemens Healthineers for years – by always striving for the best imaging to provide the best treatment for their patients. Simple! I love the feeling that my work has a value that I can observe and assess.

What would you do if you could spend a month doing whatever you wanted?
I would find it interesting to step out of the R&D rhythm and visit our end users who want to test our solution and set up clinical studies together. Patients could also benefit a lot from these types of meetings in the context of COVID-19.

I could imagine combining this with a one-month road trip around the Mediterranean, with a stop in France of course! Or in South America, with just a backpack and a mobile phone to arrange the travel day by day. It would open up so many opportunities to meet new people, experience different cultures, and see fascinating places – and I'd spend some time playing soccer, doing yoga, and just relaxing.

Of course, I could also take a month off work entirely for my trip! I'd love to return to my home country as a tourist and see some of the many villages, landscapes, and monuments I've never visited. A day, a place, and a culinary discovery: this triptych could be my plan B for a month.

Siemens Healthineers' global MRI community offers peer-to-peer support and information. Radiation Oncologists, Radiologists, Medical Physicists, Technologists and Cardiologists have all contributed with publications, presentations, training documents, videos, case studies and more – all freely available to you via this unique network.

MRI in Radiation Therapy
Peer-to-peer exchange of protocols, articles and tips

Overview   **Protocols**   Application Tips   **Articles & Case Studies**   Talks & Keynotes   Contact Us

Don't miss the MRI protocols and practical tips and tricks for several body regions from experts for both experts and novice users. The information can help in supporting your entire clinical team and grow your practice.

The centerpiece of the MAGNETOM World Internet platform consists of MAGNETOM users' results. Here you will find articles, case reports and application tips allowing you to optimize your daily work.

Put the advantages of the MAGNETOM World to work for you!

www.siemens-healthineers.com/magnetom-world-rt

Not for distribution in the US

On account of certain regional limitations of sales rights and service availability, we cannot guarantee that all products included in this brochure are available through the Siemens sales organization worldwide. Availability and packaging may vary by country and is subject to change without prior notice. Some/All of the features and products described herein may not be available in the United States.

The information in this document contains general technical descriptions of specifications and options as well as standard and optional features which do not always have to be present in individual cases, and which may not be commercially available in all countries.

Due to regulatory reasons their future availability cannot be guaranteed. Please contact your local Siemens organization for further details.

Siemens reserves the right to modify the design, packaging, specifications, and options described herein without prior notice. Please contact your local Siemens sales representative for the most current information.

Note: Any technical data contained in this document may vary within defined tolerances. Original images always lose a certain amount of detail when reproduced.

siemens-healthineers.com/magnetom-world-rt